

AUTOMATIC DETECTION OF DIABETIC EYE DISEASE THROUGH DEEP LEARNING USING FUNDUS IMAGES

Thesis submitted in fulfilment of the requirements for the degree of

Doctor of Philosophy

College of Engineering and Science

Victoria University

by

Rubina Sarki

March 2021

© 2021 Rubina Sarki
ALL RIGHTS RESERVED

ABSTRACT

AUTOMATIC DETECTION OF DIABETIC EYE DISEASE THROUGH DEEP LEARNING USING FUNDUS IMAGES

Rubina Sarki, Ph.D.

Victoria University 2021

Diabetes is a life-threatening disease that affects various human body organs, including eye retina. Advanced Diabetic Eye disease (DED) leads to permanent vision loss; thus, early detection of DED symptoms is essential to prevent disease escalation and timely treatment. Studies have shown that 90% of DED cases can be avoided with early diagnosis and treatment. Ophthalmologists use fundus images for DED screening to identify the relevant DED lesions. Due to the growing number of diabetic patients, it is becoming unaffordable for the volume of fundus images to be manually examined. Moreover, changes in the eye anatomy during its early stage are frequently untraceable by human eye due to subtle nature of the features, and a large volume of fundus images puts a significant strain on limited specialist resources, rendering manual analysis practically infeasible. Therefore, considering the popularity of deep learning in real-world applications, this research scrutinized deep learning-based methods to facilitate early DED detection and address the issues currently faced. Despite promising results on the binary classification of healthy and severe DED, highly accurate detection of early anatomical changes in the eye using Deep Learning remains a challenge in wide-scale practical application. Similarly, all previous fundus retinal image classification studies assigned a multi-class classification problems are still a challenge in Deep Learning. While studies conducted in the

past have released high classification performance outputs managed by hyper-parameters settings, applying the binary classification model to the actual clinical environment in which visiting patients suffer from different DED diseases is technically tricky. Nevertheless, mild and multi-class DED classification aimed studies have been very minimal. Furthermore, it is observed that previous researches lack in addressing the development of automated detection of early DED, jointly in one system. Detection of DED in one system is considered to be essential for treatment in terms of specific lesions. Identification of the abnormalities in that specific retinal region can provide specific treatment to the target region of the eye, which is mostly affected.

In this thesis, we explore different novel Deep Learning methods for automated detection of early (healthy and one mild) and multi-class (three or more) DED employing retinal fundus images. For this purpose, we explore transfer learning based models and build a new convolutional neural network method in automatic feature extraction and classification, based on deep neural networks. To develop an enhanced system certain number of original deep learning approach has been combined with various other advanced techniques such as: *(i) image pre-processing, (ii) data augmentation, (iii) DED feature extraction and segmentation (iv) model fine-tune, and (v) model optimization selection*. Therefore, the results of the analysis of several retinal image features demonstrate that deep learning can attend a state-of-the-art accuracy for early DED diagnosis.

DOCTOR OF PHILOSOPHY DECLARATION

I, Rubina Sarki, declare that the PhD thesis entitled *Automatic Detection of Diabetic Eye Disease through Deep Learning using Fundus Images* is no more than 100,000 words in length including quotes and exclusive of tables, figures, appendices, bibliography, references and footnotes. This thesis contains no material that has been submitted previously, in whole or in part, for the award of any other academic degree or diploma. Except where otherwise indicated, this thesis is my own work.

"I have conducted my research in alignment with the Australian Code for the Responsible Conduct of Research and Victoria University's Higher Degree by Research Policy and Procedures."

Signature



Date

18/03/2021

DEDICATION

This thesis is dedicated to my parents for their love, endless support and encouragement.

ACKNOWLEDGEMENTS

I owe my gratitude to all those who have made this thesis possible. I want to thank my esteemed supervisor, Professor Yanchun Zhang, Director of the Centre for Applied Informatics, for invaluable supervision, advice, and continuous support during my Ph.D. study. I am incredibly grateful to my associate supervisors Professor Hua Wang and Dr. Khandakar Ahmed, for encouraging me with your immense knowledge and ample experience in my research and daily life. Thank you for allowing me to explore my ideas and choosing the specific research topic that I had desired to pursue.

My gratitude extends to Dr. Khandakar Ahmed for shaping my experiment methods and critiquing my results with your constructive and encouraging feedback. Thank you for sharing many important professional and personal advice throughout these years.

The research presented in this thesis was supported by International Postgraduate Research Scholarship offered by Victoria University. This financial support is gratefully acknowledged. I want to express my gratitude to Research Dean Anne-Marie Hede, Elizabeth Smith, and Dr. Lesley Birch for their constant support and proper guidance.

I would like to thank all my Ph.D. friends, Sheikha, Sandra, Sarathkumar, Neda, and Dr. Sudha, who always helped me through my queries and for the endless support.

I am forever grateful to my Dear friends, Angelina, Deshna, Upashna, and Rihana for unconditional love and support in this long journey. Thanks, Elizabeth for giving me some positive energies whenever I needed to rejuvenate myself from stressful times. Profound gratitude to Dr. Dinesh and Dr. Saurav, particularly for helping me during the initial stage of my life in Australia. I want

to thank Dr. Anish for motivating me and guiding me to prepare my research proposal for my Ph.D. admission.

I am always grateful to my parents, who have sacrificed their life for me, and for their unconditional love and generous support. Thank you, Baba, for teaching me hard work and building my initial foundation. Thank you, Aama, for your unconditional love and for giving me strength under challenging circumstances. Last but not least, I thank God for bestowing his grace upon me throughout this Journey.

PUBLICATIONS

Based on this research work, the following articles, have been published or submitted in International Journals and Conferences.

Journal Articles

1. **Rubina Sarki**, Khandakar Ahmed, Hua Wang and Yanchun Zhang, "Automatic Detection of Diabetic Eye Disease Through Deep Learning Using Fundus Images: A Survey," in IEEE Access, vol. 8, pp. 151133-151149, 2020, doi: 10.1109/ACCESS.2020.3015258.
2. **Rubina Sarki**, Khandakar Ahmed, Hua Wang, and Yanchun Zhang, "Automated detection of mild and multi-class diabetic eye diseases using deep learning," in Health Inf Sci Syst 8, 32, 2020. <https://doi.org/10.1007/s13755-020-00125-5>.
3. **Rubina Sarki**, Khandakar Ahmed, Hua Wang, and Yanchun Zhang, "Image Preprocessing in Classification and Identification of Diabetic eye Diseases," (Accepted in Data Science and Engineering, 2021).
4. **Rubina Sarki**, Khandakar Ahmed, Yanchun Zhang, "Early Detection of Diabetic Eye Disease through Deep Learning using Fundus Images," PHAT, EAI, 2020, doi: 10.4108/eai.13-7-2018.164588.

International Conference Articles

1. **Rubina Sarki**, Khandakar Ahmed, Hua Wang, Sandra Michalska, Yanchun Zhang . Early Detection of Diabetic Eye Disease from Fundus Images with Deep Learning. In Australasian Database Conference 2020 Feb 3 (pp. 234-241). Springer, Cham.

TABLE OF CONTENTS

Doctor of Philosophy Declaration	5
Acknowledgements	6
Publications	iii
Table of Contents	iv
List of Tables	vii
List of Figures	ix
1 Introduction	1
1.1 Background and Motivation	1
1.2 Research Problems	4
1.3 Hypotheses	7
1.4 Contributions and Significance	7
1.5 Thesis Outline	16
2 Literature Review	18
2.1 Prevalence and Types of Diabetic Eye Disease	18
2.1.1 Diabetic retinopathy	19
2.1.2 Diabetic Macular Edema	21
2.1.3 Glaucoma	21
2.1.4 Cataract	22
2.2 Diabetic Eye Disease Datasets	27
2.2.1 Retinal Imaging for DED	28
2.2.2 Dataset Characteristics	31
2.3 Image Preprocessing Techniques	33
2.3.1 Image Quality Enhancement	33
2.3.2 Image Augmentation	34
2.3.3 Region of Interest based Segmentation	36
2.4 Machine Learning in Diabetic Eye Disease Classification	36
2.4.1 Image Feature Analysis	37
2.4.2 Review of machine learning algorithms	39
2.5 Deep Learning in Diabetic Eye Disease Classification	49
2.5.1 Convolutional Neural Networks	49
2.5.2 Transfer Knowledge	53
2.5.3 Combined Deep Learning and Machine Learning	58
2.5.4 Analysis and Review of Performance Evaluation metrics	61
2.6 Discussion and Observations	62
2.7 Chapter Summary	64
3 Deep learning for Mild Diabetic Retinopathy Classification and Detection	66
3.1 Introduction	67
3.2 Methodology	70

3.2.1	Image Data Collection	71
3.2.2	Image Data Pre-processing	72
3.2.3	Model Construction	76
3.2.4	Performance Evaluation	77
3.3	Experiment and Analysis	79
3.3.1	Experiment Design	79
3.3.2	Model and Optimiser Selection	79
3.3.3	Improvement Techniques Comparison	81
3.3.4	System Evaluation	82
3.3.5	Performance Analysis	84
3.4	Summary of Findings	87
4	Role of Image processing in detecting Mild DED Classification and Detection	89
4.1	Introduction	90
4.2	Literature Survey	93
4.3	Methodology	96
4.3.1	Image Data Collection	96
4.3.2	Image Pre-processing	98
4.3.3	Model Development	106
4.3.4	Proposed CNN Model	108
4.3.5	Performance Evaluation	110
4.4	Experiment Design and Analysis	111
4.4.1	Experiment Design	111
4.4.2	Model Training	112
4.4.3	Performance Analysis	114
4.5	Summary of Findings	124
5	Automatic Identification of Mild DED and Multi-Class DED using Pre-trained CNN models	126
5.1	Introduction	127
5.2	Literature Review	129
5.3	Dataset	131
5.3.1	Data Collection	131
5.3.2	Data Pre-processing	132
5.4	Model Construction	133
5.4.1	Model Specification	134
5.4.2	Classification Performance Analysis	135
5.5	Experimental Design	137
5.5.1	Performance enhancement	138
5.5.2	Training and Prediction Results	140
5.5.3	Accuracy Evaluation	141
5.6	Summary of Findings	142

6	Automated Classification and Detection of Multi-Class DED using proposed CNN	144
6.1	Introduction	145
6.2	Literature Review	147
6.3	Data Collection	148
6.3.1	Data Enhancement	149
6.4	Study Design	150
6.4.1	Model development	151
6.4.2	Classification Description	154
6.4.3	Classification Performance Analysis	154
6.5	Experimental Design	156
6.5.1	Performance enhancement	156
6.6	Results	158
6.6.1	Visualizing feature map	159
6.6.2	Explaining Proposed Model using Grad-CAM	159
6.7	Summary of Findings	162
7	Conclusion and Future Work	164
7.1	Summary of Contributions	164
7.2	Study Limitations	171
7.3	Future Research Directions	172
	Bibliography	175

LIST OF TABLES

2.1	Selected articles for common objectives (review target).	28
2.2	Datasets available for automatic Diabetes Eye Detection with source (link).	29
2.3	Image preprocessing techniques employed in selected studies. .	30
2.4	Different hyperparameters used in the selected studies.	35
2.5	Studies employing new network for automatic DED detection. .	52
2.6	Studies employing combined DL and ML for automatic DED detection.	53
2.7	Studies employing TL for automatic DED detection.	59
2.8	Performance metrics employed in selected studies.	61
3.1	The DR severity levels according to ETDRS and the number of images used in each experiment.	73
3.2	The CNN models pre-trained on ImageNet and their characteristics (source: https://keras.io/applications).	77
3.3	The accuracy comparison of pre-trained CNN models.	80
3.4	The Optimisers performance evaluation.	81
3.5	The effect of data augmentation (Scenario I) and contrast enhancement (Scenario II).	82
3.6	Proposing New CNN on (Scenario II).	82
4.1	Three CNN models pre-trained on ImageNet and their characteristics (source: https://keras.io/applications)	108
4.2	Hyper-parameters of the build CNN model and preferred weights in this study.	109
4.3	Confusion Matrix	111
4.4	Average performance of the models on original images	114
4.5	Average performance of the VGG16 model on pre-processed images	114
4.6	Average performance of the New proposed model on original images	115
4.7	Average performance of the new proposed model on pre-processed images	115
5.1	The layers and layer parameters of the VGG16 model	136
5.2	Parameters of the VGG16 model and preferred weights in this study.	137
5.3	Parameters of the InceptionV3 model and preferred weights in this study.	137
5.4	Average performance of the models in mild DED classification (mild multi-classes).	139
5.5	Average performance of the models in multi-class DED classification.	139

6.1	Hyper-parameters of the build CNN model and preferred weights in this study.	154
6.2	Confusion Matrix	154
6.3	Average performance of the models in multi-class DED classification.	158

LIST OF FIGURES

1.1	Overall thesis contribution.	9
1.2	Examples of a publicly available data set (Kaggle Data). (A) Under exposure fundus image; (B) Over exposure fundus image; (C) Unrelated artifacts and (D) Blurriness.	11
1.3	Contrast Limited Adaptive Histogram Equalization enhances contrast in an image: A. Before and B. After CLAHE application.	12
1.4	Learning features and knowledge transferred using Convolutional Neural Network for detection of DED.	14
2.1	Anatomical structures of the retina.	20
2.2	Complications of DED in retina; A. Microaneurysms, narrow bulges (Diabetic Retinopathy), B. Optic nerve damage (Glaucoma), C. Exudates with retinal thickening (Diabetic Macular Edema), D. Degeneration of lens (Cataract).	20
2.3	Search and filter results: A. Query1 (Q1) = <i>diabetic eye disease, fundus images, image processing, image classification, deep learning, transfer learning</i> ; B. Query2 (Q2) = <i>diabetic retinopathy, fundus images, image processing, image classification, deep learning, transfer learning</i> ; C. Query3 (Q3) = <i>glaucoma, fundus images, image processing, image classification, deep learning, transfer learning</i> ; D. Query4 (Q4) = <i>diabetic macular edema, fundus images, image processing, image classification, deep learning, transfer learning</i> ; E. Query5 (Q5) = <i>cataract, fundus images, image processing, image classification, deep learning, transfer learning</i>	26
2.4	Research method flowchart.	26
2.5	Classic Machine Learning Framework.	36
3.1	The examples of different stages of DR advancement on fundus images. A. No DR – healthy retina; B. Mild DR – abnormal growth of blood vessels and ‘cotton wool’ spots formation (early indication); C. Moderate DR – abnormal growth of blood vessels and ‘cotton wool’ spots formation (mid-stage indication); D. Severe DR – hard exudates, aneurysms and hemorrhages (advanced indication).	70
3.2	The high-level process pipeline.	71
3.3	The examples of data augmentation steps performed on Mild DR fundus image from Kaggle dataset. (A) Original; (B) Crop; (C) Rotate 90°; (D) Rotate 120°; (E) Rotate 180°; (F) Rotate 270°; (G) Mirror.	74
3.4	Contrast enhancement using CLAHE: A and C: before, B and D: after.	76
3.5	Validation accuracy achieved for the respective epochs. (A) Default; (B) Fine-tuning.	81

3.6	Confusion matrices for Scenario I and Scenario II.	83
4.1	Early DED complication in retina (A) Anatomical structure of the retina; (B) Microaneurysms - narrow bulges in blood vessels (diabetic retinopathy); (C) Soft exudates in macula (diabetic macular edema); (D) Optic nerve damage (glaucoma); and (E) cataract	90
4.2	The high-level process pipeline	97
4.3	The flowchart.	99
4.4	The proposed CNN model	108
4.5	VGG16 model performance in Diabetic Retinopathy	116
4.6	VGG16 model performance in Diabetic Macular Edema	117
4.7	VGG16 model performance in Glaucoma	118
4.8	Build CNN model performance in Diabetic Retinopathy	119
4.9	Build CNN model performance in Diabetic Macular Edema	120
4.10	Build CNN model performance in Glaucoma	121
5.1	Complications of DED in fundus images; A. Microaneurysms; narrow bulges in the side of the blood vessel(Diabetic Retinopathy) B. Progressive damage of optic nerve damage(Glaucoma) C. Exudates formation in macular region and thickening of macula(Diabetic Macular Edema) D. Degeneration of lens (Cataract).	127
5.2	Transfer Learning process.	129
5.3	Data Distribution	132
5.4	Contrast Enhancement (A) Original and (B) Enhanced Diabetic Retinopathy; (C) Original and (D) Enhanced Glaucoma; (E) Original and (F) Enhanced Diabetic Macular Edema; (G) Original and (H) Enhanced Cataract	133
5.5	Confusion Matrix in VGG16 + Adam (A) scenario I and (B) Scenario II.	140
6.1	Data Distribution	149
6.2	Confusion Matrix and ROC Curve obtained by proposed CNN	158
6.3	Visual feature maps in first layer and deep layer	160
6.4	Visualisation on fundus retinal images of Normal / DR/ DME/ Glaucoma/ Cataract infected using Grad-CAM on the proposed model.	161

CHAPTER 1

INTRODUCTION

1.1 Background and Motivation

Diabetes mellitus, widely known as diabetes, is a disease in which a person has an excessive blood sugar levels due to insufficient insulin secretion, inappropriate body cells responses to insulin, or both. Diabetes is a significant worldwide health complications, and is largely due to a sedentary lifestyle, being overweight, aging and poor eating habits. The prevalence of diabetes is increasing exponentially as average lifespan is increasing. With 116 million individuals suffering diabetes, China has the largest number of diabetes cases in the world. China is followed by India (77 million people) and the United States (31 million people) according to the International Diabetes Federation (IDF, 2019). The IDF's 2020 statement predicts that, globally, by 2045, approximately 700 million people will have developed diabetes [60]. Several other medical complications arise due to diabetes, including cardiovascular disease, diabetic eye disease, nerve damage, and kidney failure.

Diabetic eye disease (DED), one of the products of neglected and untreated diabetes, which can cause permanent vision loss. It is observed that the leading cause of vision impairment and blindness in the working-age class is DED. DED is comprised of diabetic retinopathy (DR), diabetic macular edema (DME), glaucoma (Gl), and cataract (ca) [25,40,58,97,101,126]. The symptoms of DED can be seen in different parts of the human eye's retina. These include the irregular development and rupture of the blood vessels, degradation of the lens, breakage of the optic nerve due to intraocular pressure, and formation of hard exudates

near the macula region causing swelling in the macula. Owing to its increased worldwide incidence, DR has been listed as a chronic eye disease by the World Health Organization (WHO). It is observed that the risk of DED is linked to glycemic regulation, the presence of arterial hypertension and the duration of the disease; with type 1 diabetes being the greatest risk. After a decade of type 2 diabetes, DED impacts approximately 80 % of sufferers [112]. Some extremely effective DED treatments have been developed. These include corticosteroids, laser photocoagulation, and the intravitreal injection of anti-vascular endothelial growth factor (VEGF) agents. However, the efficacy of these approaches in preventing vision loss is dependent on early DED diagnosis. In particular, in the preliminary stage, individuals experience no symptoms. That is why screening for DED in diabetic patients is highly recommended worldwide, as illustrated in international and regional guidelines [224].

Detecting these anatomical changes with fundus photography has a number of challenges. First, the continuous expansion of the patient's medical information, such as fundus images, creates ongoing challenges for examination, diagnosis and treatment. Manual extraction of features from a large volume of fundus images and subsequent diagnosis result in a loss of time between detection and treatment. Ophthalmologists often take days to study normal images. Ophthalmologists also take days to review DED disease images [181]. A further downside of an ophthalmologists' manual fundus retinal image analysis and DED evaluation is that they may not always achieve accurate results as even the most excellent specialist and professional ophthalmologist may not track tiny changes in eye anatomy. An automated DED diagnosis system that classifies and identifies DED lesions in less computational time would provide early treatment and prevent vision loss. Therefore, automated DED detection

techniques are necessary to address this problem.

Second, over the last few decades, efforts have been made to develop robust computer-based DED analytics systems using image processing methods and machine learning approaches [41, 168, 214]. Convolutional Neural Networks (CNN) have been analyzed extensively for DED detection, and mostly outperform previous image recognition methodologies. Overall, deep learning has demonstrated tremendous potential in the health care domain, enabling identifying patients likely to develop a disease in the future. The test accuracy of binary classification (healthy and severe DED) using deep learning has achieved highest accuracies. While, healthy and mild-DED (i.e., early stage) binary classification, as well as multi-class (mild, moderate, and severe) classification from colour fundus images, is still an open challenge [109, 150].

Third, DED image analysis aims to map images to class labels, especially in image classification tasks. DED images are considered input labels from which pixels are derived and characterized as feature maps or feature vectors. Output labels are defined as a probability distribution containing either a multi-class or binary problem with a probability value. Identifying a feature space that can effectively and appropriately differentiate feature maps from a probability distribution of feature vectors is one of the key problems in developing a robust image classification model. This can be done by selecting features or extraction techniques, and several reports have been produced on the adoption of CNN models to illustrate DED detection [38, 143, 234]. According to Abramoff's research team's latest findings, this learning technique showed good performance in terms of automatic DR classification compare to existing methods [3]. A promising advanced deep learning approach for diagnosing DR was intro-

duced by the Google research team [75]. How to build a robust model for DED detection is, however, a problem that remains unsolved.

Finally, our research focuses on exploring the research gaps in developing an early DED (healthy and mild-DED) and multi-class DED classification system based on deep learning, and designing a framework. From our literature review, it is noted that no prior studies address both the mild classification and detection of DED, (diabetic retinopathy, glaucoma, diabetic macular edema, and cataract) in a single system. Several research studies [9, 38, 77, 122, 135, 152, 153, 166, 223, 241, 249] have aimed to classify the stages of DR, i.e normal to severe. In our research study, we aimed to develop a binary and categorical classification system for all DED. Mild DED identification with one system is an essential. Identifying the lesions in a specific area or region of eye anatomy can provide specific treatment for the eye's most affected target region.

1.2 Research Problems

Deep Neural Network models use advanced mathematical activity to process pixel values in the image [150] where training is performed with diverse examples integrated into the network, as opposed to the solid rule-based programming underlying traditional methodologies [65]. CNN have been thoroughly explored in the imaging domain [6, 38, 122, 153, 163, 223], surpassing previous methodologies, namely the recognition of images [223]. Neural networks seek to learn the profound features to identify the sophisticated dimension of mild DED images [153]. Deep learning consistently offers high performance in severe DED cases. At the same time, mild and multi-class detection of DED remains a

challenge. Our study questions have been formulated to address this challenge:

Research Question 1: What deep learning approaches provide the highest accuracy for the classification of mild and multi-class DED features, and how can they be further enhanced?

Automated disease detection systems have become an essential solution over the past decade; reducing the workload of manual detection and providing a cost-effective method. The initial challenge in designing an automated system can be insufficient image data and pre-processing images to identify vital medical features (e.g., Mild DEDs) to develop early treatment solutions. For severe cases, a state-of-the-art system with high performance precision has been developed; mild cases remain a challenge. Therefore, the state-of-the-art pre-trained deep learning models will be built and tested against themselves and the conventional image processing algorithms. The most sophisticated methods (i.e. fine-tune, optimizer and selection of hyper-parameters) will be implemented to enhance performance. After that, we will introduce a robust deep learning model to evaluate against supervised transfer learning's efficacy on the classification of DED fundus images. Question 2, therefore, focuses on conventional image processing algorithms to enhance the image quality and evaluates a deep learning system's performance improvement. Consequently, Question 3 focuses on the specification, evaluation and enhancement of the state-of-the-art methods and building a new model in DED detection. Ultimately, the developed method, to validate the effectiveness of the proposed methods, will be deployed in medical condition.

Research Question 2: How the quality and quantity of the retinal fundus' images influence the deep learning techniques' precision?

For the classification system to serve its purpose, an appropriately pre-processed image is required. Publicly available datasets are limited, and the quality of the datasets differs significantly. For instance, Messidor ¹, despite its relatively small scale, is considered a high fidelity source with reliable labelling, while Kaggle ² includes a large number of noisy and often miss-annotated images. The raw Kaggle data more closely reflects a real-world scenario where images are taken under different conditions, resulting in various quality levels. The challenge lies in the possible eye lesions detection despite the observed noisiness of the data set.

Research Question 3: How to develop the robust, deep learning models with fundus retinal images?

After recognizing the image's enhanced pathological features and predicted outputs, the next question is how to automatically conduct the classification task to obtain human-like precision in DED classification. The manual methods of diagnosis are limited given the worldwide increase in the prevalence of diabetes and its retinal complications [71]. Thus, an automated detection system is required. To solve our first research question, we investigate various transfer learning methods with different hyper-parameters and build a new CNN-based model. To produce a robust and more precise network, we introduced a model trained with segmented images. Previous studies showed that image segmentation is the most critical aspect of image processing. The ophthalmologist's manual segmentation of retinal fundus images is a tedious and time-consuming operation. It is not very precise, especially with the increasing modalities of retinal imaging and the unmanageable amount of retinal images

¹<https://www.adcis.net/en/third-party/messidor/>

²<https://www.kaggle.com/c/diabetic-retinopathy-detection>

that must be examined. Therefore, it is vital to evaluate current image segmentation methodologies using automated algorithms that are precise and involve as little human intervention as possible, particularly for retinal fundus images. Finally, the most sophisticated conventional feature segmentation methods are integrated with deep learning to provide a robust system.

1.3 Hypotheses

The following hypotheses are developed to answer the aforementioned research questions:

1. Deep Learning models can accurately (accuracy > 90%) diagnose mild DED from the publicly available raw datasets and outperform the conventional classifiers.
2. The development of a deep Learning model trained on segmented features (region of interest) of large image datasets can further enhance classification performance and accuracy.
3. Developing a new CNN with combined advanced methods of traditional image preprocessing techniques can solve mild and multi-class image-classification problems.

1.4 Contributions and Significance

This section begins by discussing the scientific contribution that this work seeks to achieve by identifying gaps in current techniques used to detect early DED

using medical images, and describing its practical benefits. Despite the increasing popularity of automated disease detection systems using medical images, research related to the early mild DED domain is limited. This research proposes a high performing system (accuracy >90 percent). It validates a deep learning-based system to automatically classify retinal fundus images to improve the effectiveness of early and multi-class DED classification and detection for timely treatment.

This thesis aims to construct an automated classifier with a effective DED classification using DL-based techniques. The classification model should verify classification accuracy coefficients (close to or outperform than human performance) and provide healthcare professionals with detailed information about the essential aspects taken into consideration by the model to reach each specific end. Deep learning models utilize black-box inference systems to work. They can achieve high analytical trust when educated correctly, but they do not offer reasons behind each action. It is important to understand the reasons behind a diagnosis in medical imaging since part of the localized abnormalities may be linked to some treatment of the correlative elements of the DED. Therefore, our DED disease detection goal is to assist with the lesion location process, tracing subsequent abnormality changes to aid in surgery or other treatments. The thesis contribution is presented in Fig.1.1. Corresponding to the study goals, the primary anticipated contributions of this research can be outlined in the following:

Development and evaluation of data-driven deep learning classifier as a novel diagnostic method for automatic DED detection.

Most importantly, a comprehensive literature review was performed to

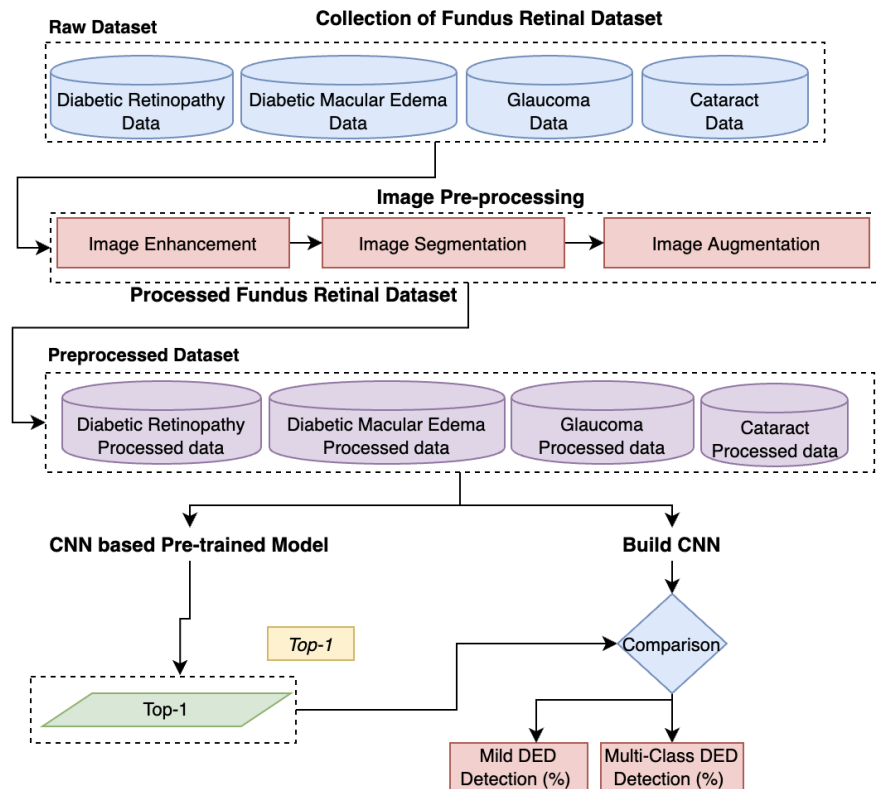


Figure 1.1: Overall thesis contribution.

achieve the research objective. From a theoretical point of view, we focus on knowledge-based learning, employing transfer learning to DED images. After that, we suggest a new conceptual structure to identify the findings to that guide our research directions. This review covers different research gaps found in previous studies on DED detection. Thorough research is essential to study the research gap and provide the solutions to develop a more robust deep neural network for early DED detection. Therefore, this thesis focuses on designing automated classification algorithms based on deep neural networks capable of achieving high performance levels like those achieved by ophthalmologists. It is observed that the quality and quantity of the dataset have a considerable impact on the development of robust models. Therefore, to reflect the real-life scenarios, our models were trained with retinal fundus images. Publicly available

images consist of low fidelity data, as they were taken with a variety of fundus cameras leading to considerable variation in image quality, size and shape. An intensive search was performed to collect data suitable for this research. After data collection, various image processing algorithms were introduced to enhance the quality and quantity of the images. Finally, this research integrates the traditional image processing and image segmentation methods with deep learning to achieve high accuracy.

Study of the effectiveness of traditional image processing algorithms in deep learning performance.

Gradual progressions in deep learning and appliance competence advancements, including computational power, storage capacity, and energy use, enhance the efficiency and cost-effectiveness of further speeding up vision-based applications. Compared to conventional image processing techniques, deep learning allows computer vision designers to obtain high precision in image analysis, image classification, image recognition tasks, and concurrent mapping and localization. However, image processing outcomes using DL are based on image resolution. Achieving an acceptable output in lesion detection involves high-resolution images – with the subsequent rise in the quantity of data needing to be analyzed, preserved, and distributed. Image resolution is extremely important for applications used to identify and analyze tiny lesions in the medical images, e.g., swelling in the blood vessels. Image size reduction techniques, edge detection techniques, data augmentation, and the identification of a region of interest are all useful for image resolution and reduce the time and data required for training. Therefore, image pre-processing before training deep learning is considered crucial for classification performance enhancement. The fun-

dus images available to the public consist of low fidelity data, and the fundus images were taken with different fundus cameras, which causes variability in quality which can be observed in Fig 1.2. Thus, the following steps are used to enhance the quality of the dataset.



Figure 1.2: Examples of a publicly available data set (Kaggle Data). (A) Under exposure fundus image; (B) Over exposure fundus image; (C) Unrelated artifacts and (D) Blurriness.

1. **Image Enhancement:** Retinal image pre-processing is considered a crucial step due to its ability to enhance the visual aspect of an image for improved classification performance. The following is a brief description of the pre-processing techniques, adopted in our research. Green Channel Extraction [237] is employed to extract the green band from the RGB of an image. The green channel of an image provides more insight into the relevant information from an image. Contrast enhancement based on CLAHE (Contrast Limited Adaptive Histogram Equalization) [251] is used in our research to enhance the contrast of the images. An example before and after CLAHE application to fundus images is presented in Fig 1.3. After contrast enhancement, illumination correction is applied to increase the brightness and luminance of the images. Finally, the noise is removed to smooth out an image using Gaussian filtering.
2. **Image Augmentation:** Another issue that needs to be addressed is the annotated data limitations. In order to train a deep learning architecture, a

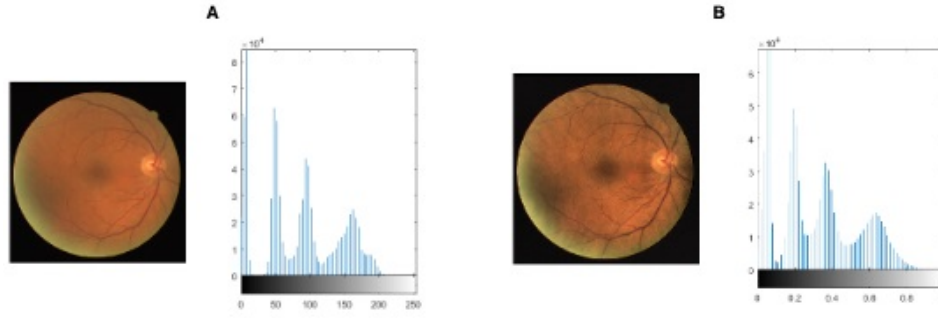


Figure 1.3: Contrast Limited Adaptive Histogram Equalization enhances contrast in an image: A. Before and B. After CLAHE application.

large set of data is required. If the training sample size is insufficient, the model can easily overfit the data resulting in poor classification performance on unseen fundus images. This problem can be solved by applying data augmentation methods such as cropping, rotating and mirroring. Data augmentation can also be used to solve the imbalanced data problem. Another method used to increase the data set volume is combining labelled data from different sources to increase the data set's volume. For example, the number of normal-labelled Kaggle image set K_0 images can be combined with the number of normal-labelled Messidor image set M_0 (Equation 1.1). Similarly, the number of mild-labelled Kaggle image set K_1 can be combined with the number of mild-labelled Messidor image set M_1 (Equation 1.2).

$$K_0 \cup M_0 = x : \forall x \in K_0 \quad or \quad \forall x \in M_0 \quad (1.1)$$

$$K_1 \cup M_1 = x : \forall x \in K_1 \quad or \quad \forall x \in M_1 \quad (1.2)$$

Hence, we can input $K_0 \cup M_0$ and $K_1 \cup M_1$ number of images into our model while training to increase the performance accuracy.

3. Image Segmentation This thesis adopts the image segmentation algo-

rithms to segment various parts of fundus images with lesions. For instance, blood vessels are segmented to detect early signs of DR, and the optic disc is segmented for identifying Gl, and macular edema for detecting exudates for diabetic macular edema. This study is intended to examine whether particular regions may help predict DED correctly, which means identifying the right region in retinal fundus images to improve the predictive capacity of DED classification models.

Design of automated DED classifiers based on ensemble traditional image processing and deep learning to improve performance accuracy.

Distorted, blurred, overexposed and underexposed fundus images have always been the issue in the publicly available datasets. Several efforts have been made to address this issue when building a robust deep learning model. One of them is the fine-tuning of the neural network, which has been the subject of studies [246,248] to create a noise-robust deep learning model, and authors like [52] proposed the improvement of the neural network model's architecture by adding a new module for image processing ahead of the neural processing model network. Therefore, in this study, we concentrate on traditional image preprocessing methods to enhance real-world images captured using various fundus image capturing devices. In this thesis, we will demonstrate that the traditional techniques of image processing can improve the neural network model's performance. Since there are very deep layers in the most current neural network models and have different filters that can derive the image's different spatial properties, in this case, conventional denoising filters on a deep neural network may not work correctly. Therefore, we employ three traditional image pre-processing methods to prepare the dataset before training the neural

network.

Experimental analysis of knowledge transfer and optimization techniques for binary and multi-class DED classification models.

Knowledge transfer or transfer learning has been employed for identifying mild and multi-class retinal disease classification, but has not shown promising results as addressed by authors [109], and [42]. In this thesis, we introduced 13 pre-trained architectures with a combination of *seven* different optimizers to evaluate the efficiency of transfer learning in DED classification. Prior research shows transfer learning is not suitable for detecting subtle abnormalities in medical images as they were initially developed for generic image identification, such as images of animals, foods, cars, etc. The concept uses information gained on primary tasks and its reuse to secondary tasks is shown in Figure 1.4. Transfer learning is beneficial in deep learning applications that involve a large amount of data and considerable computing resources.

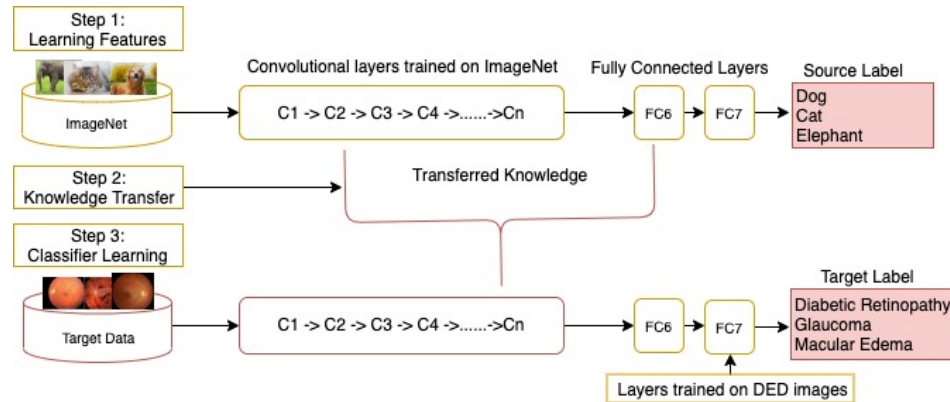


Figure 1.4: Learning features and knowledge transferred using Convolutional Neural Network for detection of DED.

As part of this analysis, following the transfer learning principle, the state-of-the-art CNN models were pre-trained on the broad public image repository. The top layers of the neural networks were trained for personalized binary and

multi-class classification from publicly accessible fundus image corpora using the weights initialized. Unlike existing methods, the research performed in this study focuses solely on instances of early DED and multi-class DED - currently challenging to classify. First, based on the comprehensive experiments performed using 13 pre-trained models, namely: *VGG16*, *VGG19*, *ResNet50*, *Inception V3*, *InceptionResNet V2*, *Xception*, *MobileNET*, *MobileNET V2*, *DenseNet 121*, *DenseNet 169*, *DenseNet 201*, *NASNetMobile*, and *NASNetLarge*, with fine-tuning, and 7 optimizer selection, the highest performing pre-trained CNN model (transfer learning) is chosen. Second, the number of efficiency enhancements, including data increase and contrast adjustment, is evaluated. Third, the most compelling scenario (in terms of accuracy achieved) is chosen to promote the creation of an accessible and efficient fully automated deep learning system in order to improve accessibility to mass screening services for at-risk populations. The concept of knowledge transfer from source task to target task can be useful in limited training data. We conclude that the results of this research will contribute to the increasing body of literature in knowledge transfer systems on DED images.

Design of the new convolutional neural network model to learn the DED features from fundus images to achieve highest accuracy.

Another option is to develop and train the CNN model entirely from scratch, without reliance on the pre-trained architectures adopted from transfer learning. This approach necessitates a large number of annotated data which can also be generated through appropriate augmentation techniques, e.g. mirroring and rotating. To increase the performance of the classifier one can increase the computational power by increasing the size of the network. Still, an extensive

evaluation has to be conducted to provide empirical validation for their practical use due to the increased computational resources required for new CNN network development.

1.5 Thesis Outline

The rest of the thesis is organized as follows:

Chapter 2 summarizes the previous research on the broader prevalence of DED and the impacts of the multiple detection approaches undertaken by different researchers and reviews on the role of image processing in developing robust automated detection systems. This study addresses the different types and sources of data required to quantify DED, and the impacts are summarised briefly with other quantitative studies using DED data.

Chapter 3 presents an approach for “Early DR classification and detection” using retinal fundus images. First, retinal fundus images are collected from a publicly available source which is labelled by a qualified ophthalmologist. Data are labelled as either “Normal” or “Mild DR” for binary classification. Retinal features are enhanced from the raw images for training. Deep learning models are adopted as state-of-the-art classification approaches. The performance of the proposed techniques is measured against the 13 different deep learning architecture with *seven* different optimizers to extract and detect of the features. Furthermore, the most informative and distinctive features between “Normal” and “Mild DR” posts are highlighted for valuable insight into the DED detection problem.

Chapter 4 proposes the various image pre-processing algorithms involved in automated DED detection systems for accuracy enhancement, integration with the state-of-the-art deep learning and transfer learning techniques, and performance evaluation in DED content classification tasks. Next is the development of the new CNN and trained with pre-processed images.

Chapter 5 introduces a method for the diagnosis of “Multi-class classification of Diabetic Eye disease”, offering insight into irreversible DED conditions. In this study, we trained the *three* state-of-the-art deep learning models. The accuracy and precision achieved are contrasted for the top *three* deep learning architectures. The image pre-processing for a region of interest is applied during model training for a further feature extraction phase to validate the models’ effectiveness in improving classification efficiency.

Chapter 6 proposes the system for “automatic classification and detection of multi-class DED using newly built CNN” from the available online dataset. The data is collected from an open source, annotated by ophthalmologists and were divided into five categories, as per the procedure explained in Chapter 4. The experiment is conducted with the newly built CNN to study its performance accuracy and validate it against other models’ in Chapter 5 performances. The image enhancement techniques are used for better feature extraction. Finally, the automated classification of the DED system is developed using the newly built CNN.

Chapter 7 summaries the results and evaluates the results obtained from the combined framework and indicates directions for future improvements.

CHAPTER 2

LITERATURE REVIEW

This chapter describes the DED background, its occurrence and severity, its high prevalence and observed effects, and finally, the different automated strategies for classification, detection, and prediction. People suffering from diabetes are at high risk of developing various eye diseases over time. As a result of advances in machine learning techniques, early detection of diabetic eye disease using an automated system brings substantial benefits over manual detection. A variety of advanced studies relating to the detection of diabetic eye disease have recently been published. This chapter presents a systematic survey of automated approaches to diabetic eye disease detection from several aspects, namely: i) available datasets, ii) image preprocessing techniques, iii) deep learning models and iv) performance evaluation metrics. The survey provides a comprehensive synopsis of diabetic eye disease detection approaches, including state of the art field approaches, which aim to provide valuable insight into research communities, healthcare professionals and patients with diabetes.

2.1 Prevalence and Types of Diabetic Eye Disease

DED comprises a group of eye conditions, which include Diabetic Retinopathy, Diabetic Macular Edema, Glaucoma and Cataract [89]. All types of DED have the potential to cause severe vision loss and blindness in patients from 20 to 74 years of age. According to the International Diabetes Federation (IDF) statement, about 425 million citizens worldwide suffered from diabetes in 2017. By 2045, this is forecast to increase to 692 million [59]. Medical, social and economic complications of diabetes impact substantially on public health, with diabetes

being the world's fourth-largest cause of death [202]. The effects of diabetes can be observed in different parts of a person's body, including the retina. Fig. 2.1 shows the normal anatomical structures of the retina. Fig. 2.2 illustrates a complication of DED in a retina. Serious DED begins with an irregular development of blood vessels, damage of the optic nerve and the formation of hard exudates in the macula region. Four types of DED threaten eye vision, and they are briefly described in the following subsection.

2.1.1 Diabetic retinopathy

DR is caused by damage to blood vessels of the light sensitive tissue (retina) at the back of the eye. The retina is responsible for sensing light and sending a signal to brain. The brain decodes those signals to see the objects around [104]. There are two stages of DR: early DR and advanced DR. In early DR, new blood vessels do not developing (proliferating) and this is generally known as non-proliferative diabetic retinopathy (NPDR). The walls of the blood vessels inside the retina weaken due to NPDR. Narrower bulges (microaneurysms) protrude from the narrower vessel surfaces, often dripping fluid and blood into the eye. Large retinal vessels also start dilating and become irregular in diameter. As more blood vessels become blocked, NPDR progresses from mild to severe. Depending on the severity, the retina's nerve fibres may begin to swell. The central part of the retina (macula) often swells (macular edema); a disease requiring treatment. NPDR is divided into three stages, namely: mild, moderate and severe [74]. Advanced DR is called proliferative diabetic retinopathy (PDR). In this case, the damaged blood vessels leak the transparent jelly-like fluid that fills the centre of the eye (vitreous) causing the development of abnormal blood ves-

sels in the retina. Pressure can build up in the eyeball because the newly grown blood vessels interrupt the normal flow of the fluid. This can damage the optic nerve that carries images from the eye to the brain, leading to glaucoma.

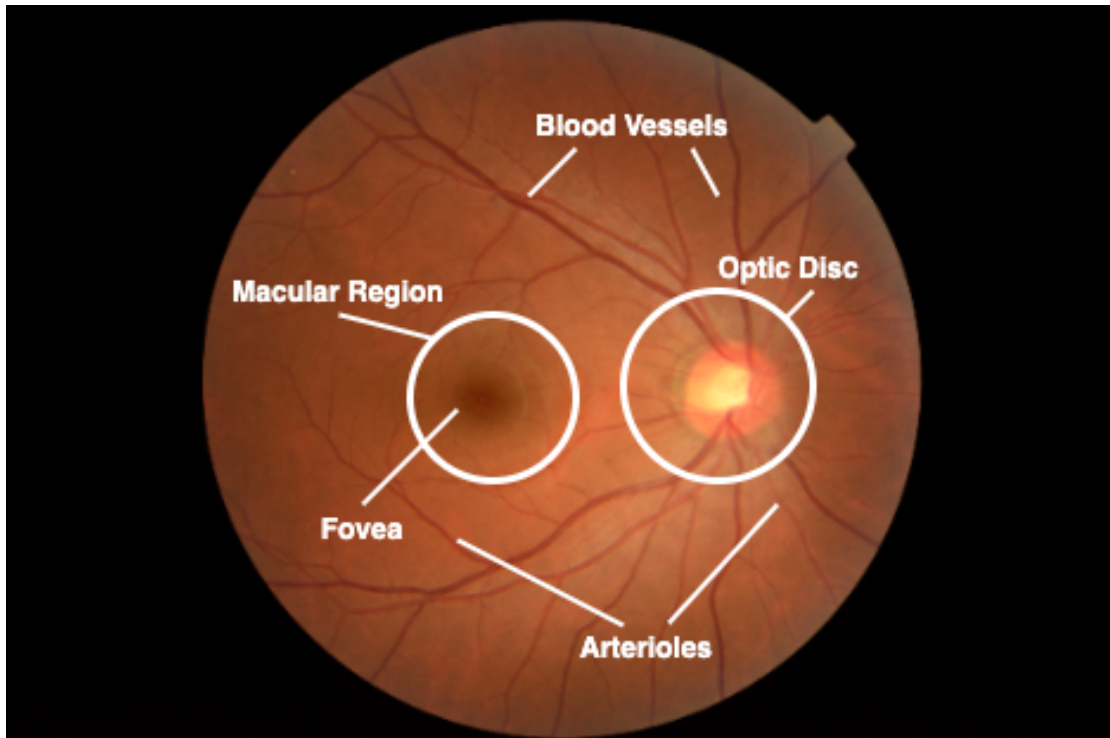


Figure 2.1: Anatomical structures of the retina.

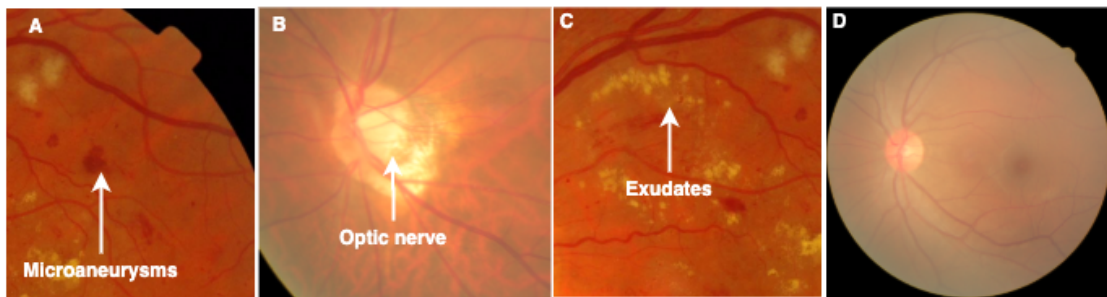


Figure 2.2: Complications of DED in retina; A. Microaneurysms, narrow bulges (Diabetic Retinopathy), B. Optic nerve damage (Glaucoma), C. Exudates with retinal thickening (Diabetic Macular Edema), D. Degeneration of lens (Cataract).

2.1.2 Diabetic Macular Edema

Diabetic Macular Edema (DME) occurs when fluid builds up in the centre of the retina (macula) due to damage to the blood vessels. The macula is responsible for sharp, straight-ahead vision. Fluid buildup causes swelling and thickening of the macula which distorts vision [104]. The stages of DME can be categorized into mild, moderate and severe based on the following points [76]:

- Retinal thickening of the fovea at or below $500\ \mu$ or $1/3$ of its disc diameter;
- Hard exudates, with subsequent retinal thickening, at or within $500\ \mu$ of the fovea;
- Retinal thickening at a size that is greater than one disc diameter ($1500\ \mu$), and which is within one fovea disc diameter.

2.1.3 Glaucoma

Glaucoma (Gl) is an ocular disease that damages the optic nerve that links the eye to the brain. When the fluid pressure inside the eye, known as intraocular pressure (IOP), is high, the optic nerve is impaired [217]. An increase in blood sugar doubles the chances of Gl, which leads to blindness and a loss of vision if not detected early. Gl can be classified into three types based on the size of the enlarged optic nerve head or optic disc and Cup-to-Disc Ratio (CDR), or cupping. The stages of Gl are mild, moderate and severe [12].

2.1.4 Cataract

Cataract (Ca) is the degeneration of the lens protein due to high sugar level causing blurry lens growth, which in turn leads to blurred vision. Diabetic people are more prone to growing cloudy lenses and developing Ca earlier than non-diabetic people. Usually Ca is graded into four classes: non-cataractous, mild, moderate and severe [242].

Patients suffering from diabetes display a significantly higher predisposition to develop DED. As a consequence, early detection of DED has become paramount in preventing vision loss in adults and children. Studies have already shown that 90% of patients with diabetes can avoid DED development through early detection [218]. Manual detection of DED involves no computer assistance, resulting in longer waiting times between early diagnosis and treatment. Moreover, the initial signs of DED are so minute that even an expert may struggle with its identification.

Advancements in Artificial Intelligence (AI) offer many advantages to automated DED detection over the manual approach. They include a reduction in human error, time-efficiency and detection of minute abnormalities with greater ease. Automated DED detection systems can be assembled through joint image processing techniques using either Machine Learning (ML) or Deep Learning techniques (DL). In DL approaches, images with DED and without DED are collected. Then, the image preprocessing techniques are applied to reduce noise from the images and prepare for the feature extraction process. The pre-processed images are input to DL architecture for the automatic extraction of features and their associated weights to learn the classification rules. The features weights are optimized recursively to ensure the best classification results.

Finally, the optimized weights are tested on an unseen set of images. This type of architecture demands a large number of images for training. Therefore, a limited number of images can severely restrict its performance.

DL techniques require a substantial amount of computational memory and power. Normally, to develop and evaluate the classification model, DL architecture requires a Graphical Processing Unit (GPU). In real world DL applications, this assumption does not always hold. Training images using the DL model can be costly, challenging in terms of *annotated* data collection, and time and power consuming. To account for the above mentioned shortcomings, the approach called Transfer Learning (TL), or Knowledge Transfer (KT), has been introduced by the researchers. In TL, previously derived knowledge (e.g. in terms of features extracted) can be re-adapted to solve new problems. Not only does TL drastically reduce the training time, it also reduces the need for a large amounts of data. The latter point proves particularly convenient in niche applications where high-quality input images annotated by specialists are often limited or expensive to obtain.

Motivation: As mentioned above, DL and TL techniques have their advantages and disadvantages however, several researchers have used these methods to build automatic DED detection systems in recent years. Overall, there are very few review studies published in academic databases which simultaneously address all of the types of DED detection. Thus, this literature review is essential to collate the work in the DED detection field.

Ting et al. [210] published a review article focusing on eye conditions such as diabetic retinopathy, glaucoma, and age-related macular diseases. They selected papers published between 2016 and 2018 and summarised them in their report.

They summarized those papers which used fundus and optical coherence tomography images, and TL methods. Their research did not include current (2019-2020) publications that incorporated TL methods into their approach, and they omitted the identification of eye cataract disease from their study scope. Similarly, Hogarty et al. [85] provided a review of current state articles using AI in Ophthalmology, but their focus lacked comprehensive AI methodologies. Mookiah et al. [125], reviewed computer aided DR detection studies, which are largely DR lesion based. Another author, Ishtiaq et al. [91], reviewed comprehensive DR detection methods from 2013 to 2018 but their review lacked studies from 2019 to 2020. Hagiwara et al. [77], reviewed an article for the computer aided diagnosis of Gl using fundus images. They addressed computer aided systems and systems focused on optical disc segmentation. There are a variety of studies using DL and TL methods for Gl detection that have not discussed in their review paper. It is, therefore, important to review papers that consider existing approaches to DED diagnostics. In fact, most scholars in their review article did not address the period of publication years covered by their studies. Current reviews were too narrow, either in terms of disease (DR, Gl, DME and Ca) or in aspects of methodology (DL and ML). Therefore, to address the limitations of the above-mentioned studies, this chapter offers a thorough analysis of both DL and TL approaches to automated DED detection published between 2014 and 2020 to cover the current DR detection methods built through DL or TL based approaches.

Contribution: To provide a structured and comprehensive overview of the state of the art in DED detection systems using DL, the proposed chapter surveys the literature from the following perspectives:

1. *Datasets available for DED;*
2. *Preprocessing techniques applied to fundus images for DED detection;*
3. *DL approaches proposed for DED detection;*
4. *Performance measures for DED detection algorithm evaluation.*

Research Method: The overall research method followed is shown in Fig. 2.4. Initially, a keyword search was conducted using 10 academic databases considering our specific review target. Seven filters were applied to select the primary review target. Afterwards, the selected articles were critically analysed and grouped into three categories based on the following aspects, namely: (i) *papers employing TL*, (ii) *papers proposing a new DL network* and (iii) *papers discussing with DL and ML combined*.

Selection of Articles A systematic review of automated detection methods of various Diabetic Eye Diseases from databases including *IEEE Xplore, MedLine, Scopus, Science Direct, Springer, ACM Digital Library, PubMed, Web of Science and Google Scholar* was performed. The subsequent seven filters applied were: (i) *Target keywords*, (ii) *Publication year*, (iii) *Publication type*, (iv) *Duplicate check*, (v) *Article title, Abstract and Keyword screening for article selection*, (vi) *References of selected articles checked* and (vii) *Final quality assessment of selected article*. Review target keywords were searched using 'AND' Boolean operator and included: "*deep learning*", "*transfer learning*", "*image processing*", "*image classification*", "*fundus images*", "*diabetic eye disease*", "*diabetic retinal disease*", "*diabetic retinopathy*", "*glaucoma*", "*diabetic macular edema*" and "*cataract*".

Papers published between 2014 and 2020 were considered eligible for this study due to rapid advances in the field. We then narrowed our search to *Con-*

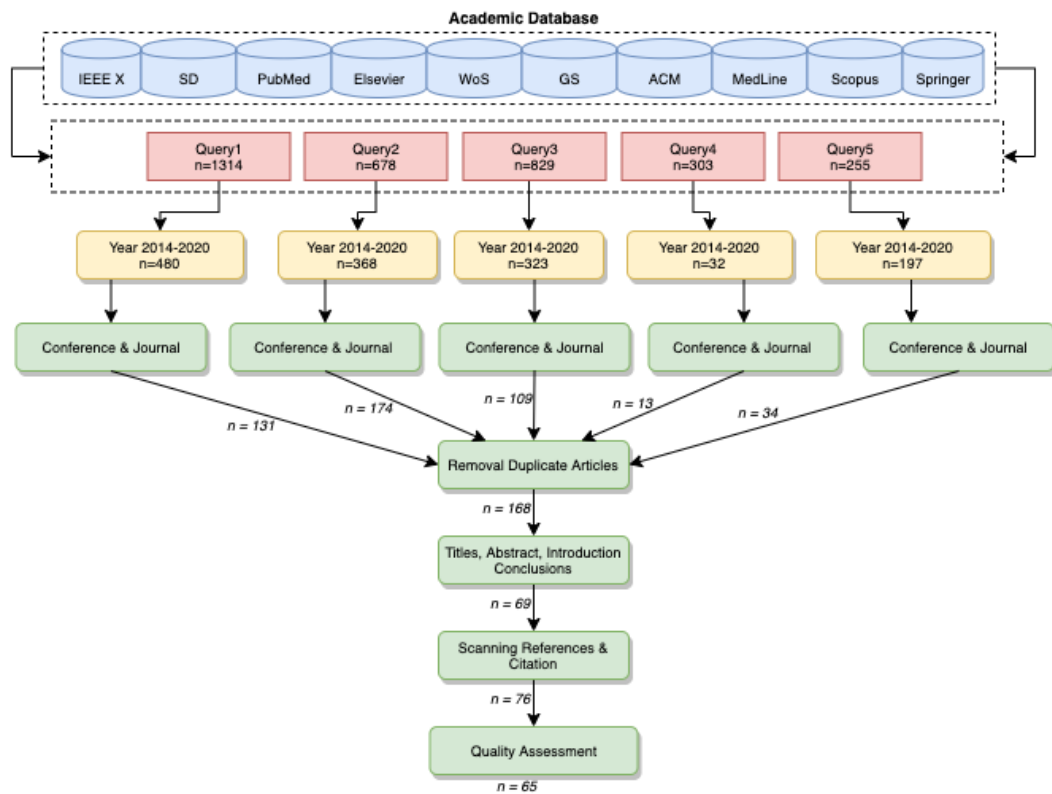


Figure 2.3: Search and filter results: A. Query1 (Q1) = *diabetic eye disease, fundus images, image processing, image classification, deep learning, transfer learning*; B. Query2 (Q2) = *diabetic retinopathy, fundus images, image processing, image classification, deep learning, transfer learning*; C. Query3 (Q3) = *glaucoma, fundus images, image processing, image classification, deep learning, transfer learning*; D. Query4 (Q4) = *diabetic macular edema, fundus images, image processing, image classification, deep learning, transfer learning*; E. Query5 (Q5) = *cataract, fundus images, image processing, image classification, deep learning, transfer learning*.



Figure 2.4: Research method flowchart.

ference Papers and *Journal Articles*. After the selection process, we encountered several duplicates as a result of using 10 different databases. After duplicates removal, titles, abstracts and conclusions of the remaining publications were carefully read. 69 articles were obtained focusing on fundus images, DL methods and classification of DED. We studied the bibliography and citation of the selected 69 articles, in which we found 7 more articles for the potential inclusion. Finally, during a quality assessment by reading 76 papers, our selection was narrowed down to 65 studies. The details of the process followed during our systematic review are presented in Fig. 2.3. We subsequently distributed the final sample of articles into three target groups. The distribution of 65 articles concerning the review target is represented in Table 2.1. The first group includes papers that use a pretrained network also referred to as the TL Approach. The second group categorizes articles that use their own built in DL network to detect DEDs. Finally, the third group summarises the articles that use combined DL and ML methods.

2.2 Diabetic Eye Disease Datasets

The authors of the selected articles use private and public datasets which are divided into training and testing examples. The most common datasets used for the detection of DR are Kaggle and Messidor [50]. Authors in [48, 55, 66, 68, 73, 75, 94, 114, 121, 147, 153, 157, 161, 172, 187, 215, 229, 232] used Kaggle data and [1, 14, 114, 116, 136, 212, 215] used Messidor [50] data. The Kaggle dataset consists of 88,702 images, of which 35,126 are used for training and 53,576 are used for testing. Messidor [50] is the most widely used dataset which consist 1,200 fundus images. The Kaggle and Messidor dataset, is labeled for DR stages.

Table 2.1: Selected articles for common objectives (review target).

Served purpose	DED	No. of Articles	References
<i>Employed TL</i>	DR	19	[3,42,73,75,78,102,114,116,117,121,128,144,157,161,172,203,209,212,215]
	Gl	15	[5,9,13,17,32,49,53,72,113,134,135,146,177,184]
	DME	3	[78,117,163]
	Ca	1	[152]
<i>Proposed New DL network</i>	DR	11	[48,55,66,68,83,94,147,153,229,232,240]
	Gl	5	[38,139,158,176,185]
	DME	3	[7,155,204]
	Ca	2	[54,242]
<i>DL combined with ML</i>	DR	3	[1,15,136]
	Gl	1	[8]
	DME		
	Ca	2	[160,231]

Legend: DL = Deep Learning, TL = Transfer Learning DED = Diabetic Eye Disease, DR = Diabetic Retinopathy, Gl = Glaucoma, DME = Diabetic Macular Edema, Ca = Cataract.

Table 2.2 describes the datasets included in the chosen articles, listed from the viewpoint of the individual DED analyzed; i.e. DR, Gl, DME, and Ca. The table contains the name of the DED, the name of the dataset, the summary of the particular dataset, the sources of the publications that used the dataset and finally, the path where the dataset can be retrieved (if accessible publicly)

2.2.1 Retinal Imaging for DED

Fundus Photography: Color Fundus images are a valuable method for scanning diabetic eye disease. Historically, fundus images were collected using film, but recently digital fundus images have been broadly adopted. Fundus photography is also important for evaluating DED improvement or development over

Table 2.2: Datasets available for automatic Diabetes Eye Detection with source (link).

DED	Dataset	Description	Reference	Link
DR	<i>Kaggle</i>	Dataset made available by EyePACS. It consists of 35,126 training images and 53,576 testing images (total of 88,702). These images are labelled with stages.	[48, 55, 66, 68, 73, 75, 94, 114, 121, 128, 147, 153, 157, 161, 172, 187, 215, 229, 232]	urlhttps://www.kaggle.com/c/diabetic-retinopathy-detection/data
	<i>Messidor</i>	Dataset consists of 1,200 fundus images. The images were obtained from three ophthalmological branches in France. Of the 1,200 images, 800 images are with pupil dilation, while 400 are without pupil dilation. Images are labelled with DR stages. Decenciere et al. [50]	[1, 14, 83, 114, 116, 136, 212, 215]	https://www.adcis.net/en/Download-Third-Party/Messidor.html
	<i>Messidor-2</i>	Dataset consists of 1,748 fundus images. Camera used was Topcon TRC NW6 non-mydiatic with 45 degrees field of view. Images are labelled with DR stages. Decenciere et al. [50].	[3]	urlhttp://www.latim.univ-brest.fr/indexfco.html
	<i>STARE</i>	Dataset consists of 400 fundus images. The images were taken with Topcon TRV-50 with 35 degrees field of view. Farnell et al. [57]	[42, 212]	http://www.cecac.clemson.edu/~ahoover/stare/
	<i>DR₁</i>	Dataset is presented by the Department of Ophthalmology, Federal University of Sao Paulo, Brazil and consists of 1,014 color fundus images (687 - normal, 327 - abnormal). Abnormal images are further split into 191 with red lesions, 245 with bright lesions and 109 with both red and bright lesions.	[114, 116]	http://www.recod.ic.unicamp.br/site/asdr
	<i>APTOS</i>	The APTOS 2019 repository incorporates 3662 fundus images classified into five levels (normal - 0, mild - 1, moderate - 2, extreme non-proliferative DR - 3, and proliferative DR - 4) as per the severity of DR labelled.	[102]	https://www.kaggle.com/c/aptos2019-blindness-detection/data
	<i>E-optha</i>	This dataset consists 47 images with exudates, 148 with microaneurysms and 268 images with no lesion.	[240]	http://www.adcis.net/en/third-party/e-optha/
	<i>DeepDR</i>	Dataset include 2696 images from 748 patients for classification of DR	[243]	https://isbi.deepdr.org/data.html
GI	<i>RIGA</i>	Dataset contains three different sources: 1) MESSIDOR (dataset consists of 460 original images marked manually by six different ophthalmologists (total of 3220 marked images); 2) Bin Rushed (dataset contains 195 original images marked by six different ophthalmologists (total of 1,365 images); 3) Magrabi Eye Center (dataset contains 95 original images marked by six different ophthalmologists (total of 665 images). Almazroa et al. [11]	[9]	https://deepblue.lib.umich.edu/data/concern/data_sets/3b591905z?locale=en
	<i>ORIGA</i>	A quantified objective benchmarking method was proposed, focusing on optic disc and cup segmentation and Cup-to-Disc Ratio (CDR). ORIGA(-light) contains 650 retinal images annotated by trained professionals from Singapore Eye Research Institute. A wide collection of image signs, critical for GI diagnosis were annotated Zhang et al. [244].	[38]	Publicly unavailable.
	<i>DrishTi-GS</i>	Dataset contains a total of 101 images. The images were divided into 51 testing and 50 training examples. The images were marked by four eye experts and collected from Aravind Eye Hospital. Sivaswamy et al. [190]	[135, 139]	http://cvit.iiit.ac.in/projects/mip/drishTi-gs/mip-Dataset2/Dataset_description.php
	<i>BIOMISA</i>	Dataset contains 462 images collected a local hospital. TopCon TRC 50EX camera was used. Hassan et al. [79].	[103]	http://biomisa.org/index.php/glaucoma-database/
	<i>REFUGE</i>	This dataset consist of 1200 color fundus images divided into 1:1:1 ratio for training, validation, and testing. [134]	[176]	http://ai.baidu.com/broad/download?dataset=gon
	<i>ODIR-2019</i>	This dataset consist of eight types of ocular disease, consisting of 207 training classes, 30 off-site testing cases, 58 on-site testing cases.	[92]	https://odir2019.grand-challenge.org/dataset/
	<i>DRIONS</i>	Dataset consists of 110 colour digital retinal images from Ophthalmology Service at Miguel Servet Hospital, Saragossa (Spain). Carmona et al. [30].	[1, 139]	http://www.ia.uned.es/~ejcarmona/DRIONS-DB.html
	<i>RIM-ONE (r1), RIM-ONE (r2), RIM-ONE (r3)</i>	Dataset details: (i) r1 40 GI and 118 Non-GI images, (ii) r2 200 GI and 225 Non-GI images and (iii) r3 74 GI and 85 Non-GI images. Fumero et al. [62]	[32, 139]	http://people.ee.ethz.ch/~cvlsegmentation/driu/downloads.html
<i>HRF</i>	Contains fundus images by patient condition containing 15 healthy, 15 DR, and 15 glaucoma.	[32]	https://www5.cs.fau.de/research/data/fundus-images/	
DME	<i>HEI-MED</i>	Dataset was obtained from Hamilton Eye Institute Macular Edema Data-set (HEI-MED). Dataset contains 169 fundus images to test and train for the detection of exudates and DME. Giancardo et al. [69].	[114]	https://github.com/lgiancaUTH/HEI-MED
	<i>IDRiD</i>	Dataset contains 516 images with both DME and DR cases. The severity of macular edema is based on the existence of hard exudates closer to fovea (macula center) region. This dataset contents 80 hard exudates images. Porwal et al. [151].	[123]	https://idridd.grand-challenge.org/Data/
	<i>DRiDB</i>	The retinal fundus databases including a description of all main anatomical structures including macula, blood vessels and optic disc is annotated. Prentavsic et al. [156].	[155]	https://ipg.fer.hr/ipg/resources/image_database
	<i>CLEOPATRA</i>	CLEOPATRA was a three phase randomised, parallel and single clinical experiment from fifteen ophthalmic centres in the United Kingdom. Sivaprasad et al. [189].	[204]	unavailable
	<i>Digifundus Ltd, Finland</i>	Dataset is non-open, anonymous retinal data-set of diabetic patients. Dataset contains 41,122 labelled retinal color fundus images from 14,624 patients. Sahlsten et al. [163].	[163]	Publicly unavailable.
Ca	<i>Beijing Tongren Hospital.</i>	Dataset is composed of 5,620 standard fundus images from Beijing Tongren Eye Center	[242]	Publicly unavailable.
	<i>Not Disclosed by Authors</i>	Study consists of 5,408 preprocessed images as experimental dataset. Dataset contains 1,948 noncataractous images: 1,268 slightly mild, 496 mild, 616 medium, 540 slightly severe and 540 severe images.	[160]	Publicly Unavailable.
	<i>Picture Archiving and Communication System (PACS)</i>	In this dataset each fundus image is manually graded by the ophthalmologist as non, mild, moderate, or severe cataract. There are 767 noncataractous, 246 mild, 128 moderate and 98 severe images (total of 1,239).	[231]	Publicly Unavailable.

Table 2.3: Image preprocessing techniques employed in selected studies.

GCE	HE	ROI	CLAHE	CE	Re	Au	GSC	BVS	IR	IC	GF	References
✓	✗	✓	✓	✗	✓	✓	✗	✗	✗	✗	✗	Li et al. [114]
✗	✗	✗	✗	✗	✓	✗	✗	✗	✗	✗	✗	X. Li et al. [116], Al-Bander et al. [7]
✓	✗	✗	✗	✗	✓	✓	✗	✗	✗	✓	✗	Zhang et al. [242]
✗	✗	✗	✗	✗	✗	✗	✗	✗	✗	✓	✗	Ran et al. [160]
✓	✓	✗	✗	✓	✓	✗	✗	✗	✗	✗	✗	Shaharum et al. [175]
✗	✗	✓	✗	✗	✗	✗	✗	✗	✗	✗	✗	Abbas et al. [1], Yu et al. [240], Diaz et al. [53], De et al. [49], Gomez et al. [72]
✓	✓	✗	✗	✗	✗	✗	✗	✗	✗	✗	✗	Yang et al. [231], Pratap et al. [152], Doshi et al. [55]
✗	✗	✗	✗	✗	✓	✗	✓	✗	✗	✗	✗	Sahlsten et al. [163]
✓	✓	✗	✗	✗	✓	✗	✗	✗	✗	✗	✗	Sisodia et al. [187]
✗	✗	✓	✗	✗	✗	✗	✗	✗	✗	✗	✗	Antal et al. [14]
✓	✗	✓	✗	✗	✗	✗	✗	✓	✗	✓	✗	Orlando et al. [136]
✗	✗	✓	✗	✗	✗	✗	✗	✗	✗	✗	✗	Almazroa et al. [11]
✗	✗	✓	✗	✗	✗	✓	✗	✗	✗	✗	✗	Chen et al. [38], Ceretinia et al. [32], Perdomo et al [144]
✗	✗	✓	✓	✗	✗	✗	✗	✗	✗	✗	✗	Orlando et al. [135]
✗	✗	✗	✗	✗	✓	✗	✗	✗	✓	✗	✗	Phan et al. [146]
✗	✓	✗	✗	✗	✓	✗	✓	✗	✓	✗	✗	Dong et al. [54]
✗	✗	✗	✗	✗	✗	✓	✗	✗	✗	✗	✗	Asaoka et al. [17], An et al. [13], Nguyen et al. [128], Xu et al. [229]
✗	✗	✓	✗	✗	✗	✗	✓	✗	✗	✗	✗	Pal et al. [139]
✗	✓	✗	✓	✗	✗	✗	✗	✗	✗	✗	✗	Hemanth et al. [83]
✗	✗	✗	✓	✓	✓	✗	✗	✗	✗	✗	✗	Gondal et al. [73]
✗	✗	✓	✗	✗	✓	✗	✗	✗	✗	✗	✓	Mansour et al. [121]
✗	✗	✗	✗	✗	✓	✓	✗	✗	✗	✗	✓	Quellec et al. [157]
✗	✗	✗	✗	✓	✓	✓	✗	✗	✗	✗	✓	Van et al. [215]
✓	✗	✗	✓	✓	✗	✗	✗	✗	✗	✓	✗	Umapathy et al. [212]
✗	✗	✗	✗	✗	✓	✗	✗	✗	✗	✗	✗	Diaz et al. [53]
✗	✗	✗	✗	✗	✓	✓	✗	✗	✗	✗	✗	Gargeya et al. [66], Ghosh et al. [68]
✗	✓	✗	✗	✗	✓	✗	✗	✗	✗	✗	✗	Jiang et al. [94]
✗	✗	✓	✓	✗	✓	✗	✗	✗	✗	✗	✗	Yang et al. [232]
✗	✓	✗	✗	✓	✗	✓	✗	✗	✗	✗	✗	Pires et al. [147]
✗	✗	✗	✓	✗	✗	✗	✗	✗	✗	✗	✗	Singh et al. [184]
✗	✗	✗	✗	✗	✗	✓	✗	✗	✗	✗	✗	Singh et al. [5]

time. There are various types of fundus images, such as: normal, wide-field, and stereoscopic. Digital fundus images allow an instant and straightforward analysis of images, transparent image enhancement, and the ability to manipulate and improve images effectively. Most of the studies used fundus image technology to develop DED detection system. Normal imaging of the macular fundus captures 30° of the eye's posterior pole, including the macula and the optic nerve. This type of digital photography benefits involve efficient and highly usable, which can be used for documentation assistance [164].

Fluorescein Angiography: Fluorescein Angiography (FA) is currently the gold standard for assessing the retinal blood vessels, the retina portion mostly suffering from diabetes, FA is useful in evaluating diabetic eye disease. A variety of possible side effects also arise with fluorescein angiography. Transient nausea, which occurs in about 2.9 percent of patients, and vomiting in 1.2 percent of patients, are the most common complications [108].

Optical Coherence Tomography: Optical coherence tomography (OCT) is an imaging method designed to measure, with microscopic precision, retinal morphology. OCT becomes more helpful in assessing and quantifying macular edema in diabetics, and it has become the most useful imaging method in the treatment of diabetic macular edema patients.

2.2.2 Dataset Characteristics

Most diabetic retinopathy datasets are collected at a particular device or at various websites using the same system, whereas others are acquired at a specific website or several sites with different devices. The tools used to capture an im-

age can be divided into two different groups, called uniform and non-uniform systems.

In uniform system and uniform site dataset, the data were acquired at a single location or hospital with the same unit. For example, Jichi Medical University Japan's exclusive dataset used by Takahashi, Tampo [203] contained 4709 images. These images were taken using a camera from the Fundus, i.e., AFC-230; May 2011 to June 2015: NIDEK Co., Ltd., Aichi, Japan.

The images in uniform system and non-uniform site dataset were collected on multiple sites using the same system. Antal and Hajdu [14], for example, used Messidor's data. This dataset includes 1200 images taken with the Topcon TRC NW6 non-mydratic colour video 3CCD camera by three ophthalmology departments in France.

The images in non-uniform system and uniform site datasets were collected on a single site with multiple cameras. There is no single research that comes under this category.

The images in non-uniform system and non-uniform site datasets were collected using multiple system at multiple sites. About half of the review papers selected in this thesis come under this category because of the single, distributed dataset or many datasets. The single dataset containing 298 images used [87], and it was collected at fifteen different locations, and ten various types of cameras were used. Similarly, the datasets used by Fraz, Jahangir [61], consisting of 4 publicly accessible datasets, were obtained at various locations and filmed, compared to each other, with multiple cameras. A number of studies were performed in datasets where the images were collected at a single location using

the same system. Six studies were designed on datasets in which the images were collected from the same system but at different locations or clinics. No study was performed in which the data were collected but at the same site or clinic with different equipment.

2.3 Image Preprocessing Techniques

Images are subjected to numerous image preprocessing steps for visualization enhancement. Once the images are brighter and clearer, a network can extract more salient and unique features. A brief description of the preprocessing techniques used by the researchers addressed in this section. Green channel on the RGB color space provides a better contrast when compared to the other channels. In most of the image preprocessing techniques, green channel extraction is employed. The green channel image produces more information than blue and red channels. For instance, Li et al. [114] extracted the green channel of the image for exudates detection, where the exudates reveal better contrast from the background.

2.3.1 Image Quality Enhancement

Another popular image preprocessing technique is contrast enhancement. The application of contrast enhancement further improves the contrast on a green channel image. To improve the contrast of the image, contrast enhancement is employed to the green channel of the image. For example, again Li et al. [114] have enhanced the contrast on the extracted green channel by employing

the Contrast Limited Adaptive Histogram Equalization (CLAHE) method. This enhances the visibility of exudates of a green channel image. Normally, after contrast enhancement, illumination correction is implemented to improve the luminance and brightness of the image. A noise removal filter like Gaussian Filtering is then applied to smooth out the image.

2.3.2 Image Augmentation

The resizing of an image is another popular method of image preprocessing. The image is scaled down to a low resolution image according to the appropriate system. Li et al. [114] resized their images with various sizes to the same pixel resolution of 512×512 . Similarly, X. Li [116] resized their image to 224×224 pixel resolution, for all the pretrained CNN models that used 224×224 size resolution images. The resolution of an image is resized into the resolution required by the network in use.

Researchers often have to eradicate and mask the blood vessels and optical discs so that they are not classified as wrong DED lesions. Many DED datasets consist of images with a black border, with researchers generally preferring to segment the meaningless black border to focus on the ROI. For example, Li et al. [114] removed the black border of fundus images using the thresholding method to further focus on the Region Of Interest (ROI).

Image augmentation is applied when there is an image imbalance (as typically observed in real world settings). Images are mirrored, rotated, resized and cropped to produce cases of the selected images for a class where the number of images is lower than the other large proportion of healthy retina images in

comparison with DED retina images. Augmentation is a common strategy for enhancing outcomes and preventing overfitting. It is observed that the distribution of the Kaggle dataset is uneven. The Kaggle dataset includes 35,126 fundus images annotated as No DR (25810), Mild DR (2443), Moderate DR(5292), Severe DR(873) and Proliferative DR(708). Thus, Li et al. [114], An et al. [13], Nguyen et al. [128], Xu et al. [229], Pires et al. [147], Gargeya et al. [66], Ghosh et al. [68], Van et al. [215], Quellec et al. [157] used the Kaggle dataset and the adopted augmentation technique to balance the dataset. Sometimes the RGB image is transformed into a greyscale image accompanied by further processing. Grayscale conversion is mostly used in approaches where ML is used.

Table 2.4: Different hyperparameters used in the selected studies.

R1	R2	R3	R4	R5	R6	References
VGG19	224 × 224	-	50	SGD	1e - 6	[42]
<i>o.o</i>	448 × 448	36	-	Adam	1e - 4	[157]
<i>o.o</i>	512 × 512	-	150	Adam	1e - 2	[73]
AlexNet	512 × 512	-	130	-	1e - 2	[114]
LeNet	48 × 48	64	30	-	1e - 2	[145]
OxfordNet	41 × 41	256	60	-	1e - 5	[215]
InceptionV4	779 × 779	-	-	-	-	[172]
VGG19, ResNet152	256 × 256, 512 × 512	-	-	-	-	[146]
DenseNet201						
VGG16	779 × 779	-	12	Adam, SGD	1e - 3, 1e - 4	[9]
ResNet	224 × 224	64	-	SGD	1e - 3	[17]
VGG16, VGG19	224 × 224, 299 × 299	8	100	SGD	1e - 4	[53]
ResNet50, Inceptionv3						
Xception						
OverFeat, VGG-S	231 × 231, 224 × 224	-	-	-	-	[135]
Standard CNN	231 × 231	64	50	SGD	1e - 4	[72]
VGG19, RESNET50	231 × 231	32	100; 80; 25	SGD	1e - 4	[72]
GoogLeNet, DENET						
InceptionV3	2095 × 2095	15	-	-	-	[163]
InceptionV3	224 × 224	-	14	Gradient Descent	1e - 5	[5]
CNN	224 × 224	-	600	-	1e - 2	[94]
CNN	512 × 512	15	300	Adam	3 × 1e - 4	[48]
CNN	128 × 128	-	250; 150; 70	Adam	1e - 3; 1e - 4, 1e - 5	[147]
CNN	64 × 64	-	20	Adam	1e - 5	[83]
CNN	256 × 256	-	100	-	1e - 2; 1e - 3; 1e - 4	[158]
CNN	256 × 256	15	200	Adam	1e - 5	[176]
CNN	512 × 512	15	200,250	SGD	3 × 1e - 4; 3 × 1e - 5	[7]
CNN	51 × 51	10	60	Adam	1e - 2	[204]

Legend: R1 = Model, R2 = Image Size, R3 = Mini Batch Size, R4 = Epoch, R5 = Optimizers, R6 = Initial Learning Rate.

2.3.3 Region of Interest based Segmentation

As it is called ROI extraction, the main objective of this phase is to retrieve the retinal anatomical structure of interest in order to minimise computational costs and boost overall performance; if a window is extracted around the raw retinal image's target anatomical structure area, then the pre-processing steps are applied to it. Each retinal anatomical structure has specific features and characteristics, so certain steps in pre-processing can be different.

2.4 Machine Learning in Diabetic Eye Disease Classification

The ML techniques employed for DED diagnosis are discussed in this section. For DED detection, the generic ML method is shown in Fig. 2.5. Firstly, labeled image data (training image dataset) for developing the DED detection model is gathered. The training collection consists of images belonging to various DED categories.

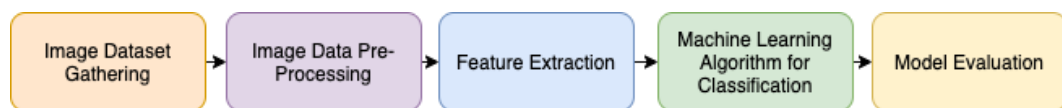


Figure 2.5: Classic Machine Learning Framework.

Afterward, to eliminate unwanted feature representations from the obtained image, multiple image preprocessing algorithms are employed. Later, different methods of extraction of features are used to discover the most discriminatory features from the preprocessed photos. The product of this step is the master feature vector (MFV). Upon understanding the classification rules from the MFV, this MFV is being given as an input to the ML model to create the DED

detection algorithm. The developed DR classification algorithm's efficiency is then tested on unseen unlabeled images (test image dataset). Therefore, in this section, we discuss the analysis of various feature and ML techniques used to develop and validate the DED detection algorithm on DED image datasets. The following subsections contain descriptions of these elements of the study.

2.4.1 Image Feature Analysis

A characteristic is a visible component of the overall operation that is under consideration in the areas of image classification and machine learning. In general, image processing and image segmentation in literature are well studied. For example, in [39], the researchers segmented images based on maximum feature coverage, while in [239], the authors explicitly suggested the Active Contour Model (ACM) for the image segmentation. Likewise, the researchers used region-based ACM for medical image segmentation in [238] via neighboring pixels' connection. Characteristics of DED may involve if the lesions (including blood vessel rupture, hard exudates, microaneurysms, soft exudates, haemorrhages, optic nerve damage) are present in the fundus image for diabetic retinopathy detection algorithms. A significant task is the choice of characteristics so that the network's learning becomes successful and precise. Independent scholars have reported and used various features in chosen research papers to detect DED. These characteristics comprise features based on structure and shape, features based on color, features based on strength, statistical features, and features based on texture. Also, as a single structure and shape-based function, the authors even integrated microaneurysm and haemorrhages [186]. A brief overview of these features is provided in the following paragraphs:

Feature based on Structure and Shape The structure and shape of different DED lesions, including haemorrhages, optic nerve damage, hard and soft exudates (yellow fluid), and microaneurysms, contain these characteristics. For example, perimeter and area, length axis, compactness, and circularity were the shape-based characteristics employed by Zhou et.al. [247] to detect microaneurysms.

Feature based on Color Here characteristics are based on the image's RGB colors. Jaya et al.[36] employed four color-based characteristics of color fundus images to identify hard exudates. Employing RGB color-space, they produced histograms. These would be the values of 'R' and 'G' normalized extraction of color-space luminosity and the channel 'Red-Green'.

Features with Intensity Intensity is the intensity of pixels represented in the planes of R, G, and B. For example, for identifying cotton-wool spots in DR pictures, Bui et al. [27] utilized features with intensity. Likewise, by measuring min and max pixels levels of intensity to identify soft and hard exudates, Joshi et al. [95] utilized intensity characteristics.

Statistical characteristics For statistical approaches of the pixels in diabetic eye disease images, statistical characteristics are being employed. Xiao et al. [227] employed statistical parameters and color characteristics to diagnose haemorrhages in fundus photographs. Mean, max, min, and deviation values were the statistical characteristics used.

Characteristics dependent on textures These characteristics provide valuable details about the texture of the photos of diabetic retinopathy. Many authors use color fundus image gray levels of intensity via GLCM (Gray Level

Co-occurrence Matrix). 4 GLCM-based characteristics, namely entropy, cluster hue, disparity, and similarity, have been used by Vanithamani et al. [216]. Likewise, GLCM was used to extract textural features by Nijalingappa et al. [129], including correlation, difference variance, energy, sum variance, homogeneity, entropy, sum entropy, contrast, sum average, difference entropy, an opposite period of variance.

The authors used distinct characteristics in machine learning techniques in the selected studies, namely appearance, color, strength, quantitative and texture-based characteristics. Statistical and shape-based features are the most commonly used combination of features. With this knowledge, we can infer that the most discriminatory features in DED detection algorithms are form, quantitative and texture-dependent characteristics that can yield impressive results for researchers in DED classification and detection based on machine learning.

2.4.2 Review of machine learning algorithms

The authors used various machine learning techniques to build the DED classification model in the selected primary studies about ML approaches. This segment is therefore committed to addressing the techniques of machine learning utilized in chosen research papers. Many of the researchers in previous work have utilized 11 discrete machine learning models, such as (RF) Random Forest, Support Vector Machine (SVM), k-Nearest Neighbor (kNN), Naive Bayes (NB), Local Linear Discrimination Analysis (LLDA), Decision Tree (DT), Artificial Neural Networks (ANN), Self-adaptive Resource Allocation Network (SRAN), AdaBoost (AB), Ensemble Classifiers and Unsupervised Classifiers (UC). The

following section discusses the specifics of these techniques.

Random Forest Algorithm: One of the most common and efficient classification algorithms for machine learning is RF. It produces forests with DT. More the number of trees, in general, the more stable the prediction is. Each tree provides a classification vote to identify a new model based on characteristics, and the design saved with the tree name. The forest determines the category with the most enormous amount of votes. In many other terms, the algorithm for RF classification is identical to the bagging strategy. In RF, a training set sub-set is generated for each sub-set a DT is developed. So all the DTs identify each input sequence for the test set, the forest eventually selects the one with the most votes. Xiao et al. [227] employed RF classifier in retinal fundus images for haemorrhage detection. They utilized the DIARETDB1 dataset, which contained 55 images and other 35 images from a unique dataset. They utilized 70 percent of the total images for the training of the machine learning framework, and the 30 percent images have been used for RF model for validation and categorization. Test results demonstrated good sensitivity by utilizing the RF algorithm.

Support Vector Machine Algorithm: A SVM is a machine learning algorithm that is used for classification purposes. It traces a distance measure (hyperplane) in the dataset close to the points located (support vectors). There have been two groups, A (+ve) and (-ve), describing the nearest distance to the extreme positives and negatives. The area that divides classes A (+ve) and (-ve) is generally referred to as the hyper-plane, in which part of the field comprises class A (+ve) while the other comprises class A (-ve).

For example, across several research [34, 127, 187, 197, 228], the researchers used SVM algorithms to identify various lesions of DED. Furthermore, using

the SVM, the authors have recorded better classification results. The efficiency of SVM, Scaled Conjugate Gradient Back Propagation Network and Generalized Regression Neural Network models for detecting and classification of exudates in retinopathy images was compared by Vanithamani et al. [216]. The researchers used the DIARETDB1 dataset containing 40 train images and 40 test images in the experimental setup. The experimental results showed that compared to Scaled Conjugate Gradient Back Propagation Network and Generalized Regression Neural Network algorithms, the SVM algorithm achieved better classification effectiveness. To identify hard exudates, Jaya et al. [93] employed a Fuzzy SVM algorithm using a complete dataset of diabetic retinopathy retinal fundus images obtained from various clinical imaging centers. The repository contains 200 eye retinal fundus images. Their machine learning network was trained on 75 images and checked on all 200 images.

As per the observational data, relative to conventional SVM, Fuzzy SVM had better discriminatory capacity. Two classification methods, specifically, DT and SVM, were used by Carrera et al. [] to classify diabetic retinopathy into four groups. They utilized a subset of 400 images of Messidor's dataset, and the results showed that SVM outperformed DT. A section of Messidor's dataset consisting of 370 images was also used by Mahendran et al. [120] to identify them according to their severities. They utilized 150 images for instruction in their studies, while 220 images were used for research purposes. Individuals analyzed the accuracy achieved by SVM and Probabilistic Neural Network, where better classification efficiency was shown by the SVM algorithm. Wu et al. [226] used the ROC dataset to compare the SVM, kNN, and LLDA microaneurysm recognition algorithms' performance. Their experimental procedure included 50 images for training and 50 test images of their algorithm. Their findings

showed that, compared to kNN and LLDA, the SVM classifier's efficiency was much higher.

k-nearest neighbor Algorithm: kNN method is the primary and most straightforward classification algorithm for machine learning. It categorizes artifacts in the feature vector present in the training dataset, depending on the closest instances. "k" indicates the proportion of neighbors nearest to the classification model to make its prediction.

Among the forty machine learning papers chosen, the kNN algorithm was used in many studies. For the classification of diabetic retinopathy into its severity ranges, Nijalingappa et al. [129] employed kNN algorithms. In their experiments, 169 images were used, namely DIARETDB1 and Messidor, and an entire dataset from two public datasets. With 119 images, they trained the machine learning model and evaluated them on the other 50 image data. With the kNN algorithm, the classification results obtained are very satisfactory. Wang et al. [220] correlated kNN, NB and SVM, classification algorithms in fundus images to localize microaneurysms.

They used three datasets for research, including DIARETDB1, ROC, and a complete dataset from Moorfields Eye Clinic. The test results demonstrated that the other two machine learning algorithms, NB and SVM, were outperformed by the kNN algorithm. Likewise, in two public datasets of diabetic retinopathy, namely DIARETDB0 and DIARETDB1, Rahim et al. [159] contrasted the findings of DT, kNN, and SVM for microaneurysm detection. In contrast with SVM, the obtained results showed that kNN and DT performed better.

Local linear discrimination analysis One of the most widely used tech-

niques of classification and dimensional reduction is LLDA. It is used to discriminate between different classes. LLDA projects a line that necessarily retains ways that are essential for the classification of data. It requires projection to a line so that information from various groups are segregated.

In the chosen primary machine learning tests, LLDA was used only once. Wu et al. [226] used the LLDA algorithm for detecting microaneurysms and compare these results on the ROC dataset with two other machine learning algorithms, namely SVM and kNN. The LLDA method was unable to function effectively, as per their experimental findings, and when compared to LLDA and kNN, SVM demonstrated high performance.

Naive bayes The classification technique for NB is a probability-based algorithm. It operates on numerical information, and that in the categories generates a probabilistic model. It only requires a small amount of numerical information for the classification prediction. It is, therefore, a fast and convenient algorithm for classification.

In the selected studies, the NB method was also utilized once only. Wang et al. [220] analyzed three identification techniques to predict microaneurysms, namely kNN, SVM, and NB. In two public and exclusive data collection, they conducted their experiments. The NB algorithm was unable to classify images of microaneurysms better than conventional classification techniques, and in their experimental conditions, kNN was more suitable.

Artificial neural networks There are typically three main layers of the ANN, called the input, hidden, and output layer. There are several nodes in the input and hidden layers, and the output layer includes just one node. An activation

node is a neuron in a neural network. The input layer forwards patterns where actual processing is performed to the hidden layer. In the hidden layer, arbitrary weights are allocated to the nodes. The hidden layer is attached to the output layer that the result is responsible. This can be regarded as a sigmoid function, which generates one output and takes multiple inputs. In the relevant literature, different varieties of ANN were used by different authors, including,

- Generalized Regression Neural Network;
- Scaled Conjugate Gradient Back Propagation Network;
- Probabilistic Neural Network;
- Multi-Layer Perceptron (MLP) and Lattice Neural Network;
- Pattern Recognition network;
- Levenberg-Marquardt neural network;
- Hopfield Neural Network;
- Probabilistic Neural Network;
- Feedforward Backpropagation Neural Network;
- Radial Basis exact fit;
- Radial Basis fewer neurons;
- Meta-cognitive Neural Network;
- Radial Basis Neural Network.

A specific ANN classification method on fundus retinal images has been used by several authors and achieved more reliable results. Authors have used a single ANN algorithm in [10,27,95] and have stated this to be a more robust

classification technique in the diabetic retinopathy image classification domain. Shirbahadurkar et al. [180] contrasted Levenberg-Marquardt NN with SVM and demonstrated that the Levenberg-Marquardt neural network algorithm's classification efficiency was superior in their experimental design. They used the DIARETDB1 database and carried out their lesion-level experiments. Using 652 specimens derived from the corpus, they trained their machine learning model and evaluated them with the same number of specimens. The test results demonstrated that with greater precision, the Levenberg-Marquardt neural network algorithm outperformed the support vector machine. Santhi et al. [167] and Ganesan et al. [63] contrasted the Probabilistic NN to various classifiers, and they reported after experimenting that the efficiency of the Probabilistic Neural Network classification model in their experimental design was more substantial than the others.

Decision tree Algorithm A DT is a general technique which is used particularly for problems with classification. This one has a tree structure, in which a node represents a reflection of an attributes test, a section signifies a test result, and a class mark is included in the terminal node. A root-node is the top-most node in a tree. A DT is used in strategic planning to describe the decisions. In DT, grouping, in a tree-like framework, is performed hierarchically. A few of the benefits of DT is that it includes little to no preparation of data. The drawback of DT is that over-complex DTs are often made, also recognized as overfitting. DTs can become unpredictable because merely the absence in the data can generate a complete variance in the information. Thus, several trees-based frameworks were implemented for improving performance of DTs, i.e. RF. Rahim et al. [159] measured the effectiveness of decision tree, k-near neighbor, and support vector machine to identify microaneurysms employing DIARETDB0 and DIARETDB1

datasets retinal fundus images. For training, 90 percent of the whole images were employed, whereas evaluation of these different classifiers was done on the remainder 10 percent of retinal fundus images. The researchers stated that with 91 percent accuracy obtained by decision tree and k-near neighbor algorithm outperforming support vector machine.

Adaptive Boosting A standard strategy which can apply to several statistical models is Adaptive Boosting (AdaBoost). It operates sequentially and then each node is installed on a changed version of the primary database and a strong classifier is finally generated. The AdaBoost classification model has been used once in the chosen research articles. Prentasic et al. [154] used the Adaboost for identifying exudates in diabetic retinopathy images. They utilized discontinuous training sets and testing set containing 50 images from the DRiDB dataset in their experimental setup. The test results demonstrated that the sensitivity of the AdaBoost was 75 percent.

Self-adaptive resource allocation network classifier While the names imply selecting the training examples, a self-adaptive allocation of resources framework algorithm employs a self-regularized concept and later eliminates the repetitive training samples, thereby using less memory and processing resources. For both the training stage, the chosen samples with more data are now used. In the chosen primary machine learning tests, the SRAN algorithm was used twice but did not execute well compared to the other classification techniques. The SRAN classification model contrasted Ponnibala et al. [149] and Bala et al. [148] with both the SVM and McNN algorithms and the classification of various eye-based lesions. Authors employed an unique dataset obtained in Coimbatore, India, at the Lotus Eye Hospital. Their studies showed that SRAN's

performance in their experiments was unsatisfactory, although McNN provided them with better precision.

Unsupervised classifiers Unsupervised classification is currently used where existing information is not available. Just the set of data and the features corresponding to such cases are identified in that scenario. A very methodology is intended to examine groups of items in the pixel values in unsupervised learning, generally achieved with protocols for clustering.

In the selected studies, unsupervised classification algorithms were employed many times. Zhou et al. [247] used an unsupervised microaneurysm identification classification using the ROC database comprising 100 images. They used half the pictures in their tests for preparation and a half for evaluation. The study noted that, in their observational data, unsupervised classification methods obtained fair efficiency. Likewise, Kusakunniran [106] and Biyani [23] used an unsupervised classification model to identify exudates in diabetic retinopathy images and recorded that the unsupervised classification algorithms provided 89 percent and 88 percent of sensitivities.

Ensemble classifiers The learning algorithm may be referred to as group learning, in which many classification techniques merge to construct a more precise model. This can be achieved, i.e., bagging and enhancing, in 2 ways. Numerous classification methods work in parallel during bagging and eventually decide the most reliable one. The final classification model becomes one with a plurality vote. Similar classification algorithms are used in series during boosting. The weights are modified based on the previous model for each model. Firstly, the dataset is partitioned into several sections, and using others, one of them is validated and so on.

In the selected papers, Ensemble classifiers were embraced by a few authors. A classification model developed by Mane [61] was an aggregate of FFNN and HDT. They independently compared their diabetic retinopathy image recognition potential with LMNN and HDT, using two datasets, DIARETDB0 and DIARETDB1, to achieve an accuracy of 98%.

Fraz et al. [61] used 478 images from DIARETDB1, e-Ophtha, and Messidor datasets to design a classifier model with bootstrapped DT for the segmentation of exudates. They used 137 images for the training of the machine learning network and 341 images for the evaluation of their ensemble-based classification model in their experimental design. In their experimental data, they achieved 98 percent accuracy. Likewise, in order to classify diabetic retinopathy images, Somasundaram et al. [194], Antal et al. [14], and Barkana et al. [21] also used ensemble-based classification techniques, and their experimental data provided accuracies of 95 percent, 87 percent, 90 percent, respectively.

It can be seen above, and the better classification results were shown by ANN in most of the experiments, followed by SVM and ensemble classifier. Furthermore, tree-based classifiers, including decision trees, random forest, have seldom been used in the studies. In four selected experiments, the Euclidean distance-based classifier, namely kNN, also showed promising results. The single best classification model should not be inferred, as the classification algorithm performed in various indifference situations. Thus, to determine the highest score on collected images, it is suggested to compare different machine learning algorithms' performance.

2.5 Deep Learning in Diabetic Eye Disease Classification

In this section, we review the DL based approaches for DED detection. DL is defined as the extension of the ML with a multilayer network for extracting features. In DL architecture the term "deep" refers to the depth of the layers. The classification process is as follows: (i) The annotated dataset is split into testing and training samples for DL architecture, (ii) The dataset is preprocessed using image preprocessing techniques for quality enhancement and (iii) The preprocessed images are fed into DL architecture for features extraction and subsequent classification. Each layer in DL architecture considers the output of the previous layer as its input, processes it and passes it onto the next layer. Many authors fine tune the hyperparameters of existing DL algorithms, such as VGG16 or CNN, to improve classification performance. Hyperparameter observed in this study is shown in Table 2.4. Finally, the last layer of the architecture produces the required result, i.e. classification of DED as for the scope of the study. Out of 65 studies, 38 used TL, 21 used their proposed DL and six used a combination of DL and ML classifiers such as RF, SVM, Backpropagation Neural Network (BPNN).

2.5.1 Convolutional Neural Networks

An alternative to TL is the new network development by the researchers. Out of 65 studies, 21 of them have designed their DL architectures for automated detection of DED. Table 2.5 presents the list of studies, where the researchers have employed their own built DL models with the classifier indicated, number of layers, model used and results obtained.

Diabetic Retinopathy Doshi et al. [55] detected the severity of diabetic retinopathy using the 29 layers CNN model and detected five stages of DR, and three CNN achieved an accuracy of 39.96% on kappa matrix. Gargeya et al. [66] identified diabetic retinopathy using the DL approach. They achieved AUC of 94%, specificity of 87% and sensitivity of 93%. Ghosh et al. [68] employed a 28 layers CNN for two and five class classification of diabetic retinopathy. Using Softmax they achieved an accuracy of 95% for two class and 85% of accuracy for five class classification. Jiang et al [94] classified two classes of diabetic retinopathy using fundus images. They used 17 layers deep CNN on the Caffe framework and achieved an accuracy of 75.7%. Pratt et al. [153] employed a CNN architecture to identify the severity level of DR. They achieved an accuracy of 75%, specificity of 30% and sensitivity of 95% using Softmax classifier. Xu et al. [229] employed a 16 layer model for early detection of DR. Using Softmax classifier they achieved an accuracy of 94.50%. Yang et al. [232] employed local and global CNN architectures. Local CNN (10 layers) was used for lesion detection and the global CNN (26 layers) for grading DR. The authors achieved an AUC of 0.9687, specificity of 89.80% and sensitivity of 95.90%. Yu et al. [240] detected exudates using 16 layers CNN. With Softmax classifier, they achieved an accuracy of 91.92%, specificity of 96% and sensitivity of 88.85%. Torre et al. [48] used 17 layered CNN architecture obtaining specificity of 90.8% and sensitivity of 91.1%. Pires et al. [147] proposed 16 layer CNN architecture. They used Messidor-2 and DR2 dataset to test the model. With the neural networks classifier, they achieved AUC of 96.3% in the DR2 dataset and AUC of 98.2% in Messidor-2 and with the Random Forests classifier, they achieved AUC of 96.1% in DR2 dataset and AUC of 97.9% in Messidor-2.

Hemanth et al. [83] proposed a hybrid method based on using both image

processing and DL for improved results. using 400 retinal fundus images within the MESSIDOR [50] database and average values for different performance evaluation parameters were obtained an accuracy 97%, sensitivity (recall) 94%, specificity 98%, precision 94%, FScore 94% and geometric mean (GMean) 95%.

Glaucoma Chen et al. [38] developed six layer CNN model. With the Softmax classifier they achieved an AUC of 83.1% and 88.7% in ORIGA [244] and SCES datasets. Raghavendra et al. [158] build an eighteen layer CNN framework to diagnose Gl using 1426 fundus images in where 589 were normal and 937 were with glaucoma. They achieved an accuracy of 98.13%, sensitivity of 98% and specificity of 98.3%. Abhishek et al. [139] introduced a novel multi-model DL network named G-EyeNet for glaucoma detection using DRI-ONS [30] and Drishti-GS [190] datasets. Their experimental findings revealed an AUC of 92.3%.

Diabetic Macular Edema Al-Bander et al. [7] proposed a CNN system to grade the severity of DME using fundus images using the MESSIDOR [50] dataset of 1200images. They obtained an accuracy of 88.8%, sensitivity of 74.7% and specificity of 96.5% respectively. Prentavsic et al. [155] introduced a novel supervised CNN based exudate detection method using the DRiDB dataset [156]. The proposed network consists of 10 alternating convolutional and max-pooling layers. They achieved sensitivity of 78%, Positive Predictive Value (PPV) of 78% and FSc of 78% respectively. Tan et al. [204] used the CLEOPATRA [189] image dataset. They obtained sensitivity of 87.58% and specificity of 98.73% respectively.

Cataract Zhang et al. [242] proposed eight layers of DCNN architecture. With Softmax classifier, they achieved an accuracy of 93.52% and 86.69%. Dong

et al. [54] used Softmax classifier with five layer CNN architecture and achieved an accuracy of 94.07% and 81.91%, respectively.

Table 2.5: Studies employing new network for automatic DED detection.

DED	Classifier	Model	Layers	Ref.	Results
DR	Softmax	CNN	29	[55]	$KSc = 39.96\%$
	Decision Trees	CNN	6	[66]	$AUC = 94\%, SE = 93\%, SP = 87\%$
	Softmax	CNN	28	[68]	$ACC = 85\%, KSc = 75.4\%, Prec = 88.20\%, SE = 95\%$
	Softmax	CNN	17	[94]	$ACC = 75.70\%$
	Softmax	CNN	13	[153]	$SE = 95\%, SP = 30\%$
	Softmax	CNN	16	[229]	$ACC = 94.5\%$
	Softmax	CNN	10	[232]	$AUC = 96.87\%, SE = 95.90\%, SP = 89.90\%$
	Softmax	CNN	16	[240]	$ACC = 91.92\%, SE = 88.85\%, SP = 96\%$
	Softmax	CNN	17	[48]	$SE = 91.1\%, SP = 90.8\%$
	Softmax	CNN	16	[147]	$AUC = 96.1\%$
GI	Softmax	CNN	6	[38]	$AUC = 83.1\%, 88.7\%$
	Softmax	CNN	18	[158]	$ACC = 98.13\%, SE = 98\%, SP = 98.3\%$
	Softmax	CNN	6	[139]	$AUC = 92.3\%$
	Softmax	CNN	6	[176]	$ACC = 90\%, SE = 96\%, SP = 84\%$
	Softmax	CNN	12	[185]	$AUC = 8.31\%, 88.7\%$
DME	Softmax	CNN	13	[7]	$ACC = 88.8\%, SE = 74.7\%, SP = 96.5\%$
	Softmax	CNN	10	[155]	$SE = 78\%, PPV = 78\%, FSc = 78\%$
	Softmax	CNN	10	[204]	$SE = 87.58\%, SP = 98.73\%$
Ca	Softmax	CNN	8	[242]	$AUC = 93.52\%$
	Softmax	CNN	5	[54]	$ACC = 94.07\%, 81.91\%$

Legend: CNN = Convolutional Neural Network, SSAE = Stacked Sparse Auto Encoder, ACC = Accuracy, SE = Sensitivity, SP = Specificity, AUC = Area Under Curve, FSc = F-Score, KSc = Kappa Score, Prec = Precision, PPV = Positive Predictive Value, GMean = Geometric mean.

Table 2.6: Studies employing combined DL and ML for automatic DED detection.

DED	Model	Layers	Features	Ref.	Classifier	Results
DR	CNN	3	DColor-SIFT, GLOH	[1]	Softmax	$AUC = 92.4\%$, $SE = 92.18\%$, $SP = 94.50\%$
	CNN	10	Shape, Intensity	[136]	RF	$AUC = 93.47\%$, $SE = 97.21\%$
	DBN	3	Shape, Intensity	[15]	SVM	$ACC = 96.73\%$, $SE = 79.32\%$, $SP = 97.89\%$
GI	CNN	23	-	[8]	RF	$ACC = 88.2\%$, $SE = 85\%$, $SP = 90.8\%$
Ca	DCNN	17	Shallow, residual, pooling	[160]	RF	$ACC = 90.69\%$
	CNN	2	Wavelet, Sketch, Texture	[231]	SVM, BPNN	$ACC = 93.2\%$, 84.5%

Legend: CNN = Convolutional Neural Network, DBN = Deep Belief Network, RF = Random Forests, SVM = Support Vector Machine, BPNN = Back-Propagation Neural Network, SE = Sensitivity, SP = Specificity, AUC = Area Under Curve, Acc = Accuracy, DColor-SIFT = Dense Color Scale-Invariant Feature Transform, GLOH = Gradient Location Orientation Histogram.

2.5.2 Transfer Knowledge

The concept of TL is based on the reuse of the features learned by DL models on the primary task and its adaptation to the secondary task. The idea is to reduce the computational complexity while training Neural Network architecture (resource intensive). Additionally, TL is found to be beneficial in cases where there is insufficient data to train a Neural Network from scratch (high volume of data required). Using TL, the parameters are initialized from the prior learning instead of random generation. Intuitively, the first layers learn to extract basic features such as edges, textures, etc., while the top layers are more specific to the task, e.g. blood vessels and exudates. Therefore, TL is commonly adopted in image recognition applications as the initial features extracted are shared regardless of the tasks. Table 2.7 shows the records of works, which applied TL for the detection of DED. The details regarding a particular type of DED recognition, network architecture and model used were further extracted. Additionally,

the classification results were retrieved for the comparison between the studies and state of the art overview. Overall, 38 of the 65 studies adopted the TL approach for the detection of DED through DL (19-DR, 15-GI, 3-DME and 1-Ca).

Diabetic Retinopathy Abramoff et al. [3] used a CNN model based on *AlexNet* with RF classifier for the detection of DR. Using Messidor-2 data they achieved AUC of 98.0%, sensitivity of 96.8%, specificity of 87.0% and the predictive negative value was 99.0%. Choi et al. [42] used a STARE dataset [57] to perform the binary classification (normal and abnormal) for 10 retinal diseases. They used VGG-19 architecture with SGD optimizer with Random Forests classifier and achieved AUC of 90.3%, sensitivity of 80.3% and specificity of 85.5%. Ting et al. [209] used VGGNet architecture to classify DR and other diseases like Age-related Macular Degeneration (AMD) and GI. They collected dataset from the Singapore National Diabetic Retinopathy Screening Program (SIDRP) from 2010 to 2013 and achieved AUC of 93%, specificity of 91.6% and sensitivity of 90.5%. For the GI, they achieved AUC of 94.2%, specificity of 87.2% and sensitivity of 96.4%. Last, for the referable DME, they achieved sensitivity of 92%. Quellec et al. [157] and Gondal et al. [73] used a 26 layered *o.O* solution proposed by Bruggemann and Antony ¹, which ranked second in DR Kaggle competition. [157] achieved AUC of 95.4% on the Kaggle dataset and on the eophtha dataset they obtained AUC of 94.9%. Similarly, Gondal [73] used *o.O* solution to detect DR lesions such as red dots, soft exudates, hemorrhages and microaneurysms. They replaced the last dense layer to the global average pooling layer. They achieved AUC of 95.4% on the DIARETDB1 dataset. Gulshan et al. [75] detected DR using Inception-v3 on the Kaggle dataset and also datasets collected from three Indian hospitals. They achieved specificity of 98.2% and

¹<https://www.kaggle.com/c/diabetic-retinopathy-detection/discussion/15617>

sensitivity of 90.1% for a moderate and worse stage of DR respectively. Mansour et al. [121] modified AlexNet for the classification of 5 stages of DR. They achieved an accuracy of 97.93%, specificity of 93% and sensitivity of 100% on the Kaggle dataset. Roy et al. [161] used the Random Forest classifier on the Kaggle dataset and achieved a Kappa Score ² (KSc) of 86%. Li et al. [114] detected exudates using a modified U-Net. U-Net was designed for the segmentation of neuronal membranes. They modified the architecture using unpooling layers rather than deconvolutional layers of U-Net. The authors trained the model using the e-ophtha dataset and achieved AUC of 96% on DIARETDB1. X. Li et al. [116] used various pretrained CNN models such as AlexNet, GoogLeNet and VGGNet. They achieved an AUC of 98.34%, accuracy of 92.01%, specificity of 97.11% and sensitivity of 86.03%. They achieved an AUC of 97.8% and KSc of 77.59%, following accuracy of 95.21%, specificity of 97.80% and sensitivity of 77.79%, respectively. Perdomo et al. [144] classified normal DR images and images with exudates using LeNet architecture. Using the e-ophtha dataset the authors achieved an accuracy of 99.6%, specificity of 99.6% and sensitivity of 99.8%. Takahashi et al. [203] applied a modified GoogLeNet for detecting various stages of DR. They modified GoogLeNet by deleting the five accuracy layers and reduced the batch size to four and achieved an accuracy of 81% and Kappa value of 74%. Van et al. [215] used a nine layered CNN, which consisted of five convolution layers with 32 filters inspired by OxfordNet. They achieved AUC of 97.2%, specificity of 91.40% and sensitivity of 91.90% using the Messidor dataset [50]. Sayres et al. [172] classified five different stages of DR with an accuracy of 88.4%. The accuracy on the normal images was 96.9% and accuracy on images with mild and worse NPDR was 57.9%. Umapathy et al. [212] used

²Diabetic Retinopathy Detection, Evaluation Available; <https://www.kaggle.com/c/diabetic-retinopathy-detection/overview/evaluation>

images from STARE [57], HRE, MESSIDOR [50] and images acquired from the Retina Institute of Karnataka datasets. The authors proposed two methods for automated detection, Decision Trees classifier and TL. They retrained the last layer of Inception-V3 to classify the normal and DR images. They achieved an accuracy of 88.8%. Nguyen et al. presented an automated method of DR screening using DL models such as CNN, VGG-16 and VGG-19. The system classifies five categories of DR range 0-4, in which 0 is no DR and 4 is PDR. They obtained an AUC of 90.4%, sensitivity of 80%, specificity of 82% and accuracy of 82% respectively.

Glaucoma A number of studies have been conducted for the automated detection of Gl using TL. Phan et al. [146] applied the Deep Convolutional Neural Network to 3,312 images, which consisted of 369 images of Gl eyes, 256 Gl-suspected images and 2687 images of non-glaucoma eyes³. The AUC achieved was 90%. Ghamdi et al. [9] presented a semi-supervised TL CNN model for automatic detection of Gl. They used the RIM-ONE [62] database and achieved an accuracy of 92.4%, specificity of 93.3% and sensitivity of 91.7%. Asaoka et al. [17] used ResNet architecture and tested two datasets obtained from multiple institutes. They used the method of data augmentation to increase the data volume and measure their accuracy using the area under the receiver operating characteristic curve (AROC). Hence, they obtained two results, an AROC of 94.8% in an augmented dataset and an AROC of 99.7% in a dataset without augmentation. An et al. [13] used TL to detect Gl using color fundus images and 3 dimensional optical coherence tomography (OCT). To evaluate the model AUC the tenfold cross-validation (CV) was used. The Random Forest combined with five separate CNN models improved tenfold CV AUC to 96.3%.

³Data Collected; Yamanashi University glaucoma outpatient clinic and Yamanashi Koseiren Hospital

Andres et al. [53] used five different publicly available datasets resulting in the AUC of 96.05%, specificity of 85.80% and sensitivity of 93.46%. Cerentinia et al. [32] used GoogLeNet architecture for the detection of the presence of Gl. They used datasets from various databases and achieved an accuracy of 90% from the High Resolution Fundus (HRF) database, 94.2% of accuracy from RIM-ONE(r1) [62], 86.2% of accuracy from RIM-ONE(r2) [62], 86.4% of accuracy from RIM-ONE(r3) [62] and by combining all three databases the accuracy obtained was 87.6%. Orlando et al. [135] used two different CNN models from OverFeat and VGG-S to develop an automated Gl detection system. The proposed architecture yielded AUC value for OverFeat and VGG-s of 76.3% and 71.8%, respectively. Alan et al. [49] used VGG-16, VGG-19, ResNet50, InceptionV3 and InceptionResNetV2 to diagnose Gl on RIM-ONE [62] datasets. Promising results were obtained by combining ResNet and Logistic Regression, on RIM-ONE-r2 [62], with AUC of 95.7% and on InceptionResNet with the same classifier yielded AUC of 86% on RIM-ONE-r3 [62]. Fei et al. [113] used the VGG network to classify glaucoma and non-glaucoma visual fields based on the results of the visual field (VF) study and, for this test, they obtained VF samples from three different ophthalmic centres in mainland China. They obtained an accuracy of 87.6%, while the specificity was 82.6% and sensitivity was 93.2%, respectively. In the Gomez et al. [72] study VGG-19 was used to identify glaucoma and non-glaucoma using two publicly available datasets RIM-ONE [62] and DRISHTI-GS [190] and one private dataset from a screening campaign performed at Hospital de la Esperanza (Parc de Salut Mar) in Barcelona (Spain).

Diabetic Macular Edema Various researchers also investigated the use of a pretrained model to detect DME. Sahlsten et al. [163] performed binary classification of Non-Referable DME and Referable DME (NRDME/RDME) and

achieved AUC of 98.7%, specificity of 97.4% and sensitivity of 89.6% in binary classification using TL.

Cataract Finally, cataract detection using DL was performed by Pratap et al. [152]. Authors have collected data from various sources such as HRF, STARE [57], DIARETDB0, MESSIDOR [50], FIRE, etc. In total, they collected 800 images (200 - normal, 200 - mild, 200 - moderate, 200 - severe). The accuracy achieved was 92.91%.

2.5.3 Combined Deep Learning and Machine Learning

Out of 65 studies, six proposed a combination of DL and ML classifiers. Table 2.6 shows the studies in which the authors applied a combination of DL and ML classifiers namely: RF, SVM and BPNN based architectures for DED detection. Abbas et al. [1] developed a DL Neural Network (DLNN) to discover the severity degree of DR in fundus images using studying Deep Visual Features (DVF). For feature extraction, they used Gradient Location Orientation Histogram (GLOH) and Dense Color Scale Invariant Feature Transform (DColor-SIFT). They converted the features through the use of Principle Component Analysis (PCA). Afterwards, a three layer deep neural network was used to learn these features and subsequently, an SVM classifier was applied for the classification of DR fundus images into five severity stages, including no-DR, moderate, mild, severe NPDR (Nonproliferative Diabetic Retinopathy) and PDR (Proliferative Diabetic Retinopathy). They obtained sensitivity of 92.18%, specificity of 94.50% and AUC of 92.4% on three publicly available datasets (Foveal Avascular Zone Messidor [50], DIARETDB1) and one extraor-

Table 2.7: Studies employing TL for automatic DED detection.

DED	Architecture	Model	Ref.	Results	
DR	AlexNet	CNN	[3]	$AUC = 98.0\%$, $SE = 96.8\%$, $SP = 87.0\%$	
	VGGNet	CNN	[42]	$AUC = 90.3\%$, $SE = 80.3\%$, $SP = 85.5\%$	
	VGGNet	CNN	[209]	$AUC = 93.6\%$, $SE = 90.5\%$, $SP = 91.6\%$	
	<i>o</i> -OSolution	CNN	[73]	$AUC = 95.4\%$, $SE = 93.6\%$, $SP = 97.6\%$	
	Inception-V3	CNN	[75]	$SE = 90.1\%$, $SP = 98.2\%$	
	AlexNet	CNN	[121]	$ACC = 97.93\%$, $SE = 100\%$, $SP = 93\%$	
	<i>o</i> -OSolution	CNN	[157]	$AUC = 95.4\%$	
	ImageNet	CNN	[161]	$KSc = 86\%$	
	U-Net	CNN	[114]	$AUC = 96\%$	
	AlexNet, GoogLeNet, VGGNets	CNN	[116]	$AUC = 98.34\%$, $ACC = 92.01\%$, $SE = 86.03\%$, $SP = 97.11\%$	
	LeNet	CNN	[144]	$ACC = 99.6\%$, $SE = 99.8\%$, $SP = 99.6\%$	
	GoogLeNet	CNN	[203]	$ACC = 81\%$, $PABAK = 74\%$	
	OxfordNet	CNN	[215]	$AUC = 97.2\%$, $SE = 91.90\%$, $SP = 91.40\%$	
	Inception-V4	CNN	[172]	$ACC = 88.4\%$	
	Inception-V3	CNN	[212]	$ACC = 88.8\%$	
	VGG-16, VGG-19	CNN	[128]	$AUC = 90.4\%$, $ACC = 82\%$, $SE = 80\%$, $SP = 82\%$	
	ResNet50	CNN	[117]	$ACC = 96.3\%$, $AUC = 92.6\%$	
	AlexNet	CNN	[78]	$ACC = 90.07\%$	
	GI	VGG19, ResNet152, DenseNet201	CNN	[146]	$AUC = 90\%$
		VGG-16	CNN	[9]	$ACC = 92.4\%$, $SE = 91.7\%$, $SP = 93.3\%$
ResNet		CNN	[17]	$AUC = 99.7\%$	
VGG-19		CNN	[13]	$AUC = 96.3\%$	
VGG-16, VGG-19, Inception-V3, ResNet50, Xception		CNN	[53]	$AUC = 96.05\%$, $SE = 93.46\%$, $SP = 85.80\%$	
GoogLeNet		CNN	[32]	$ACC = 90.0\%$, 94.2% , 86.2% , 86.4% , 87.3%	
OverFeat, VGG-S		CNN	[135]	$AUC = 76.3\%$, 71.8%	
VGG-16, VGG-19, ResNet50, InceptionV3, InceptionResNetV2		CNN	[49]	$AUC = 95.7\%$, 86.0%	
VGG		CNN	[113]	$ACC = 87.6\%$, $SE = 82.6\%$, $SP = 93.2\%$	
VGG-19		CNN	[72]	$AUC = 94\%$, $SE = 87.01\%$, $SP = 89.01\%$	
ResNet50, 101, 152		CNN	[134]	$AUC = 84.58\%$, $SE = 72.50\%$	
Xception		CNN	[134]	$AUC = 93.48\%$, $SE = 85.00\%$	
VGG19		CNN	[134]	$AUC = 88.06\%$, $SE = 73.18\%$	
ResNet18, CatGAN		CNN	[134]	$AUC = 95.55\%$, $SE = 89.18\%$	
ResNet		CNN	[134]	$AUC = 95.24\%$, $SE = 85\%$	
SENet		CNN	[134]	$AUC = 95.87\%$, $SE = 89.17\%$	
ResNet50		CNN	[134]	$AUC = 98.17\%$, $SE = 97.60\%$	
ResNet101, 152, DensNet169, 201		CNN	[134]	$AUC = 93.27\%$, $SE = 92.50\%$	
DeepLabv3		CNN	[134]	$AUC = 95.08\%$, $SE = 87.50\%$	
ResNet		CNN	[177]	$AUC = 96.5\%$	
InceptionV3		CNN	[184]	-	
InceptionV3		CNN	[5]	$AUC = 92.2\%$, $AUC = 88.6\%$, $AUC = 87.9\%$	
DME		Inception-V3	CNN	[163]	$AUC = 98.7\%$, $SE = 89.6\%$, $SP = 97.4\%$
	AlexNet	CNN	[102]	$ACC = 97.9\%$	
	ResNet50	CNN	[117]	$ACC = 91.2\%$, $AUC = 92.4\%$	
	AlexNet	CNN	[78]	$ACC = 96.85\%$	
Ca	AlexNet	CNN	[152]	$ACC = 92.91\%$	

dinary dataset (from the, Hospital Universitario Puerta del Mar, HUPM, Cádiz, Spain). Orlando et al. [136] combined ML and DL for the detection of lesions (red). They used three public datasets, namely Messidor [50], DIARETDB1 and e-optha. They extracted intensity and shape as features using knowledge transferred LeNet architecture, which consists of 10 layers. They achieved AUC of 93.47% and sensitivity of 97.21%, respectively. Arunkumar et al. [15] employed a Deep Belief Network (DBN) for diabetic retinal image classification. At first, with three hidden layers, the deep features were extracted with Deep Belief Network (DBN), then those features were decreased by applying the Generalised Regression Neural Network (GRNN) technique and finally, the retinal images were classified using SVM. On their publicly available ARIA dataset, the authors achieved an accuracy of 96.73%, specificity of 97.89% and sensitivity of 79.32%, respectively. Al-Bander [8] used CNN for feature extraction and SVM for Gl and non Gl classification. They achieved an accuracy of 88.2%, specificity of 90.8% and sensitivity of 85%, respectively. Ran et al. [160] used a 17 layer DCNN feature extractor, which adopts a residual network to learn more detailed features of fundus images. The DCNN contains three modules, namely shallow, residual and pooling. Here, the shallow and residual modules extract features on a deep, medium and shallow level and the final feature vectors for Random Forests are output from the pooling module. The authors detected six classes of cataract with an accuracy of 90.69%. Last, [232] proposed 2 layers stacking architecture with Support Vector Machine and backpropagation neural network classifier. The ensemble classifier achieved an accuracy of 93.2% and 84.5%.

Table 2.8: Performance metrics employed in selected studies.

ACC	AUC	SE	SP	KSc	FSc	Prec	PPV	Pabak	GMean	References
✓	✗	✓	✓	✗	✗	✗	✗	✗	✗	[7–9, 15, 54, 113, 121, 144, 158, 176, 240]
✗	✓	✓	✓	✗	✗	✗	✗	✗	✗	[1, 3, 42, 53, 66, 72, 73, 136, 209, 215, 232]
✗	✗	✓	✓	✗	✗	✗	✗	✗	✗	[48, 75, 153, 204]
✗	✗	✗	✗	✓	✗	✗	✗	✗	✗	[55, 161]
✓	✗	✓	✗	✓	✗	✓	✗	✗	✗	[68]
✗	✗	✓	✗	✗	✓	✗	✓	✗	✗	[155]
✓	✗	✓	✓	✗	✓	✓	✗	✗	✓	[83]
✓	✗	✗	✗	✗	✗	✗	✗	✓	✗	[203]
✓	✓	✓	✓	✗	✗	✗	✗	✗	✗	[116, 128]
✓	✗	✗	✗	✗	✗	✗	✗	✗	✗	[54, 78, 78, 94, 102, 152, 160, 172, 212, 229, 231]
✗	✓	✗	✗	✗	✗	✗	✗	✗	✗	[5, 13, 17, 38, 49, 114, 135, 139, 146, 147, 157, 242]

Legend: ACC = Accuracy, AUC = Area Under Curve, SE = Sensitivity, SP = Specificity, KSc = Kappa Score, FSc = F-Score, Prec = Precision, PPV = Positive Predictive Value, Pabak = Prevalence And Bias Adjusted Fleiss' Kappa, GMean = Geometric Mean.

2.5.4 Analysis and Review of Performance Evaluation metrics

Detailed description of performance measures, namely: specificity, sensitivity, accuracy, AUC, precision, f-score, and positive predictive value can be found in [192]. Likewise, Kappa Score, PABAK Index discussions can be found in [36], respectively. In the majority of listed academic papers, the authors used specificity, sensitivity, accuracy and AUC as their assessment metrics to evaluate the effectiveness of the classifier. The combined effect of performance metrics found to be used frequently was Sensitivity, Specificity and Accuracy. This variation was used 12 times out of a total 60 trials, accompanied by 12 uses of and sensitivity, specificity, AUC and two use of sensitivity, specificity, accuracy and AUC. Instead of Sensitivity, some researchers used Recall. We accommodated Recall under Sensitivity, rather than using it as another success indicator. The performance measurements frequently used include Sensitivity (32 times), Specificity

(25 times), Accuracy (26 times), and AUC (25 times). Other performance metrics not commonly used by research groups were: F-Score (twice), Precision (twice), PABAK (once), Kappa Score (3 times), Positive Predictive Value (once) and GMean (once).

2.6 Discussion and Observations

AI is one of the most intriguing technologies used in the material science toolset in recent decades. This compendium of statistical techniques has already shown that it is capable of significantly accelerating both fundamental and applied research. ML, already has a rich history in biology [206,245] and chemistry [130], and it has recently gained prominence in the field of solid state materials science. Presently, DL models in ML are effectively used in imaging for classification, detection [20], segmentation [141] and pre-processing. The most famous and commonly employed DL architecture in the selected 65 studies is CNN, which is used in 64 cases, while DBN is implemented once. We can infer that CNN is currently the most preferred deep neural network, particularly for the detection of DED as well as the diagnosis of other pathological indications from the medical images.

We have noticed that DL performed well on binary classification tasks (eg. DR and Non DR), whereas its performance significantly dropped when the number of classes increased. As an example, Ghosh et al. [68] obtained an accuracy of 95% on DR and Non DR classification task and accuracy of 85% on a multi class problem (five stages of severity), with 10% loss in accuracy. Else, Choi et al. [42] classified 10 distinct retinal diseases and achieved an accuracy

of 30.5%. Also, Dong et al. [54] performed cataract classification based on two features, namely: i) features extracted using DL and ii) features extracted using wavelet. Classification for the binary problem (Cataract and Non Cataract) achieved an accuracy of 94.07% and 81.91%. Then, the authors performed the classification of four classes of cataract and obtained an accuracy of 90.82% and 84.17%. This shows that features extracted using wavelet increased an accuracy of the Softmax classifier by 4% in the four class problem. Still, the overall highest accuracy was observed for a binary classification task.

This study reveals the research gap for more rigorous approaches to the development of multiclass DED classification problems. Furthermore, we have observed that binary classification is mostly conducted between the normal and the affected DED cases. For instance, Ghosh et al. [68] and Choi et al. [42] classified DR and Non-DR. Also, Al-bander et al. [8] and Phan et al. [146], identified glaucomatous and nonglaucomatous retinal images, while Dong et al. [54] detected cataract and noncataract conditions. The methods used in these articles are effectively identifying the vast proportion of severe cases where pathological signs are more prominent. Thus, there is a need for classifiers that perform equally well for mild stages of DED developments, where the lesions are tiny and difficult to detect.

Early detection of DED or mild DED is especially necessary to take effective preventive steps and to avoid possible blindness due to deterioration condition over time. As we can see, DL has shown an extensive capacity in the field of health care and especially in the field of DED detection. However, there are some limitations in its large-scale implementation. In terms of the validation of the proposed methods, the authors predominantly used Accuracy, Specificity

and Sensitivity to report their classification performance. For instance, Perdomo et al. [144] used LeNet CNN to detect exudates and reported accuracy (99.6%), specificity (99.6%) and sensitivity (99.8%) for the approach proposed. Another widely used metric was AUC, accuracy and sensitivity. This combination is appropriate in DL methods where image classes are imbalanced. However, data imbalance has been solved using geometric transformation (augmentation techniques) or re-sampling images from each class. For example, Chen et al. [38] used augmentation to overcome the overfitting on image data and obtained AUC (83.10%), and AUC (88.7%) on the ORIGA and SCES datasets. Other metrics have been used to measure performance such as Kappa Score (Ksc) used by Roy et al. [161], AROC used by Asaoka et al. [17], and Prevalence And Bias Adjusted Fleiss' Kappa (PABAK) used by Takahashi et al. [203].

2.7 Chapter Summary

This review chapter provides a comprehensive overview of the state of the art on DED detection methods. To achieve this goal, a rigorous systematic review of relevant publications was conducted. After the final selection of relevant records, following the inclusion criteria and quality assessment, the studies have been analyzed from the perspectives of 1) Datasets used, 2) Image preprocessing techniques adopted and 3) Classification method employed. The works were categorized into the specific DED types, i.e. DR, Gl, DME and Ca for clarity and comparison. In terms of classification techniques, our review included studies that 1) Adopted TL, 2) Build DL network architecture and 3) Used combined DL and ML approach. Details of the findings obtained are included in Section 2.6.

We have also identified several limitations associated with our study. First, we narrowed down the review conducted from *April 2014 - January 2020* due to rapid advances in the field. Second, we limited our review to DL based approaches due to their state of the art performance, in particular on the image classification task. Finally, our review focused on a collection of predefined keywords that provides a thorough coverage of the DED area of detection but may not be exhaustive. Furthermore, we hope that our research can be further expanded in the future to include an all encompassing and up-to-date overview of the rapidly developing and challenging field of DED detection.

CHAPTER 3

DEEP LEARNING FOR MILD DIABETIC RETINOPATHY CLASSIFICATION AND DETECTION

The previous chapter discusses the background of automated classification and detection of DED, its occurrence and severity, its high prevalence, and observed effects. This chapter discusses various computational techniques like image pre-processing, image augmentation, and pre-trained DL techniques to detect early DR (one of the DED).

Diabetes and the associated DR instances are currently increasing at an alarming rate, followed by an extensive research in DR detection from fundus photography. The classification of *severe* cases of pathological indications in the eye has already achieved over 90% accuracy. Still, the *mild* cases are challenging to detect due to model's inability to identify the subtle features, discriminative of a disease. Thus, in this thesis, a comprehensive evaluation of numerous CNN architectures was conducted in order to facilitate an *early* DR detection. Furthermore, several performance improvement techniques were applied to address existing CNN limitation in subtle eye lesions identification. The data used, i.e. annotated fundus photographs, was obtained from *two* publicly available sources - Messidor and Kaggle. The experiments were conducted on 13 CNN models, pre-trained on large-scale ImageNet database as part of the Transfer Learning approach implementation. Several performance improvement techniques were adopted, including: (i) fine-tuning, (ii) optimiser selection, (iii) data augmentation, and (iv) contrast enhancement. Maximum accuracy of 89% on No DR/Mild DR classification task was obtained for *ResNet50* model with fine-tuning and RMSProp Optimiser trained on augmented and enhanced Messidor

and Kaggle data sets.

3.1 Introduction

Approximately 420 million people worldwide have been diagnosed with Diabetes [31], and its prevalence has doubled in the past 30 years [133]. The number of people affected is only expected to increase, particularly in Asia [33]. Nearly 30% of those suffering from Diabetes are expected to develop the DR - a chronic eye disease that is considered a leading cause of vision loss among working-age adults [31,44]. The eventual blindness resulting from DR is irreversible, though it can be prevented through regular fundus examination [243].

Effective treatment is available for patients identified through *early* DR identification [225]. Needless to say, a timely detection of pathological indication in the eye leading to DR is critical. It not only allows to avoid the late invasive treatments and high medical expenses, but most importantly - to reduce the risk of potential sight loss. The manual methods of diagnosis prove limited given the worldwide increase in prevalence of both Diabetes and its retinal complications [71]. Currently, the ophthalmologist-to-patient ratio is approx. 1:1000 in China [243]. Furthermore, the traditional approaches reliant on human assessment require high expertise, as well as promote inconsistency among the readers [31]. Labour and time-consuming nature of manual screening services has motivated the development of automated detection methods [188], in particular early stages of DR and other diabetic related eye disease [169]. DNN model is a sequence of mathematical operations applied to the input, such as pixel value in the image [150], where the training is performed by presenting the network with multiple examples, as opposed to unflexible rule-based pro-

gramming underlying the conventional methodologies [65].

Deep learning, in particular CNN, has been widely explored in the field of DR detection [122,153,155,166,222], largely surpassing previous image recognition methodologies [222]. Overall, Deep learning has demonstrated tremendous potential in healthcare domain, enabling the identification of patients likely to develop a disease in the future [170,225]. In terms of DR, the applications range from binary classification (No DR/DR), to multi-level classification based on condition severity scale (No DR/Mild DR/Moderate DR/Severe DR). CNNs, with their multi-layer feature representations, have already shown outstanding results in discovering the intricate structures in high-dimensional datasets. The models have proven successful at learning the most discriminative, and often abstract aspects of the image, while remaining insensitive to irrelevant details such as orientation, illumination or background.

Motivation: The diagnosis for DR is particularly difficult for patients in early stage, which is the challenge identified in prior literature [31]. As highlighted by Pratt et al. [153], Neural Networks struggle to learn sufficient deep features to detect intricate aspects of Mild DR. In the same study, approx. 93% of mild cases were incorrectly classified as healthy eye instances. A problem is illustrated in Fig. 3.1, displaying various stages of DR and the associated visibility of the features. Numerous accuracy improvement techniques such as dimensionality reduction or feature augmentation have been proposed in the literature. Still, the studies using deep learning for DR detection consistently report high performance on binary classification (No DR/ Severe DR) cases, while classification of (No DR/ Mild DR) cases still remains a challenge. This limitation impedes wider application of fully automated mass-screening due to potential omission

of early phase of DR, leading to more advanced condition development in the future. In this chapter, we will employ image pre-processing techniques and train 13 pre-trained CNN models to enhance the accuracy in the classification of No DR/ Mild DR.

Contributions: Transfer learning has already been validated and demonstrated promising results in medical image recognition. The concept uses knowledge learned on primary task, and its re-purpose to secondary task. TL is particularly useful in DL applications that require vast amount of data and substantial computational resources. The state-of-the-art CNN models, pre-trained on the large public image repository have been used as part of this study, following the concept of transfer learning. Using the weights initialised, the top layers of Neural Networks have been trained for customised No DR/Mild DR binary classification from publicly available fundus image corpora. The improved classification performance via Transfer learning has already been reported in prior research on automated DR detection [219]. Unlike previous approaches, the study conducted in this thesis focuses entirely on *Mild* DR instances - currently challenging to identify.

- First, the highest performing CNN model is selected based on the extensive experiments conducted, i.e. fine-tuning, optimiser selection.
- Second, the number of performance improvements are evaluated, including data augmentation and contrast enhancement.
- Finally, the most optimal scenario in terms of achieved accuracy is selected to facilitate an efficient and effective fully-automated Deep learning-based system development in order to increase the access to mass-screening services among the population-at-risk.

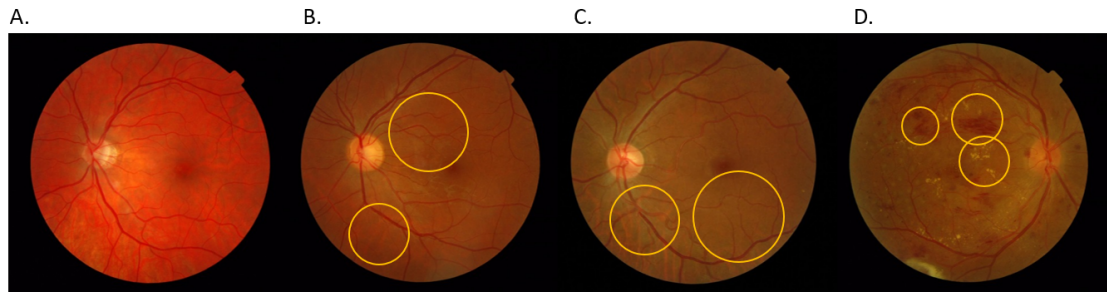


Figure 3.1: The examples of different stages of DR advancement on fundus images. A. No DR – healthy retina; B. Mild DR – abnormal growth of blood vessels and ‘cotton wool’ spots formation (early indication); C. Moderate DR – abnormal growth of blood vessels and ‘cotton wool’ spots formation (mid-stage indication); D. Severe DR – hard exudates, aneurysms and hemorrhages (advanced indication).

3.2 Methodology

The overarching aim of the study is the performance improvement of early DR detection of Mild DR from fundus images through an empirical evaluation of various classification improvement techniques. The associated objectives can be identified as follows:

- Comparison of 13 CNN architectures using concept of Transfer Learning;
- Effect of fine-tuning evaluation on models’ performance;
- Effect of optimiser selection on models’ performance;
- Evaluation of data augmentation and contrast enhancement techniques for further classification improvement on Mild DR detection task.

To illustrate the steps followed, the high-level process pipeline is presented in Fig. 3.2.

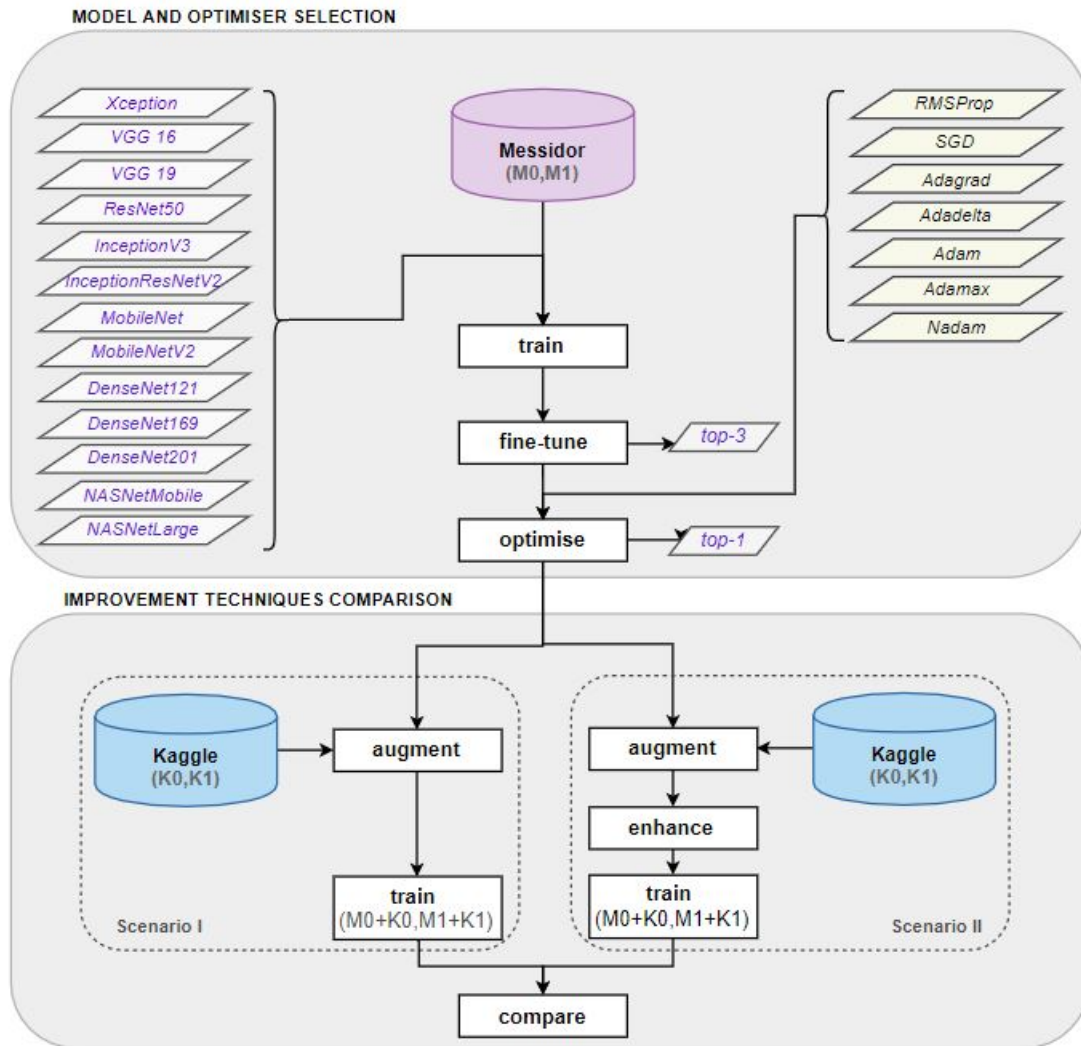


Figure 3.2: The high-level process pipeline.

3.2.1 Image Data Collection

Data was acquired from publicly available corpora, i.e. Kaggle and Messidor. Kaggle data set contains 35, 126 fundus images annotated as *No DR*, *Mild DR*, *Moderate DR*, *Severe DR*, *Proliferative DR* (5-class in total), while Messidor data set contains 1, 200 fundus images annotated as *No DR*, *Mild DR*, *Moderate DR*, and *Severe DR* (4-class in total). Both data sets consist of colour photographs of right and left eye. The images dimensions vary between low-hundreds to

low-thousands. The quality of data differs significantly between the data sets. Messidor, despite its relatively small scale, is considered a high fidelity source with reliable labelling, while Kaggle includes a large number of noisy and often misannotated images. The raw Kaggle data more closely reflects a real-world scenario, where images are taken under different conditions, thus resulting in various quality levels. The challenge lies in the potential eye lesions detection despite the observed noisiness in the data set.

3.2.2 Image Data Pre-processing

Data augmentation: Deep learning benefits from high-volume data. The larger number of both No DR as well as Mild DR instances can increase model's reliability and allow for more distinctive patterns detection. Thus, the small-scale Messidor dataset has been combined with large-scale Kaggle dataset, i.e. the respective No DR and Mild DR classes have been merged together. Table 3.1 presents the number of images for each class used in each scenario (before and after augmentation), along with the descriptions of the particular DR stages. The severity scale used is in accordance with the Early Treatment Diabetic Retinopathy Study (ETDRS) [243].

Given the large volume and proportion of No DR to Mild DR instances of Kaggle data, subsequent augmentation was performed to alleviate the resulting data imbalance issue. Data imbalance is generally encountered in machine learning implementations [115]. Another reason for using data augmentation is relatively low fidelity character of Kaggle data set. The Kaggle images were captured with different fundus cameras, resulting in various quality levels.

Table 3.1: The DR severity levels according to ETDRS and the number of images used in each experiment.

Severity level	Id	Description	M	K (raw)	K (aug)	M + K (aug)
<i>No DR</i>	0	No abnormalities.	546	25810	50976	51522
<i>Mild DR</i>	1	Microaneurysms only.	153	2443	55410	55563
<i>Moderate DR</i>	2	More than just microaneurysms, but less than severe NPDR.	247	5292	-	-
<i>Severe DR</i>	3	Any of the following and no signs of proliferative retinopathy: (1) severe intraretinal hemorrhages and microaneurysms in each of four quadrants; (2) definite venous beading in two or more quadrants; (3) prominent IRMA in one or more quadrants.	254	873	-	-
<i>Proliferative DR</i>	4	One or both of the following: (1) neovascularisation; (2) vitreous/preretinal hemorrhage.	-	708	-	-

M - Messidor, K - Kaggle, NPDR - Non-Proliferative Diabetic Retinopathy, IRMA - Intraretinal Microvascular Abnormalities.

The relatively noisy character of images is observed through their blurriness, under/over-exposure, presence of unrelated artifacts, and so on. The raw format of Kaggle data set closely reflects the nature of DR detection in real-world settings, where substantial variability in data quality is observed between the practitioners.

In order to evaluate the potential classification improvement due to pre-processing techniques applied, the following steps have been performed: (1) *crop*, (2) *resize*, (3) *rotate* and (4) *mirror*. The example of the original image, and the augmentation steps implemented are presented in Fig. 3.3. *Cropping and*

resizing (1 + 2) allows to focus on pathological indications with greater level of detail, which proves important for DR discrimination. Additionally, the subsequent *rotating and mirroring* (3 + 4) substantially expands the dataset, alleviating the imbalance issues between the classes.

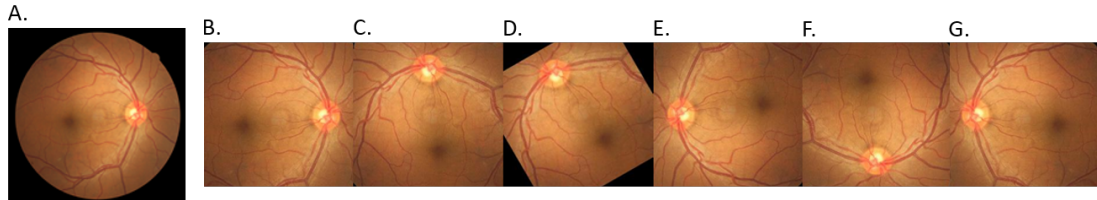


Figure 3.3: The examples of data augmentation steps performed on Mild DR fundus image from Kaggle dataset. (A) Original; (B) Crop; (C) Rotate 90°; (D) Rotate 120°; (E) Rotate 180°; (F) Rotate 270°; (G) Mirror.

Contrast Enhancement: Applying CLAHE on each component of RGB color corrupts its originality. A more coherent approach is the uniform dispersion of colour intensities, while leaving the colours (e.g. hues) unchanged. However, CLAHE on RGB image proves much more luminous and unnatural. Furthermore, the inevitable improvement of noise in smooth area is identified. Thus, contrast enhancement is performed by converting RGB to HSV colour space, and then CLAHE is applied on HSV colour model. HSV colour characterise colours in Hue (H), Saturation (S) and Value (V). This model was introduced by A.R. Smith [191], and is as follows (3.1, 3.2, 3.3):

$$V = \max(R, G, B); \quad (3.1)$$

$$\text{Let, } m = V - \min(R, G, B); \quad (3.2)$$

$$S = \frac{V - m}{V}; \quad (3.3)$$

Amount of widely separated RGB values determine the saturation (S) in HSV. That is, when the values are close collectively, the colour is close to grey, and when they are far, the colour is more extreme towards pure. Finally, Hue (H) decides whether or not the coloration is Green, Blue, Red, Yellow, etc. Therefore, the calculation of r1, g1, and b1 has been performed to calculate Hue (H) (3.4, 3.5, 3.6).

$$r1 = \frac{V - R}{V - m}; \quad (3.4)$$

$$g1 = \frac{V - G}{V - m}; \quad (3.5)$$

$$b1 = \frac{V - B}{V - m}; \quad (3.6)$$

If $S = 0$, then H is undefined, otherwise (3.7):

$$H = \begin{cases} 5 + b1 & R = \max(R, G, B) \text{ and } G = \min(R, G, B) \\ 1 - g1 & R = \max(R, G, B) \text{ and } G \neq \min(R, G, B) \\ r1 + 1 & G = \max(R, G, B) \text{ and } B = \min(R, G, B) \\ 3 - b1 & G = \max(R, G, B) \text{ and } B \neq \min(R, G, B) \\ 3 + g1 & B = \max(R, G, B) \\ 5 - r1 & \text{otherwise} \end{cases} \quad (3.7)$$

Thus, Hue discontinuity can be observed around 360° , therefore it is difficult to perform arithmetic operations in all of the HSV components. Hence, CLAHE is applied on S and V and it is shown in Fig. 3.4.

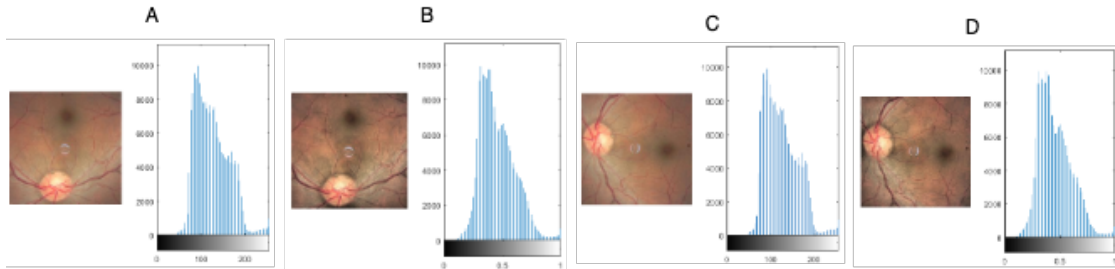


Figure 3.4: Contrast enhancement using CLAHE: A and C: before, B and D: after.

3.2.3 Model Construction

The knowledge transfer from primary to secondary task frequently acts as an only solution in highly-specialised disciplines, where the availability of large-scale quality data proves challenging. The adoption of already pre-trained models is not only the efficient optimisation procedure, but frequently supports the classification improvement. The first layers of CNN learn to recognise the generic features such as edges, patterns or textures, whereas the top layers focus on more abstract and task-specific aspects of the image, such as blood vessels or hemorrhages. Training only the top layers of target dataset, while using the initialised parameters for the remaining ones is the commonly employed approach, in particular in computer vision domain. Apart from efficiency gains, fewer parameters to train also reduce the risk of overfitting, which is a major problem in Neural Networks training process [153]. The CNN models used in the experiments along with their characteristics are presented in Table.3.2.

Table 3.2: The CNN models pre-trained on ImageNet and their characteristics (source: <https://keras.io/applications>).

Model	Size	Top-1 Accuracy *	Top-5 Accuracy *	Parameters	Depth **	Reference
<i>Xception</i>	88 MB	0.790	0.945	22,910,480	126	Chollet [43]
<i>VGG16</i>	528 MB	0.713	0.901	138,357,544	23	Simonyan and Zisserman [183]
<i>VGG19</i>	549 MB	0.713	0.900	143,667,240	26	
<i>ResNet50</i>	98 MB	0.749	0.921	25,636,712	-	He et al. [82]
<i>InceptionV3</i>	92 MB	0.779	0.937	23,851,784	159	Szegedy et al. [201]
<i>InceptionResNetV2</i>	215 MB	0.803	0.953	55,873,736	572	Szegedy et al. [199]
<i>MobileNet</i>	16 MB	0.704	0.895	4,253,864	88	Howard et al. [86]
<i>MobileNetV2</i>	14 MB	0.713	0.901	3,538,984	88	Sandler et al. [165]
<i>DenseNet121</i>	33 MB	0.750	0.923	8,062,504	121	Huang et al. [87]
<i>DenseNet169</i>	57 MB	0.762	0.932	14,307,880	169	
<i>DenseNet201</i>	80 MB	0.773	0.936	20,242,984	201	
<i>NASNetMobile</i>	23 MB	0.744	0.919	5,326,716	-	Zoph et al. [250]
<i>NASNetLarge</i>	343 MB	0.825	0.960	88,949,818	-	

* The top-1 and top-5 accuracy refers to the model’s performance on the ImageNet validation dataset.

** Depth refers to the topological depth of the network. This includes activation layers, batch normalisation layers etc.

3.2.4 Performance Evaluation

Fine-tuning: The CNN models adopted in the study were pre-trained on a large-scale ImageNet data set that spans numerous categories such as flowers, fruits, animals, etc. The models obtain high performance on classification tasks for the objects present in the training data set, while prove limited in their application to niche domains, such as DR detection. Diagnosis of pathological indications in fundus images depends on a wide range of complex features and their localisations within an image [31]. In each layer of CNN, there is a new representation of input image by progressive extraction of the most distinctive characteristics [122]. For example, the first layer is able to learn edges, while the last layer can recognise exudates - a DR classification feature [31]. As a result, the following scenarios were considered in the experiments: (1) only the top layer removal and network re-train (the current pre-trained approach); and

(2) the n top layers removal and network re-train (the proposed approach). The parameter n vary across the CNNs used and depends on the total number of layers present in each model structure. The threshold of 100 was selected, and the subsequent layers of each model were 'un-frozen' and fine-tuned. The initial 100 layers were treated as a fixed feature extractor [132], while the remaining layers were adapted to specific characteristics of fundus photography. The potential classification improvement on DR detection task was evaluated as a result of the proposed models customisation. In the study conducted by Zhang et al. [243], the performance accuracy of Deep learning-based DR detection system improved from 95.68% to 97.15% as a result of fine-tuning.

Optimiser selection: During the training process, the weights of Neural Network nodes are adjusted accordingly in order to minimise the loss function. However, the magnitude and direction of weights adjustment is strongly dependent on the Optimiser used. The most important parameters that determine the Optimiser's performance are: Learning rate and Regularisation. Too large/too small value of Learning rate results in either non-convergence of the loss function, or in the reach of the local, but not absolute minima, respectively. At the same time, the Regularisation allows to avoid model overfitting by penalising the dominating weight values for the correct predictions. Consequently, the classifier generalisation capability improves, when exposed to a new data. The Optimisers used in the experiments were as follows: (1) *RMSprop*, (2) *SGD*, (3) *Adagrad*, (4) *Adadelata*, (5) *Adam*, (6) *Adamax* and (7) *Nadam*.

3.3 Experiment and Analysis

The algorithms were implemented using Keras library¹, with TensorFlow² as a back-end. The images resolution has been standardised to a uniform size in accordance with input requirements of each model. The number of epochs, i.e. complete forward and backward passes through the network, was set to 20 due to the already pre-trained models use. The training/testing split was set to 80/20. The stratified random sampling was performed to ensure proportional class distribution. Mini-batch size was set to 32, and the cross-entropy loss function was selected due to its suitability for binary classification task. The default Optimiser was RMSProp. The standard evaluation metric of Accuracy, Sensitivity and Specificity on testing data set was used for final results validation.

3.3.1 Experiment Design

The algorithms is implemented using MatLab for contrast enhancement, and Keras 2.3 library, with TensorFlow 2 as a back-end and Python 3.8 programming language in jupyter notebook with a processor of 2.3 GHz Intel Core i9 and RAM of 16 GB 2400 MHz DDR4 with Intel UHD Graphics 630 1536 MB.

3.3.2 Model and Optimiser Selection

The 13 pre-trained CNNs were compared in terms of yielded accuracy on testing data set (Table. 3.3). Additionally, the fine-tuning was applied as an alternative

¹<https://keras.io/>

²<https://www.tensorflow.org/guide/keras>

to the default option. After removal and re-training of n layers from 100 onwards (n was CNN-dependent), the performance obtained for each model was used for comparison purposes. The fine-tuning effect was calculated in terms of percentage accuracy increase/decrease. Then, the maximum accuracy was selected for each model (either default or after fine-tuning). Finally, the top 3 CNN architectures with highest classification performance on Messidor data set progressed to the subsequent optimisation step, as set out in process pipeline (Fig. 3.2).

Table 3.3: The accuracy comparison of pre-trained CNN models.

Model	Accuracy	Accuracy (F-T*)	F-T* effect	Accuracy (max)
Xception	0.809	0.809	±00.0%	0.809
VGG16	0.809	0.809	±00.0%	0.809
VGG19	<u>0.813</u>	0.813	±00.0%	0.813
ResNet50	0.813	<u>0.816</u>	+00.4%	0.816
InceptionV3	0.806	0.795	-01.3%	0.806
InceptionResNetV2	0.812	0.582	-28.4%	0.812
MobileNet	0.583	0.556	-04.7%	0.583
MobileNetV2	0.781	0.656	-16.0%	0.781
DenseNet121	0.795	0.778	-02.2%	0.795
DenseNet169	0.569	0.642	+12.8%	0.642
DenseNet201	0.797	0.795	-00.2%	0.797
NASNetMobile	0.799	0.802	+00.4%	0.802
NASNetLarge	<u>0.813</u>	0.809	-00.4%	0.813

* Fine-Tuning

The accuracy after each epoch was further plotted in order to investigate the models convergence capabilities in the default and fine-tuning scenario (Fig. 3.5). As a result, the computational intensity was additionally evaluated.

Following the top 3 CNN models selection (Table. 3.3), the 7 most common in Deep learning applications Optimisers were evaluated as part of the opti-

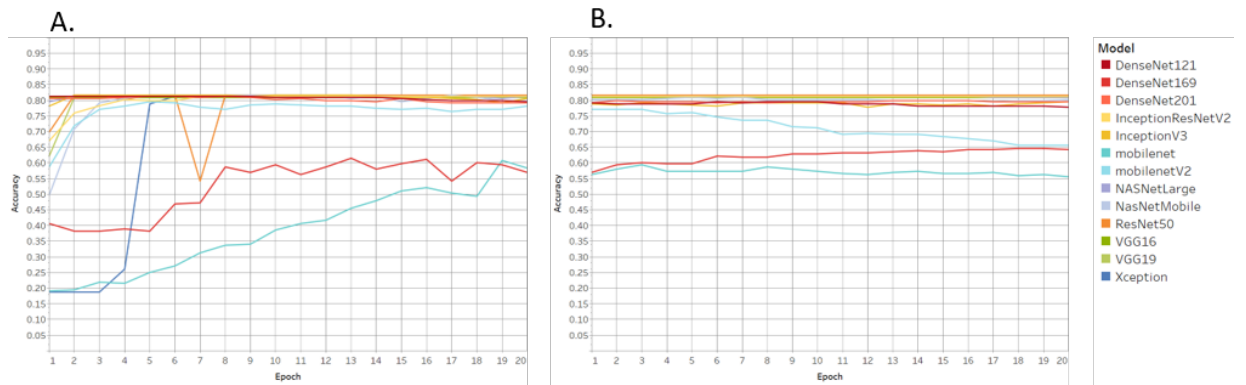


Figure 3.5: Validation accuracy achieved for the respective epochs. (A) Default; (B) Fine-tuning.

miser selection process (Table. 3.4). The most robust Optimiser in terms of validation accuracy for each of the 3 models was indicated. The highest performing model+Optimiser was selected for further data augmentation step.

Table 3.4: The Optimisers performance evaluation.

	VGG19	ResNet50	NASNetLarge
Optimiser	Accuracy	Accuracy	Accuracy
RMSprop *	0.813	0.816	0.813
SGD	0.812	0.812	0.812
Adagrad	0.812	0.802	0.815
Adadelta	0.812	0.812	0.812
Adam	0.812	0.812	0.792
Adamax	0.812	0.739	0.802
Nadam	0.812	0.756	0.809

* default

3.3.3 Improvement Techniques Comparison

The respective classes of both Messidor and Kaggle data sets (M0+K0,M1+K1) were merged together and used to train the max-accuracy model, as deter-

mined. The increase in data set volume was expected to contribute towards performance improvement. Next, the augmentation of imbalanced low quality Kaggle data was conducted to further evaluate impact of image pre-processing on classification accuracy. The results of both scenarios (i.e. (I) Messidor + Kaggle (augmented) data; and (II) Messidor + Kaggle (augmented) + enhanced) are presented in Table. 3.5.

Table 3.5: The effect of data augmentation (Scenario I) and contrast enhancement (Scenario II).

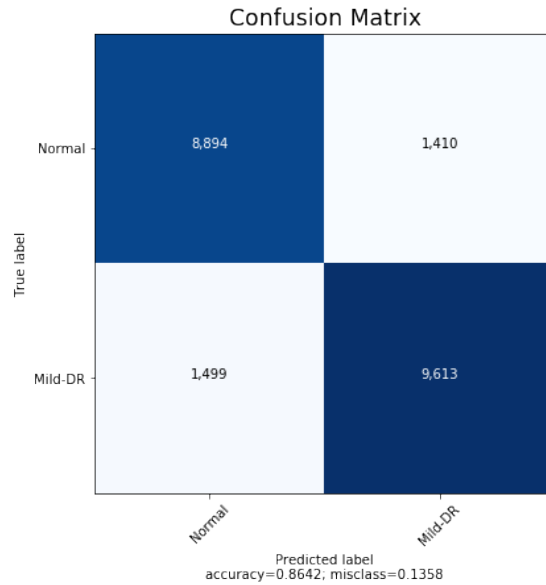
	Dataset	Accuracy	Sensitivity	Specificity
Scenario I	Messidor + Kaggle (aug)	86.42%	0.87	0.86
Scenario II	Messidor + Kaggle (aug + enh)	<u>89.15%</u>	<u>0.88</u>	<u>0.91</u>

Table 3.6: Proposing New CNN on (Scenario II).

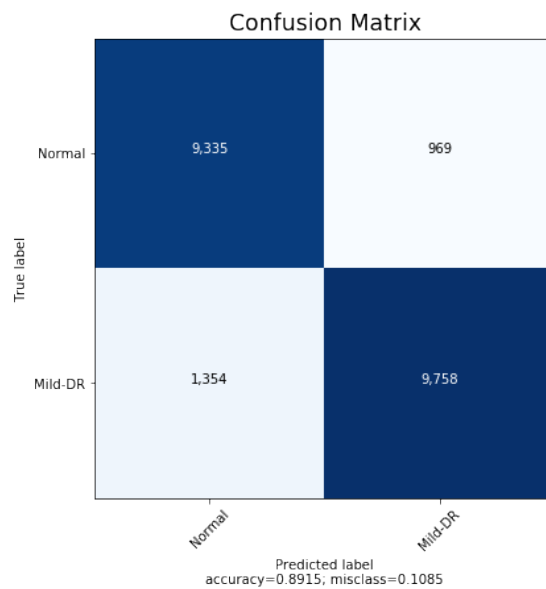
	Dataset	Accuracy	Sensitivity	Specificity
Scenario II	Messidor + Kaggle (aug + enh)	<u>100%</u>	<u>100</u>	<u>100</u>

3.3.4 System Evaluation

Increasing life expectancy, popular indulgent lifestyles and other contributing factors indicate that the number of people with Diabetes is projected to raise [153,173]. This in turn places an enormous amount of pressure on available resources and infrastructure [186]. For instance, most of the patients with DR in China often neglect their condition and fail to secure timely interventions resulting in severe state development [243]. Early identification of pathological indications effectively prevents further condition aggravation, and its impact on the affected individuals, their families, and associated medical expenses.



(a) Data augmentation (Scenario I)



(b) Contrast enhancement (Scenario II)

Figure 3.6: Confusion matrices for Scenario I and Scenario II.

Thus, DR detection system allows to either (i) fully-automate the eye-screening process; or (ii) semi-automate the eye-screening process. First option requires sufficient level of accuracy, equivalent to that of retinal experts. According to British Diabetic Association (BDA) guidelines, a minimum standard of 80% sen-

sitivity and 95% specificity must be obtained for sight-threatening DR detection by any method [18]. After evaluation of our approach on Mild DR detection task, the maximum sensitivity of 88% and the maximum specificity of 91% were obtained. Thus, the early DR detection proved sufficient given the BDA standards, but still falling 4% short in terms of its specificity. Second option allows to downsize the large-scale mass-screening outputs to the potential DR cases, followed by human examination. Both scenarios significantly reduce the burden on skilled ophthalmologists and specialised facilities, making the process accessible to wider population, especially in low-resource settings.

3.3.5 Performance Analysis

The first part of the experiment included feature extraction initialised via Transfer learning using the pre-trained CNN models, followed by the removal of the top layer (existing approach). The comprehensive evaluation of 13 CNN architectures (including state-of-the-art) was performed. In the second part, the N layers were 'un-frozen' (over the threshold of 100), and subsequently re-trained to better adapt to the specifics of the application case-study (proposed approach). The combination of Messidor and Kaggle datasets was conducted to further support model generalisation, given the variety of images provided for system training, as well as to benefit the model performance due to higher volume of training examples. The size of data used in training greatly affects the outcome of Neural Networks process [65]. The numerous pre-processing steps were implemented to measure potential accuracy improvement for No DR/Mild DR image classification. As Mild DR proves extremely challenging to differentiate from healthy retina due to only subtle indications of the disease,

the data augmentation undertaken was expected to enhance pathological features visibility (e.g. zoom and crop).

The top 3 CNN architectures with the top layer removed and re-trained were *VGG19*, *ResNet50* and *NASNetLarge*, yielding the accuracy of 81.3% for each (Table. 3.3). The lowest performance was obtained by *DenseNet169* (56.9%) and *MobileNet* (58.3%), respectively. In terms of *DenseNet169*, the characteristic feature of its structure that connects each layer to every other layer in a feed-forward manner did not prove to enhance the performance on No DR/Mild DR classification task. As for *MobileNet*, the results only confirmed its intended purpose for mobile applications due to its lightweight and streamlined architecture, which comes at a cost of the accuracy.

The effect of fine-tuning (un-freezing the layers from 100 onwards) differed across the models. Accuracy improvement observed was only minor, suggesting the relative suitability of default pre-trained models to DR detection task. In other words, the CNN models were able to identify Mild DR from healthy retina despite being trained on un-related pictures from ImageNet repository. If no accuracy increase is achieved, the un-freezing of further layers is not recommended due to unnecessary computational time and cost incurred.

To complete the analysis on the effect of fine-tuning, the graphs depicting each CNN architecture performance at the respective epochs (single pass of the full training set) has been performed, as illustrated in Fig. 3.5. Despite no major influence on the classification accuracy, faster model's convergence was observed following the fine-tuning. The higher number of layers un-frozen and re-trained made the models more task-specific, leading to an improved use of resources due to reduced training time for the most optimal performance. The

finding was particularly noticeable for the following models *Xception*, *MobileNet* and *DenseNet169*.

Next, the various optimisers have been evaluated on the top 3 CNN architectures (Table. 3.4). While there was no major impact on the classification performance for *VGG19*, the higher variability was observed for *ResNet50*, proving its sensitivity to the most suitable optimiser selection. Overall, RMSProp proved the most optimal choice for 2 out of 3 models. *ResNet50*+RMSProp was selected as the max-accuracy model+optimiser option for No DR/Mild DR classification task.

In the final step, the 2 scenarios were considered, namely (i) data augmentation, and (ii) contrast enhancement. As expected, data augmentation applied to lower quality Kaggle data, and its combination with Messidor data resulted in classification accuracy improvement from 81.6% to 86.4%. Images augmentation (i.e. crop, zoom, mirror, rotate) also helped to address data imbalance problem due to large number of healthy retina instances. The improved accuracy can further be attributed to greater variability in terms of training examples that in turn impact the generalisability of the approach. Additionally, contrast enhancement was applied on the augmented images, which has increased the classification performance to 89.3% (the maximum accuracy achieved). As a result, the max classification accuracy on No DR/Mild DR classification task was achieved for *ResNet50* model with fine-tuning and RMSProp optimiser trained on the combined Messidor + Kaggle (aug) + (enh) data sets.

Future work: As it is the initial study focusing on binary No DR/Mild DR classification, future work will cover finer-grained information extraction from cases previously identified as Mild DR. For instance, upon sufficient data avail-

ability, the model will allow to recognise the particular lesions such as exudates or aneurysms. The more in-depth classification will further assist the retinal practitioners in more efficient eye-screening procedure. Also, the highly varied input data (e.g. in terms of ethnicity, age group, level of lighting) will support model robustness and flexibility. Additionally, different scenarios with respect to the number of layers and nodes will be evaluated as increased convolution layers are expected to learn deeper features by the model [65, 153]. This in turn will enable the most optimal CNN architecture design (depth and width of the network) for maximum classification accuracy. An increase network dimensionality is the most direct way to enhance model performance [219]. Future work will also place more emphasis on outputs visualisation in order to obtain greater insight into the models internal workings. In particular, the identification of exact image regions that are associated with specific classification results will be highlighted, as well as the magnitude of each feature intensity (so called attention/saliency maps [150]). Improved understanding of algorithm workings will facilitate the automated system wider adoption and acceptance among physicians [225]. Finally, the experiments with ensemble approach will be conducted, where the results of Neural Network models trained on the same data will be averaged in order to evaluate further classification accuracy gains.

3.4 Summary of Findings

Early detection and immediate treatment of DR is considered critical for irreversible vision loss prevention. The automated DR recognition has been a subject of many studies in the past, with main focus on binary No DR/DR classification [153]. According to the results, an identification of moderate to

severe indications do not pose major difficulties due to pathological features high visibility. The issue arises with Mild DR instances recognition, where only minute lesions prove indicative of the condition, frequently undetected by the classifiers. Mild DR cases prediction is further challenged by the low quality of fundus photography that additionally complicates the recognition of subtle lesions in the eye. Thus, the study proposed the system that focuses entirely on Mild DR detection among the No DR instances, as unaddressed sufficiently in prior literature. Given the empirical nature of Deep learning, the numerous performance improvement techniques have been applied (i.e. (i) fine-tuning, (ii) optimiser selection, (iii) data augmentation, and (iii) contrast enhancement). Additional benefit of Deep learning incorporates the automatic features detection that are most discriminative between the classes. Such approach allows to avoid the shortcomings associated with empirical, and often subjective manual feature extraction methods. Furthermore, the study used the combined datasets from various sources to evaluate system robustness in its ability to adapt to the real-world scenarios. As stated by Wan et al. [219], the single data collection environment poses difficulty in accurate model validation. The system successfully facilitates the streamlining of labour-intensive eye-screening procedure, and serves as an auxiliary diagnostic reference whilst avoiding human subjectivity.

CHAPTER 4

ROLE OF IMAGE PROCESSING IN DETECTING MILD DED CLASSIFICATION AND DETECTION

DED is a cluster of eye problem that affects diabetic patients. Identifying DED is a crucial activity when using retinal fundus images because early diagnosis and treatment can eventually minimize the risk of visual impairment. The retinal fundus image plays a significant role in early DED classification and identification. The development of an accurate diagnostic model using a retinal fundus image depends highly on image quality and quantity. Therefore, this chapter presents a methodical study on the significance of image processing for DED classification with a compelling image processing technique that will enhance the classification system's performance. The proposed automated classification framework for DED was achieved through several steps: image quality enhancement, image segmentation (region of interest), image augmentation (geometric transformation), and classification. The dataset was obtained from various open sources. The optimal results were obtained using traditional image processing methods with a newly built CNN architecture. The classification outcomes were highly dependent on image processing. The transfer learning based on VGG-16 integrated with the traditional image processing approach provided an accuracy of 83.43% for diabetic retinopathy (DR), 89.13% for diabetic macular edema (DME), and 88% for glaucoma (GL). However, the newly built CNN combined with the traditional image processing approach presented the best performance with an accuracy of 93.33% for DR, 91.43% for DME, 100% for GL in the early stage of DED classification. The results of the experiments conducted show the necessary accuracy, specificity, and sensitivity.

4.1 Introduction

DED is the most common complication in diabetes, for which retinal fundus imaging is the most commonly adopted procedure because of its sensitivity in the diagnosis of DED [88]. The analysis of the severity and intensity of DED correlated with a patient having diabetes is typically conducted by ophthalmologists based on the lesion present in retinal fundus images [207]. For instance, Fig. 4.1 presents the details on lesions that must be identified from retinal images: (i) extra growth of blood vessels and damage or rupture in the tiny blood vessels in the retina (microaneurysms), often known as an early stage of DR; (ii) built-up fluid causing swelling in the macular region or often forming soft exudates known as DME, the common reason for blindness and vision loss, and (iii) damage to the optic nerve and blood vessel rupture causing intraocular pressure that damages the optic nerve causing Gl which is irreversible.

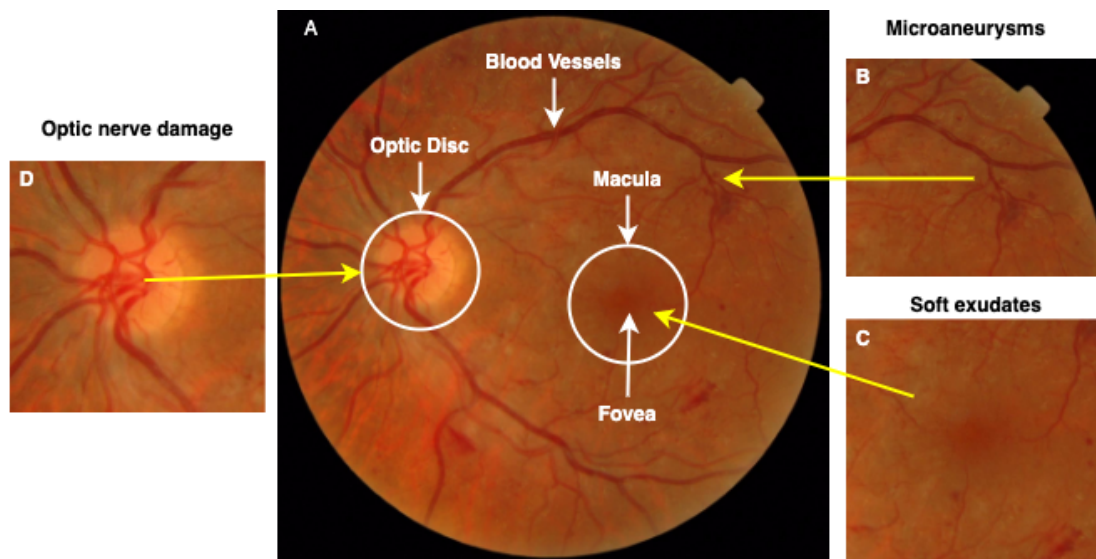


Figure 4.1: Early DED complication in retina (A) Anatomical structure of the retina; (B) Microaneurysms - narrow bulges in blood vessels (diabetic retinopathy); (C) Soft exudates in macula (diabetic macular edema); (D) Optic nerve damage (glaucoma); and (E) cataract

While the number of diabetic patients is growing exponentially, there is also a rise in the number of retinal fundus images obtained from screening campaigns, which, has resulted in considerable labour-intensive, time-consuming and complex work for medical experts. This complexity has driven the development of an automated retinal lesions detection system. In the past few years, a CNN in the DL system has played a significant role in medical image classification. CNN's widespread use in image classification came after Krizhevsky et al. [105] won the 2012 Imagenet [162] Large Scale Visual Recognition Challenge (ILSVRC) with a CNN with an error rate of 15%. The studies employing DL for DED detection demonstrate maximum performance in binary classification (normal / severe) cases. Lam et al. [109] used the GoogLeNet model and obtained a maximum sensitivity of 95% and specificity of 96% using real-time data augmentation with preprocessing techniques.

In DL, a pre-trained CNN can be used to *transfer learning* from source task to target task with a limited number of images or minimise training time. The most popular *transfer learning* method is to fine-tune the pretrained network. Regardless of the nature of the training model (pre-trained model or a new model), image data sets are typically pre-processed prior to training CNN architectures in various ways, such as image resizing, image quantity, image standardisation, and image enhancement. Improving the classification performance of the CNN model is limitless, and the image quality in the data set has a significant impact on the overall performance of the architecture.

Motivation: DL has had a significant impact on a number of scientific fields over the last few years. These include advancements in image and speech recognition, the ability to train artificial data that beat human players in games like

ATARIS [124] and GO [182], and the development of new creative images using methods like Generative Adversarial Networks (GAN) [205], and music [26]. Several of these activities were considered onerous, needing to be accomplished by algorithms before the development of DL. The DL framework is also extremely relevant for imaging. Image detection, recognition, segmentation, registration, and computer-aided diagnosis are some of the areas that have been primarily affected by its rapid development.

However, in medical imaging (e.g., retinal fundus images), early-stage identification of lesions and abnormalities is still an open issue reported in previous literature by Lam. et al. [109]. Pratt et al. [153] and Carson et al. [109] mentioned that deep neural networks are struggling to learn enough in-depth features to identify aspects of mild disease, with 93% of mild cases are wrongly classified as a healthy eye. Therefore, this research presents a system in which traditional image processing techniques and state-of-the-art CNN are combined to analyze early-DED disease. This chapter presents a research study using a small volume of the open-source retinal images for in-depth learning evaluation for normal and mild DED classification.

Contribution: Therefore, in this thesis, the main objective is to achieve the highest accuracy, sensitivity, and specificity compared to existing deep learning models. The technique used is a combination of traditional image processing methods for image enhancement and segmentation, and then training in DL algorithms. We explore the significance of traditional image pre-processing for enhancing early stage DED detection accuracy using DL models. The advancement of this technology does not indicate the complete substitution of an ophthalmologist. Rather, it allows ophthalmologists to more reliably diagnose DED.

The contribution of this chapter in the diagnosis of early DED can be classified into the following:

- Image enhancement: green channel extraction, contrast limited adaptive histogram equalization (CLAHE), and illumination correction were used to enhance the original image
- Image segmentation: Regions of Interest (ROI) such as blood vessels, macular region and optic nerve segmented from retinal fundus images
- Pre-trained model: High-performance models were selected to classify the processed and segmented retinal fundus images
- Build a new CNN model and train the model from scratch with processed and segmented retinal fundus images.

4.2 Literature Survey

Early detection of DED in retinal fundus images relies on a clinical technique to visualize a comprehensive set of features and localization within the image. Detection is challenging for diabetic patients with early DED stages because it depends on the existence of microaneurysms (bulges in blood vessels), fluid leakage from blood vessels, soft exudates formation, and damage to the optic nerve. The stages of diabetic eye disease are shown in Fig.4.1.

In the past, automated DED diagnostics have been explored to ease the burden on ophthalmologists and minimise diagnostic inconsistencies [125]. Studies, have used lesion-based detection. Gharaibeh et al. [67] presented a new

approach to detect microaneurysms in retinal fundus images. Their work includes pre-processing methods like blood vessel segmentation, fovea localization, and elimination. They used a combination of neural networks and fuzzy logical models for feature extraction and classification. Their study addressed the binary classification of DR into two categories (microaneurysms and non-microaneurysms). Moreover, a range of features other than microaneurysms are appropriate for the diagnosis of DED.

Similarly, Kaur et al. [100] proposed region-based segmentation and detection of the lesion and then classified it using pixel-based classification to determine the severity level of the retinal disease. Karegowda et al. [98] detected exudates in DR using decision tree and GA-CFS techniques as input to back-propagation neural network. They classified the normal eye and eye with exudate. The results obtained were insufficient to provide reliable classification accuracy and did not result in efficient noise removal. Sopharak et al. [195] presented a fuzzy C-means and clustering-based exudate identification method. Their work mostly relied on the identification of optic disc and the elimination of blood vessels. According to the results obtained, the exudates are identified without their characteristics. Jenuja et al. [96] presented a method based on the optic disc and optic cup segmentation. The proposed method uses dual neural networks that operate in combination with the optical cup and disc parts. The aim of this proposed method is to efficiently segment the optic cup and disc of a retinal fundus image. The results of the classification of various stages of GL are not given. Earlier, Gulshan et al. [75] and Gargeya et al [66] presented CNN for DR detection using fundus images. They achieved specificity and sensitivity in the range of 90% for (normal/mild to moderate/severe) binary classification in private wider data sets comprising 80,000 to 120,000 fundus images.

There are many traditional strategies for DED diagnosis and classification. Most techniques use neural networks, mathematical morphology, region of interest techniques, pattern recognition, clustering of fuzzy C-means, and Gabor filter techniques. Chaudhuri et al. [35] used 2D matched filters, to detect the blood vessels present in the retina. Vallabha et al. [213] used Gabor filter bank outputs to identify the mild, moderate, and extreme stages of retinopathy. Automated detection and classification of abnormalities present in the vascular network are carried out. Sinthanayothin et al. [186] detected haemorrhages, microaneurysms, and exudates, by developing a system based on recursive area growth and Moat operator. Numerous methods have been suggested for optic disc detection. PCA is one of the methods by which the clustering of brighter pixels shows the candidate regions for the optical disc. Noronha et al. [131] used Hough Transform for Optic Disc detection. For the detection of exudates, a NN-based approach is used by Gardner et al. [65]. A fuzzy C-means clustering method was employed by Bezdek et al. [22] and a computational intelligence-based approach by Osareh et al. [137]. The automatic classification of normal, mild, moderate, severe, and proliferative DR was carried out by measuring the areas of several characteristics, such as haemorrhages, microaneurysms, exudates, and blood vessels classified by the support vector machine [4].

However, the accuracy metrics for the diagnosis of the four categories of DR (i.e., no DR, mild, moderate, and severe), are based on disease-grade selection ratios. Although the no DR and severe stages are likely to achieve high sensitivity, the mild and moderate recall levels are often deficient. Research studies using publicly available datasets reveal difficulties in detecting early stage DEDs.

4.3 Methodology

This study's overarching objective is to improve the performance of early detection of DED from fundus images through the empirical assessment of image preprocessing and classification improvement techniques. The related objectives can be described as follows:

- Implementing traditional image processing techniques such as (i) image Enhancement, (ii) image Augmentation, (iii) image Segmentation
- Implementing various hyperparameters and evaluating their effect on CNN model performance
- Evaluating the accuracy obtained by pre-trained CNN models: *ResNet50*, *VGG-16*, and *Xception* with original and preprocessed fundus images
- Developing a new CNN model to train preprocessed fundus images for classification accuracy improvement
- Evaluating the results of the pre-trained and new CNN model by performance metrics.

The process pipeline is shown in Fig. 4.2.

4.3.1 Image Data Collection

Data was collected from publicly accessible sources, i.e., Messidor, Messidor-2, DRISHTI-GS, and the Retinal Dataset from GitHub. This section explains the data sets used in this chapter. The labelling of each image is generated

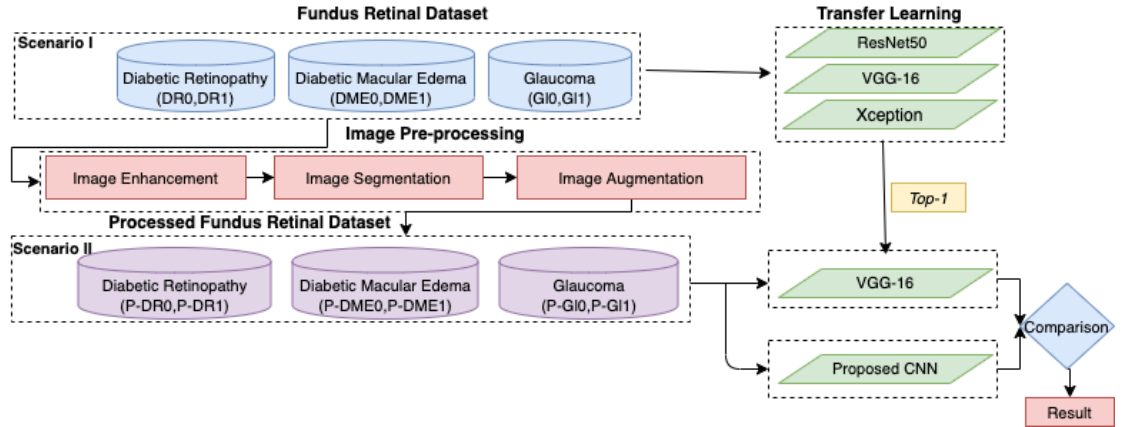


Figure 4.2: The high-level process pipeline

by the ophthalmologist. Depending on the number of haemorrhages, microaneurysms, and the presence of neovascularisation, each image is classified as one of three lesion grades. The *Messidor Dataset* was formed to promote computer-assisted DED studies. It contains 1200 retinal fundus images of the posterior pole from three departments of ophthalmology using a 3CCD colour video camera placed on a Topcon TRC NW6 non- retinograph with a 45° field of view (FOV). The medical experts offered two diagnostics for each image: *Retinopathy grade* and *Macular edema risk*. The *Messidor-2 Dataset* is a publicly accessible dataset used by individuals to evaluate DED algorithm performance. Messidor-2 comprised of 1,748 colour retina images of 874 subjects. Messidor-2 varies from the actual Messidor dataset of 1200 images and ensures that it has two images for each subject; one for each eye. Using the previously published ICDR and DME gradings, Messidor-2 provided four disease rates for each subject. *DRISHTI-GS Dataset* [190] There are 101 retinal images in the Drishti-GS1 dataset with 31 normal images and 70 GL lesion images. Due to the limited images obtained from DRISHTI-GS, we considered the GL dataset from the GitHub¹ *Retina Dataset* which contains 100 retinal images indicating GL lesions.

¹https://github.com/yiweichen04/retina_dataset/tree/master/dataset

Therefore, imbalance in the dataset caused us to perform under-sampling of the dataset. Thus, we selected 100 images from each class to perform our experiment.

4.3.2 Image Pre-processing

The preprocessing step is used to eliminate noise/variation in the retinal fundus image and improve the quality and contrast of the image. Apart from contrast enhancement and noise reduction, the preprocessing step can be used for image normalization and non-uniform intensity correction to eliminate artifacts and increase the accuracy of the process steps. Furthermore, DED features are localized, extracted and segmented from fundus images for further classification in pre-trained models. The pre-processing techniques utilized in this article are briefly discussed in this section.

Image enhancement: To enhance the original images' appearance and information value before processing, we used popular image enhancing techniques: contrast enhancement, and illumination correction. *Contrast enhancement:* Contrast limited adaptive histogram equalization (CLAHE) [251] is utilized to improve the visibility of images. CLAHE is an adapted part of the Adaptive Histogram Equalization (AHE) process. In this method, the enhancing function is introduced to all neighbourhood pixels, and the transformation function is derived. This is distinct from AHE for its limited contrast. In CLAHE, the contrast of the image is improved by implementing contrast limited histogram equalization (CLHE) to small data areas called tiles rather than the entire image. The resulting adjacent tiles are then perfectly stitched back utilising bilinear inter-

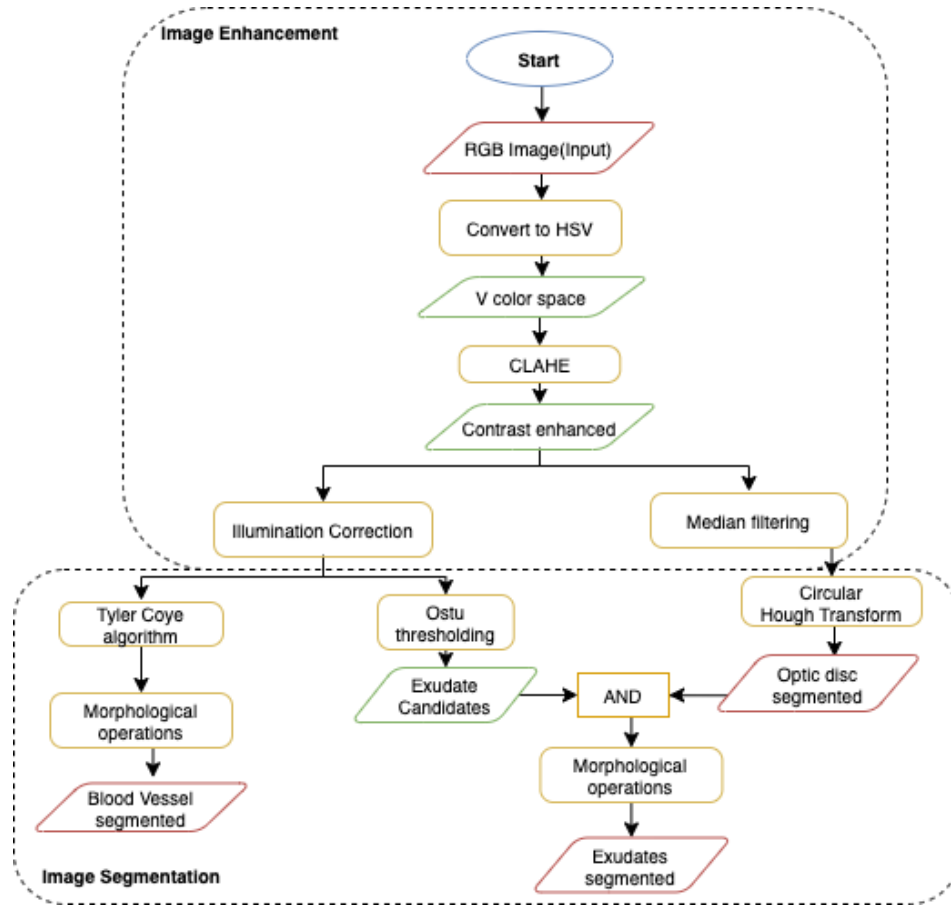


Figure 4.3: The flowchart.

pulation. CLAHE is applied to greyscale retinal images. The 'cliplimit' function is applied to limit noise in an image. Create grey level mapping and clip the histogram. In the contextual area, pixel numbers are divided equally at each grey level so that the average number of pixels is grey as follows:

$$n_{avg} = \frac{n_{CR-x_p} * n_{CR-y_p}}{n_{gray}} \quad (4.1)$$

Where, n_{avg} = average number of pixels, n_{gray} = number of gray level in contextual region,

n_{CR-x_p} = number of pixels in x direction of contextual region

n_{CR-y_p} = number of pixels in y direction of contextual region after that calculate the actual cliplimit.

$$n_{CL} = n_{CLIP} * n_{avg} \quad (4.2)$$

CLAHE [251] is an useful technique in biomedical image processing because it is very effective at making the normally important salient sections more accessible.

Illumination correction: This pre-processing method aims to reduce the scenario effect caused by the uneven illumination of retinal images. Every pixel intensity is calculated using the following equation:

$$p' = p + \mu_D - \mu_L \quad (4.3)$$

Where p , p' is the initial and the latest pixel size values, respectively, μ_D is the desired average intensity, and μ_L is the local average intensity [237]. Microaneurysms forming on the surface of the retina are enhanced with this method.

Image segmentation: To build an effective deep learning-based classification system for detecting mild DED, we need to consider the importance of the architecture of the network as well as the importance of input data. To obtain efficient results, input images play a significant role. In retinal fundus images, variability such as the number of images, luminosity, contrast, and anatomical features, determines the result of the automatic disease detection algorithm. Therefore, features segmentation enhances the value of the images for classification and contribute to better accuracy. The process and associated theory is explained in the following sections.

Blood vessels extraction: For the detecting early stages of DR, the blood vessels are one of the most significant anatomical features in retinal images. Thus, retinal blood vessel segmentation is performed with following steps: (i) image enhancement, (ii) Tyler Coye algorithm [45] and (iii) morphological operation for further improvement in results.

We performed image enhancement techniques as mentioned above, green channel of the RGB colour space presents better contrast between vessels network and background. The variation of contrast and luminosity in the background of a fundus image, can be estimate using method introduced by Zuiderveld [251] and Youssif et al. [237]. After contrast and luminosity adjustment, ISODATA used in Tyler Coye algorithm is used to extract the threshold level. After the Tyler Coye algorithm, morphological operation (erosion and dilation) is used for further enhancement. Using these two essential fundamental operations, we reduce noise or remove of gaps in the background and foreground. Erosion is a procedure used to eliminate or spike the edge of the area, which is represented in the following equation:

$$A \ominus B = \{p|B_p \subseteq A\} \quad (4.4)$$

Dilation is a procedure employed to broaden the rim of the background or foreground image configuration. This procedure is widely used to fill a gap, and can be defined in the following equation:

$$A \oplus B = \{x|B_x \cap X \neq 0\} \quad (4.5)$$

Closing is to perform the dilation, followed by erosion, to create a relation between each pixel of the image in order to bring them closer to one another. This procedure can be defined in the following equation:

$$A \cdot B = (A \oplus B) \ominus B \quad (4.6)$$

Where, \oplus denote the dilation; \ominus denote the erosion; A = Structuring element and B = the erosion of the dilation of that set. However, several gaps remain in Tyler Coye algorithm. This morphological process is to fill these small gaps in order to cover some of the required regions of the blood vessels.

Optic disc detection and extraction: GL occurs when the optic nerve is damaged so segmentation of the optic disc (OD) helps to obtain a clearer view of the anatomical changes in the optic nerve. Fig. 4.1 shows a fundus image of an eye from our collected data set with anatomical parts showing OD. To segment the OD, we applied the following steps: (i) image enhancement, (ii) Circular Hough Transform (CHT) to detect circular object, (iii) median filter to reduce noise, and (iv) optic disc segmentation using the threshold values. Image processing attempts to improve the quality of the retinal fundus image to enable the identification of clinical features for DED. A flowchart of the image processing and image segmentation approach is depicted in Fig. 2.3. CLAHE can not be employed in the entire image, but only on a specific area 'tile' of the image.

Image enhancement calculation is adjusted on the basis of the user-specific maximum contrast rate level by setting its rate to l , $0 \leq l \leq 1$ [193]. Further contrast enhancement is performed in those images which have low contrast estimated by

$$\phi(i, j) = \left(\frac{\mu(i, j) - \Delta}{\delta - \Delta} \right) (\Gamma - 1) \quad (4.7)$$

Where, $\phi(i, j)$ and $\mu(i, j)$ are pixels after transformed and pixels before transformed in (i, j) coordinates, respectively; Δ is maximum pixel value; δ is minimum pixel value of input image and Γ is maximum value of gray scale.

The median filtering has a strong noise reduction efficiency and it is very common in image processing for noise removal. Mean filtering replaces the pixel value in the middle of the sliding window with the median value of the pixels in the window. Mathematically median filtering is represented by:

$$f(x, y) = \text{median}_{(s,t) \in S_{xy}} \{g(s, t)\}. \quad (4.8)$$

Segmentation is a pixel classification method for extracting objects or segmenting regions with a similar to the background [178]. Therefore, we used the Circular Hough Transform (i.e. CHT) method for optical disc detection. The CHT method is often used to identify the circular shape in an image. The key benefit of the CHT approach is that it is sensitive of differences in feature specification descriptions as well as being largely unaffected by image noise. The CHT is provided by the equation:

$$(x - a)^2 + (y - b)^2 = c^2 \quad (4.9)$$

The procedure to detect circles involves the following steps:(i) obtain a binary edge map of the image, (ii) values for a and b are set, (iii) obtain the value of c radius that satisfies Equation 4.7, (iii) adjust the accumulator corresponding to (a,b,c) , (iv) change the values for a and b within the scope of interest and return to Phase (iii).

Exudate localization and detection: Exudates in two-dimensional retinal images acquired via a digital fundus camera, usually appear as a bright area with varying scale, brightness, position and form. Precise exudate segmentation is a difficult activity given the large variety of scale, intensity, contrast and shape. It comprises of three major processing stages: (i) image enhancement; (ii) optic disc detection and removal; (iii) blood vessel removal; and (iv) exudate

extraction. When exudate are acquired from the mild dataset, the classification of the DME can be performed according to the grading criteria mention in the messidor dataset. Early DME can be diagnose early by detecting the presence of exudates in fundus images. Fig. 4.1 shows the exudates formation in the macular region. After *optic disc detection and removal* performed, Otsu thresholding is applied to obtain candidate areas of exudates. Threshold value T relying on the input image is estimated by Ostu method, automatically. First, the intensity value i of histogram is calculated using Equation 4.10:

$$p(i) = \frac{n_i}{N}, p(i) \geq 0, \sum_1^{256} p(i) = 1 \quad (4.10)$$

The number of pixel images N and the number of pixels n_i with I intensity. Subject weight and background are described in Equations 4.12 and 4.13:

$$w_1(t) = \sum_{i=1}^t p(i) \quad (4.11)$$

$$w_2(t) = \sum_{i=t+1}^L p(i) = 1 - w_1(t) \quad (4.12)$$

Here, the number of the gray level is L . The mean of the object and the background is then determined using Equations 4.14 and 4.15:

$$m_1(t) = \sum_{i=1}^t i.p(i)/w_1(t) \quad (4.13)$$

$$m_2(t) = \sum_{i=1}^t i.p(i)/w_2(t) \quad (4.14)$$

Hence, variance is estimated by Equations 4.16 and 4.16, while the total of variance is expressed in Equation 4.18 as follows.

$$\sigma_1^2(t) = \sum_{i=1}^t (1 - m_1)^2 \cdot \frac{p(i)}{w_1(t)} \quad (4.15)$$

$$\sigma_2^2(t) = \sum_{i=t+1}^t (1 - m_2)^2 \cdot \frac{p(i)}{w_2(t)} \quad (4.16)$$

$$\sigma^2(t) = \sigma_w^2(t) + \sigma_B^2(t) \quad (4.17)$$

Here, σ_w is called as within-class variance (WVC) that is expressed in Equation 4.19, while σ_B called between-class variance (BVC) that is expressed in Equation 4.20. WVC is the amount of individually class variance that has been weighted with probability of each class. Average total is calculated using Equation 4.21. Threshold value can be obtained from the minimisation of WVC or maximisation of BVC; but BVC has less computation time:

$$\sigma_w^2(t) = w_1(t) \cdot \sigma_1(t)^2 + w_2(t) \cdot \sigma_2(t)^2 \quad (4.18)$$

$$\sigma_B^2(t) = w_1 \cdot [m_1(t) - m_T]^2 + w_2 \cdot [m_2(t) - m_T]^2 \quad (4.19)$$

$$m_T = \sum_{i=1}^N i \cdot p(i) \quad (4.20)$$

Morphological is a set of discrete coordinates that are related to a pixel object of an image that involves a logical operation, such as “or” and “and”. The opening operation aims to refine the object contour and repair the object contour with an eliminated pixel area that is smaller than the structure element.

$$AoB = (A \odot B) \oplus B \quad (4.21)$$

Image Augmentation: DL models perform well with high volume training data. Therefore, data augmentation is comprised of a collection of techniques that improve the quantity of training data without actively acquiring new data. Thus, the image augmentation algorithms addressed in this chapter include geometric transformations such as flipping, rotating, mirroring, and cropping. We used the Keras *ImageDataGenerator*² class for real-time image augmentation, which ensures that the selected model will obtain variations of the images at every epoch. The advantage of using the *ImageDataGenerator* class in our work is that transformed images will not add to the range of original images, which avoid overfitting the selected model.

4.3.3 Model Development

In this research, we are using CNN-based transfer learning to implement the DED retinal fundus image classification. To accomplish the absolute best classification outcomes, we explore pre-trained CNN model transfer learning techniques. The precise details of the pre-trained models will be presented in this section.

According to Pan et al. [140] transfer learning is defined as; $D = \Phi, P(X)$ with $X = x_1, x_2, \dots, x_n \in \Phi$, where, D is domain, Φ is feature space and $P(X)$ is the marginal probability distribution. Given, $T = Y, F(*)$ where, T is given task, Y is refers to a label space and $F(*)$ is an objective predictive function that is

²<https://keras.io/api/preprocessing/image/>

learned from the feature vector and label pairs. Specifically, given a source domain D_s with learning task T_s and a target domain D_t with learning task T_t , then transfer learning is the process of improving the learning of the target predictive function $F_t(*)$ in D_t based on the knowledge learned from source domain D_s and learning task T_s , where $D_t \neq D_s$, or $T_t \neq T_s$. It should be noted that the single source domain described above can be expanded across multiple source domains.

The concept behind transfer learning for the classification of images is that, if a network is typically trained on a broad scale and enough data set (e.g., ImageNet), it can effectively train in the particular target task, which has fewer labelled examples than the pre-training dataset. One can benefit from these learned feature maps without training a large model from scratch on a large dataset.

In this chapter, we will customize pre-trained models in two ways: (i) *Feature Extraction*: features learned from the source task to extract useful features from the target task. We added a new classifier, which can be trained from scratch to the top of the pre-trained network to modify the features maps initially learned for the sample. (ii) *Fine-Tuning*: unfreeze some of the last layers of the frozen base network and collectively train the last layers of the base network and the newly added classifier layers. This helps to "fine-tune" the higher-order character representations in the base network to make them more appropriate to the target task. We fine-tune three pre-trained CNNs (Xception, VGG-16, and DenseNet21) to implement DED image classification. Three CNN pre-trained networks on ImageNet and their characteristics are described in Table 4.1.

Table 4.1: Three CNN models pre-trained on ImageNet and their characteristics (source: <https://keras.io/applications>)

Model	Size	Top-1 Accuracy *	Top-5 Accuracy *	Parameters	Depth **	Reference
<i>Xception</i>	88 MB	0.790	0.945	22,910,480	126	Chollet [43]
<i>VGG16</i>	528 MB	0.713	0.901	138,357,544	23	Simonyan and Zisserman [183]
<i>DenseNet21</i>	33 MB	0.750	0.923	8,062,504	-	Huang et al. [87]

* The top-1 and top-5 accuracy refers to the model’s performance on the ImageNet validation dataset

** Depth refers to the topological depth of the network. This includes activation layers, batch normalisation layers etc

4.3.4 Proposed CNN Model

CNNs are the most popular DL algorithms which train the medical images for the classification of medical image abnormalities [118]. The explanation for this is that while analyzing input images, the CNN preserves distinctive features. Spatial relationships, such as where the blood vessels start rupturing or how yellow fluid starts accumulating near the macular region, are of primary importance in retinal images, as we discussed above. The framework of the process is shown in Fig. 4.4, and Table 4.2 shows the selected hyperparameters. There are five convolution layers in this proposed CNN model, which take as its input a retinal fundus image tensor of 244×244 .

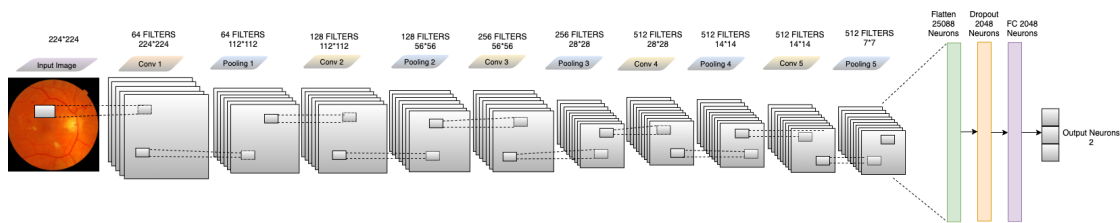


Figure 4.4: The proposed CNN model

The first convolution layer uses $5 \times 5 \times 3$ kernel filters with stride 1×1 , and a total of 64 such filters are employed. The next layer, which receives the output from the first layer, is a max-pooling layer with 2×2 stride, reducing the input

Table 4.2: Hyper-parameters of the build CNN model and preferred weights in this study.

R1	R2	R3	R4	R5	R6	R7	R8
CNN	224*224	RMSprop	32	10-fold	3e-4	BCE	50

Legend: R1 - Model, R2 - Image Size, R3 - Optimizers, R4 - Mini Batch Size, R5 - Cross validation, R6 - Initial Learning Rate, R7 - Loss function, R8 - Epoch, BCE - Binary cross-entropy

to half of its size 112×112 . For all layers, the output from the pooling layer passes through the ReLU activation feature. The nonlinear output obtained is now fed into the next convolution layer with $5 \times 5 \times 64$ with 128 filters, and the stride value is the same 1×1 . The obtained output pass through a max-pooling layer with the same 2×2 strides, which again reduces the input to half of its size 56×56 . After the output passes through ReLU activation, it is fed into the third convolution layer with 256 filters and the kernel size $5 \times 5 \times 128$ with 1×1 stride. The output is passed to a max-pooling layer, which results in a tensor of shape 28×28 . Again, the output passes through ReLU activation, fed into the fourth convolution layer with 512 filters and kernel size $5 \times 5 \times 256$ and with the same stride 1×1 . The output from the fourth convolution is max-pooled to a size of 14×14 . After ReLU is activated and it is passed to a fifth convolution layer with 512 filters and $14 \times 14 \times 512$ kernel size to accommodate the output of all the filters from previously configured layers, and max-pooling of output from that layer with a stride of size 2×2 produces an output of size 14×14 . Now the resulting tensor has the shape $7 \times 7 \times 512$. The obtained tensor is flattened with 25,088 neurons. The weighed values that emerge as neurons demonstrate the proximity to the symptoms of DED. The dropout layer is applied here to drop values to handle network overfitting. In this work, we used a dropout rate of 0.5 during training. The fully connected layer converts the tensor with 25,088 neurons to 64 neurons and adds ReLU activation to the output. These

64 neurons is the product of the fully connected layers; these 64 neurons are translated into neuron counts equal to the number of categories to which the retinal image belongs: healthy, DR, GL, and DME.

4.3.5 Performance Evaluation

Different metrics have been used to evaluate the effectiveness of the highest performing DL model. To calculate the true or false classification of the DED diagnosed in the fundus images evaluation is as follows. Initially, the cross-validation estimator [192] is adopted and plotted in a confusion matrix as shown in Table 4.3. The confusion matrix has the following four predicted outcomes. True Positive (TP) has been identified with the right diagnosis and a variety of abnormalities. True Negative (TN) is an erroneously calculated number of periodic instances. False positives (FP) are a set of periodic instances. The following performance metrics are used to calculate the values of possible outcomes in the confusion matrix.

Accuracy: Accuracy is an essential metric for the evaluation of the results of DL classifiers. It is a summary of the true positive and true negatives divided by the confusion of the matrix components' total values. The most accurate model is an excellent one, but it is imperative to ensure that symmetric sets of data with almost equal false positive values and false negative values. Thus, the elements of the confusion matrix mentioned above will be calculated to evaluate the effectiveness of our proposed classification model for the DED dataset:

$$Accuracy(\%) = \frac{TP + TN}{TP + FN + TN + FP} 100\%. \quad (4.22)$$

Table 4.3: Confusion Matrix

	P Positive	P Negative	Total
A Positive	TP	FN	$TP + FN$
A Negative	FP	TN	$FP + TN$
Total	Se	Sp	

Legend: A Positive = Actual Positive, A Negative = Actual Negative, P Positive = Predicted Positive, P Negative = Predicted Negative, TP = True Positive, FN = False Negative, FP = False Positive, TN = True Negative, Se = TP + FP, Sp = FN + TN

Sensitivity (Recall): Sensitivity is measured as the number of accurate positive predictions divided by the sum of positive. The best sensitivity is 1.0, whereas the worst is 0.0. We calculate sensitivity using following equation:

$$Sensitivity = \frac{TP}{TP + FN} \quad (4.23)$$

Specificity: Specificity is measured as the number of correct negative predictions divided by the sum of negatives. The best specificity is 1.0, and the worst is 0.0. We calculate sensitivity using the following equation:

$$Specificity = \frac{TN}{TN + FP} \quad (4.24)$$

4.4 Experiment Design and Analysis

4.4.1 Experiment Design

All the experiments were implemented using MatLab, Python, Keras library1, with TensorFlow2 as a back-end and Python 3.8 programming language in a

Jupyter Notebook with a processor 2.3 GHz Intel Core i9 and RAM of 16 GB 2400 MHz DDR4 with Intel UHD Graphics 630 1536 MB. The training/testing data split was set at 80/20. The segregated generic selection was conducted to ensure an approximately equal distribution of the class. Mini-batch size was set to 32, and the cross-entropy loss function was chosen due to its suitability for binary classification tasks. The Optimiser was set as default (Adam) and RMSprop for build CNN. The standard performance evaluation metric accuracy, sensitivity and specificity of the test dataset were used to validate the results.

4.4.2 Model Training

We compared and analysed performance accuracy for three distinct pre-trained DL models with the newly built CNN model. The three pre-trained models, namely; *Xception*, *VGG16*, and *DenseNet21* and five-layered convolutional model were evaluated for test data set accuracy (Table 4.1). The pre-trained models adopted for this research were trained and tested with large-scale ImageNet data, covering a wide range of categories such as cars, animals, flowers, etc. Models acquire excellent performance image classification for objects while demonstrating a limitation in their application to narrow product areas, such as medical lesion (DED) detection. The prognosis of pathological indications in the retinal fundus images depends on various complex characteristics and lesion localization in the retinal fundus image. There is a new representation of the input image in each CNN layer by progressive extraction of the most distinctive features. For instance, the first layer is capable of learning edges, while the last layer can identify a lesion as a DED classification feature. As a result, the following scenarios were considered in the experiments: Region of Interest

such as blood vessels, macular regions and the optic disc were detected, localized and segmented.

We employed a combination of multiple traditional image segmentation algorithms for each phase of the proposed system. All of these algorithms provided effective results in the segmentation of the Region of Interest. We performed a series of procedures to build a high-performance system, such as image enhancement, blood vessel segmentation, identification and then extraction of optic discs, extraction of macular region, blood vessels removal, elimination of optic discs, extraction of features, and classification of features. After segmentation, the image size of the images has been optimised to a suitable size following the input specifications of each network. To minimise the risk of model overfitting, the imbalance dataset was augmented using the real-time augmentation *ImageDataGenerator* class from Keras. Fine-tuning was used for pre-trained models after eliminating and re-training n layers (n was CNN layer-dependent). The final output acquired for each model was used for comparison in terms of percentage accuracy, and these are represented in Tables 4.4 and Table 4.5. VGG16 classification surpassed the other two fully-trained DL models, Xception and DenseNet121. Similarly, among all pre-trained models, the newly built CNN model using pre-processed retinal images performed well. Tables 4.6 and Table 4.7 compare the accuracy of results. The built CNN's accuracy surpasses all the models used for classification.

To detect retinal anomalies, we developed more general screening classification models. The confusion matrix and ROC curves of each pre-trained deep learning model and a built CNN model for binary classification of healthy and other DED disease status are shown in Fig. 4.5, 4.6, 4.7, and Fig. 4.8, 4.9, 4.10.

Table 4.4: Average performance of the models on original images

DED	Model	Accuracy	Sensitivity	Specificity	Precision
Normal /Mild DR	<i>Xception</i>	60.87%	67%	58%	43%
	<i>VGG16</i>	80.43%	76.92%	85%	74%
	<i>DenseNet121</i>	56.67%	71.43%	53.85%	96%
Normal /Mild DME	<i>Xception</i>	62.07%	65%	60%	52%
	<i>VGG16</i>	85.79%	90%	81%	78%
	<i>DenseNet121</i>	51.72%	100%	51%	28%
Normal /Mild GL	<i>Xception</i>	63.41%	85.71%	58.82%	95%
	<i>VGG16</i>	87.80%	94.12%	83.33%	95%
	<i>DenseNet121</i>	80.49%	77%	84%	76%

Legend: DED = Diabetic Eye Disease DR = Diabetic Retinopathy, DME = Diabetic Macular Edema, GL = Glaucoma.

Table 4.5: Average performance of the VGG16 model on pre-processed images

DED	Model	Accuracy	Sensitivity	Specificity	Precision
Normal /Mild DR	<i>VGG16</i>	83.43%	86%	85.71%	78%
Normal /Mild DME	<i>VGG16</i>	89.13%	85%	95%	96%
Normal /Mild GL	<i>VGG16</i>	88%	95%	90%	90%

Legend: DED = Diabetic Eye Disease DR = Diabetic Retinopathy, DME = Diabetic Macular Edema, GL = Glaucoma.

4.4.3 Performance Analysis

This research is a study of binary classification DL algorithms to identify three mild diabetic eye diseases automatically. This research has shown that the complexity of the DL algorithms arises from the quality and quantity of data (fundus images), not from the algorithm. In this research, we used publicly available an-

Table 4.6: Average performance of the New proposed model on original images

DED	Model	Accuracy	Sensitivity	Specificity	Precision
Normal /Mild DR	<i>CNN</i>	63.33%	53.33%	73.33%	61%
Normal /Mild DME	<i>CNN</i>	82.86%	83.33%	82.35%	82%
Normal /Mild GL	<i>CNN</i>	96.77%	100%	93.75%	100%

Legend: DED = Diabetic Eye Disease DR = Diabetic Retinopathy, DME = Diabetic Macular Edema, GL = Glaucoma.

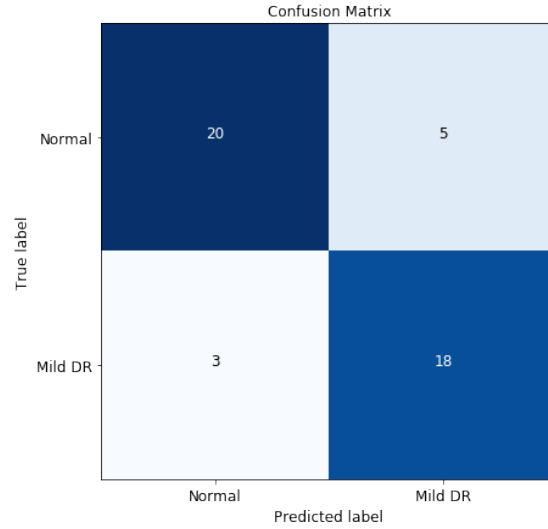
Table 4.7: Average performance of the new proposed model on pre-processed images

DED	Model	Accuracy	Sensitivity	Specificity	Precision
Normal /Mild DR	<i>CNN</i>	93.33%	100%	86.67%	100%
Normal /Mild DME	<i>CNN</i>	91.43%	94.44%	88.24%	94%
Normal /Mild GL	<i>CNN</i>	100%	100%	100%	100%

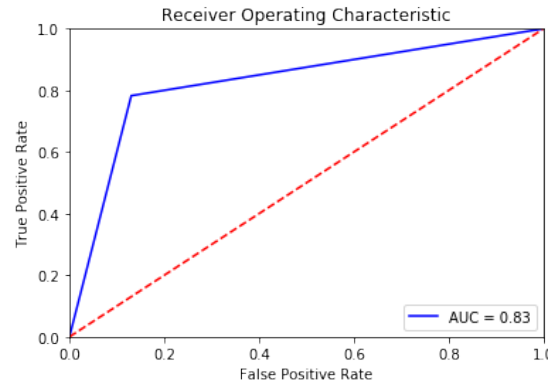
Legend: DED = Diabetic Eye Disease DR = Diabetic Retinopathy, DME = Diabetic Macular Edema, GL = Glaucoma.

notated data (fundus images). For a computer-aided clinical application, more robust, practical, and realistic results can be obtained using labelled hospital fundus images. Indeed, this chapter recommends that the automatic classifier strive to classify against the binary classification of at least average, DR, DME, and GL due to each disease's significance. These three diseases are the major retinal diseases caused by diabetes. Unless an initial evaluation is conducted, these diseases always cause severe damage to the visual acuity, and it is irreversible [24, 153].

Growing life expectancy, busy lifestyles, and other factors suggest that the number of people with diabetes will increase [153]. For example, many pa-



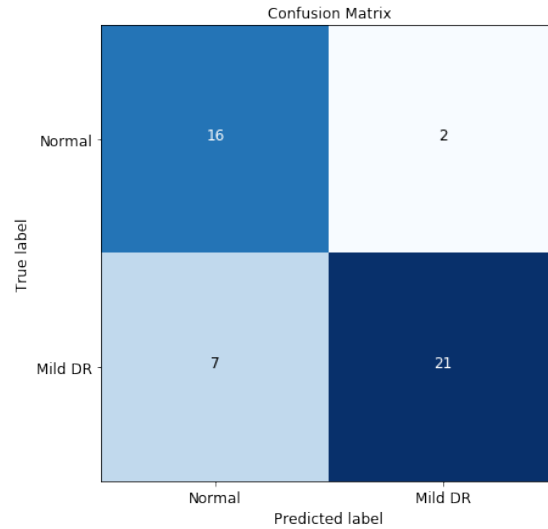
(a) Confusion Matrix



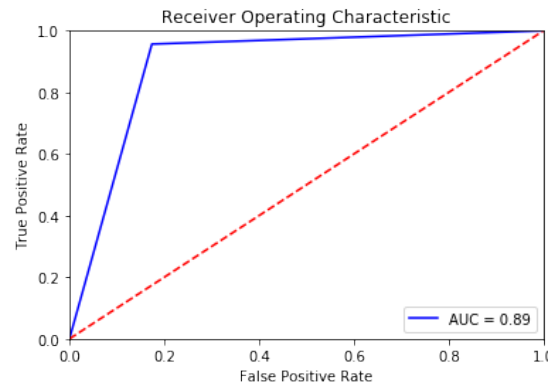
(b) ROC-AUC

Figure 4.5: VGG16 model performance in Diabetic Retinopathy

tients with DED in China often overlook their situation and lack timely treatment leading to serious state development of DR [243]. Early intervention of abnormal signs prevents further deterioration of the condition and its effect on the impacted individuals and related medical costs. Therefore, the DED identification system enables either a completely automated the eye-screening process or semi-automated eye-screening system. The first method requires a reasonable degree of accuracy which is similar to that of the retinal experts. As per the British Diabetic Association (BDA) guidelines, a minimum level of 95% speci-



(a) Confusion Matrix

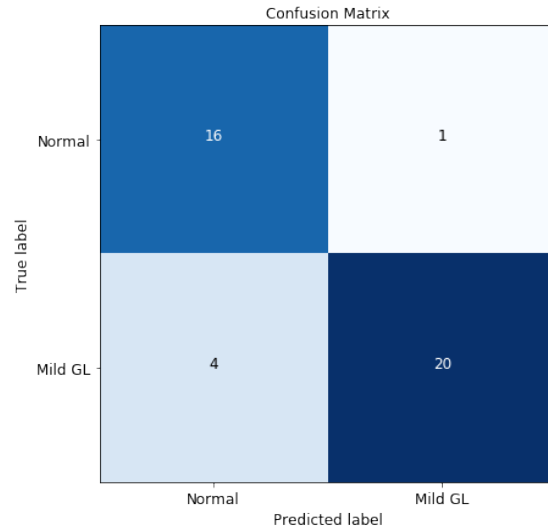


(b) ROC-AUC

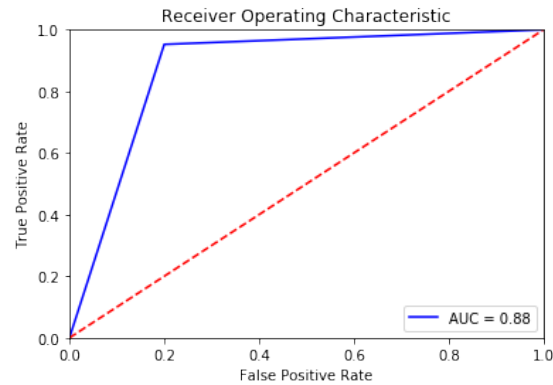
Figure 4.6: VGG16 model performance in Diabetic Macular Edema

ficiency and 80% sensitivity for sight-threatening DR detection must be obtained by the applied method [18]. Second option allows the downsizing of large-scale mass-screening outputs to potential DED cases, followed by human examination. Both scenarios significantly reduce the burden on skilled ophthalmologists and specialised facilities, making the process accessible to the population, especially in low-resource settings.

The application of DL to the clinical practice still has many challenges. An earlier research dealt with the ethical and political concerns in terms of database



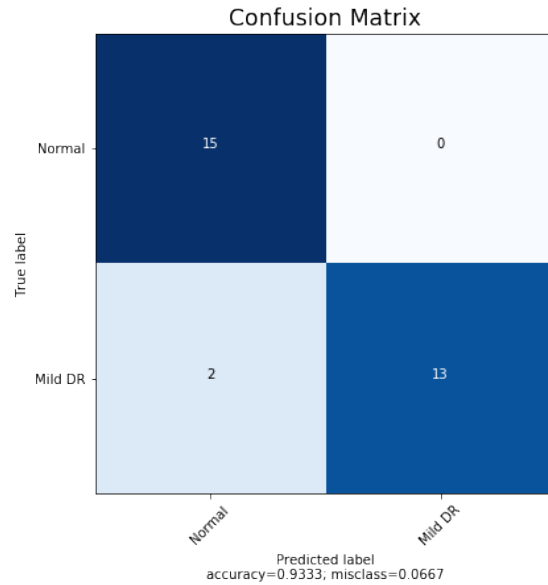
(a) Confusion Matrix



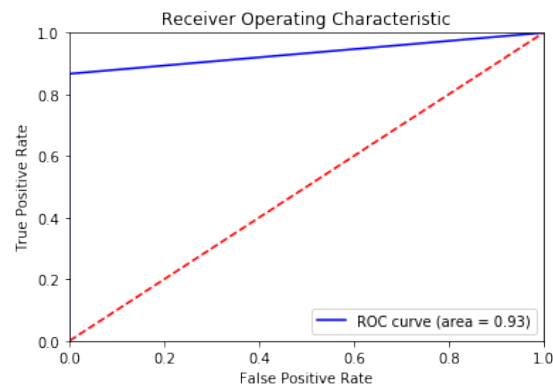
(b) ROC-AUC

Figure 4.7: VGG16 model performance in Glaucoma

creation [2]. For this purpose, it has been difficult to obtain large-scale data for many diabetic eye diseases. Another challenge is that mild (early) classification problems consist of real clinical problems. Binary classification for DED prediction was the subject of previous studies. Even though Google has built a DL model that works better than ophthalmologists, their 'Inception-v3' model was optimised for binary classification for DR identification based on the GoogLeNet structure Gulshan et al. [75]. This framework was evaluated after adding a wide image database gathered for only healthy and non-healthy DR



(a) Confusion Matrix

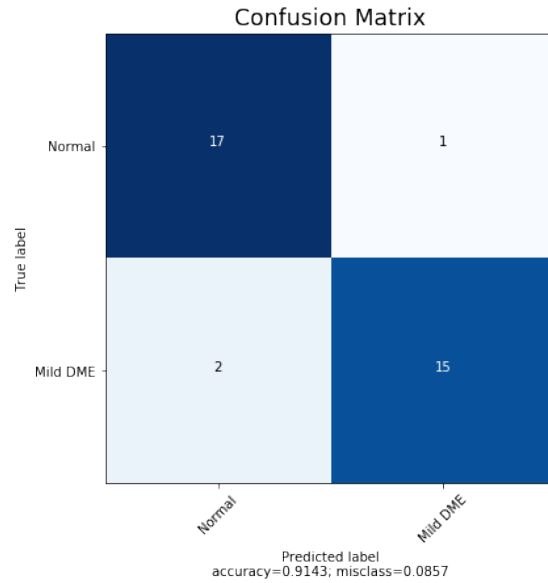


(b) ROC-AUC

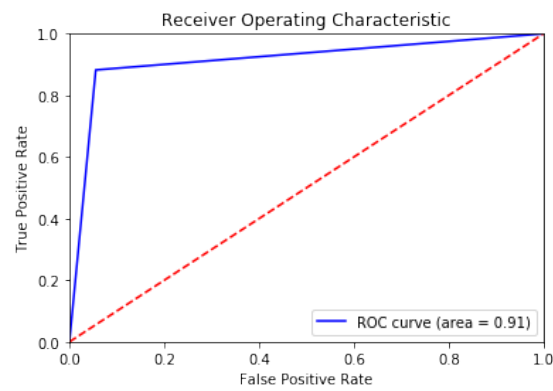
Figure 4.8: Build CNN model performance in Diabetic Retinopathy

screening of diabetes patients. For binary disease classification, Gulshan et al. stated a 93-96 % recall but noted that recall is not enhanced while practicing with 60,000 image samples contrasted with 120,000 image samples employing a private dataset.

Visual representations of the features acquired by CNNs demonstrate that the patterns being used for classification are a part of the image fully visible to the observer [236]. The moderate and severe class of the diabetic retinal images



(a) Confusion Matrix

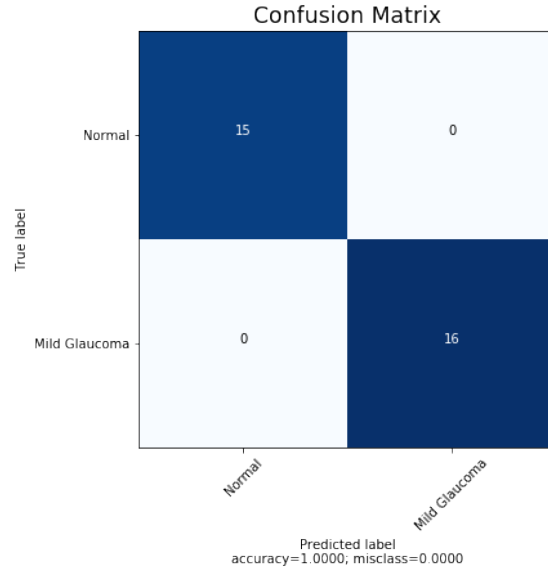


(b) ROC-AUC

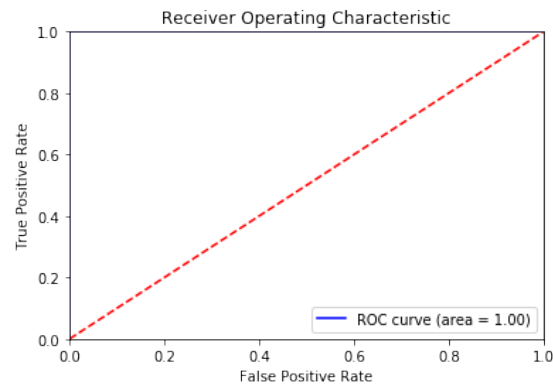
Figure 4.9: Build CNN model performance in Diabetic Macular Edema

include macroscopic features on a scale designed for classification by current CNN architectures such as those accessible from the ImageNet visual database. On the other hand, less than 1 % of the overall pixel volume, a degree of slight that is often difficult for human interpreters to identify, is the characteristics that differentiate mild disease from the normal.

This research indicates that mild-class DED classification should be established through further studies on automatic diagnosis using retinal fundus



(a) Confusion Matrix



(b) ROC-AUC

Figure 4.10: Build CNN model performance in Glaucoma

imaging. The first part of the experiment includes traditional image processing for enhancing mild DED features. Various conventional techniques for image processing have been implemented to extract DED lesions. Pre-trained CNN models using transfer learning provides excellent performance with object-oriented images such as flowers, cars and animals, but is not efficient for lesion based medical images. So, in this research we aim to objectify mild DED lesions by segmenting the region of interest and transferring it to transfer learning and building CNN for further feature extraction. Following with the elimination

of the top layer (existing approach) a detailed review of *three* CNN architectures (including state-of-the-art architectures) was conducted. Secondly, the n layers were 'unfrozen' and then re-trained to respond effectively to the details of the case study of the application (proposed approach). The Messidor and Messidor-2, retinal datasets were used for system training. Two training sets were prepared with the available dataset before, and after pre-processing to measure potential accuracy improvement for normal/mild DED image classification.

As mild DED tends to be incredibly difficult to discern from a normal retina due to only a few subtle indications of the impairment, an increase in data quality was supposed to improve the visibility of pathological features. The top 1 CNN architectures with the top layer removed and re-trained were *VGG16*, yielding the accuracy of 83.43%, 89.13%, 88% for each disease (Table. 4.5). The lowest performance was obtained by *Xception* and *DenseNet21*, respectively. The impact of fine tuning varied across the models. The observed improvement in accuracy was only minor, indicating the relative appropriateness of default pre-trained networks for DED classification tasks. In other words, the CNNs networks were able to identify mild DED from a healthy retina despite having been trained on different images from the ImageNet repository. If no improvement in accuracy is obtained, the unfreezing is not advised as it results in unnecessary computational costs and time accrued. The built CNN model yielded the accuracy of 93.33%, 91.43%, 100% respectively.

To compare the performance of the employed models, two scenarios were considered: (i) before image preprocessing, and (ii) after image preprocessing. In the before pre-processing scenario, we trained our models with a raw dataset

with data augmentation (geometric transformation) applied to the Messidor, Messidor-2, and DRISTI-GS datasets, to avoid overfitting. In the after image pre-processing scenario, the datasets were pre-processed using various traditional image processing techniques which increased the classification performance to 100% (the maximum accuracy achieved for GI).

After evaluation of our high performed approach on the Mild DR, Mild DME and Mild GL detection tasks, the maximum sensitivity of 100%, 94.44%, 100% and the maximum specificity of 86.67%, 88.24%, 100% were obtained. Thus, early DED detection proved sufficient given the BDA standards, but still fell 9% and 6% short in terms of specificity.

Approach limitations: Several research deficiencies have been established. First, the datasets acquired for this experiment were obtained from publicly available which limits the number of high quality mild DED images, only limited to-moderate data set sizes were employed in the research. The approach also emphasises the value of an effective annotation process as having a direct effect on the output of the classifier. The Messidor and Messidor-2, retinal datasets have been validated and marked by professional ophthalmologists. Transfer learning is used as a compensation procedure. Pre-trained CNN models in the wide-scale ImageNet database have been adopted in this study. To increase the size of the training sample set and to ease the data imbalance problem data were rotated, flipped, mirrored, etc. Second, the default model parameters were adopted for the classification task (i.e. dropout, batch size, loss function, optimizer, etc.). Finally, the "black-box" nature of DL-based solutions is often criticized, causing resistance in the broader approach adopted by practitioners. However, with a CNN built using binary classifiers, we achieved state-of-the-

art accuracy, the model performance degrades with the use of transfer learning. However, it is striving to ensure that training with more data might be more robust. Previous field research has confirmed that the CNN's ability to accommodate differences in size is limited and some have indicated that more data can not complement this inherent weakness in the case of retinal images [75].

4.5 Summary of Findings

Effective identification and prompt diagnosis of DED is deemed essential for the prevention of permanent vision loss. Automated DED identification has been the topic of a variety of studies in the past, with the main emphasis on binary normal / severe DR image classification [153]. The results show that the identification of normal to severe indications does not present major difficulties due to the high visibility of the pathological features. The problem occurs with the mild DED identification of instances where very few degree specimens prove representative of the condition, which is often unnoticed by classifiers. Mild DED instances prediction has been further questioned by the poor quality of fundus images which further complicates the identification of delicate lesions in the retinal images. Thus, this research proposes an approach that focuses specifically on the identification of mild DED among normal instances as not adequately discussed in previous literature.

According to the analytical aspect of DL, a variety of performance optimization techniques have been employed (i) image enhancement, (ii) feature enhancement, (iii) data balance, and (iv) fine-tuning. The additional advantage of DL involves automatic recognition capabilities that are most selective

between categories. Such an approach makes it possible to avoid technological constraints with the analytical, and sometimes subjective, approach of manual extraction of features.

In addition , the analysis used composite data sets from various sources to determine the robustness of the system and its capacity to respond to real-world scenarios. As Wan et al. [219] pointed out, the single data collection framework poses difficulties in the validation of accurate models. The developed system enables the standardisation of labour-intensive eye-screening processes and satisfies as an auxiliary diagnosing reference, while avoiding human subjectivity.

CHAPTER 5

AUTOMATIC IDENTIFICATION OF MILD DED AND MULTI-CLASS DED USING PRE-TRAINED CNN MODELS

Diabetic eye disease is a collection of ocular problems that affect patients with diabetes. Thus, timely screening enhances the chances of timely treatment and prevents permanent vision impairment. Retinal fundus images are a useful resource to diagnose retinal complications for ophthalmologists. However, manual detection can be laborious and time-consuming. Therefore, developing an automated diagnose system reduces the time and workload for ophthalmologists. Recently, the image classification using Deep Learning(DL) in between healthy or diseased retinal fundus image classification already achieved a state of the art performance. While the classification of mild and multi-class diseases remains an open challenge, therefore, this research aimed to build an automated classification system considering two scenarios: (i) mild multi-class Diabetic Eye Disease(DED), and (ii) multi-class DED. Our model tested on various datasets, annotated by an ophthalmologist. The experiment conducted employing the top two pretrained convolutional neural network(CNN) models on ImageNet. Furthermore, various performance improvement techniques were employed, i.e., *fine-tune*, *optimization*, and *contrast enhancement*. Maximum accuracy of 88.3% obtained on the VGG16 model for multi-class classification and 85.95% for mild multi-class classification.

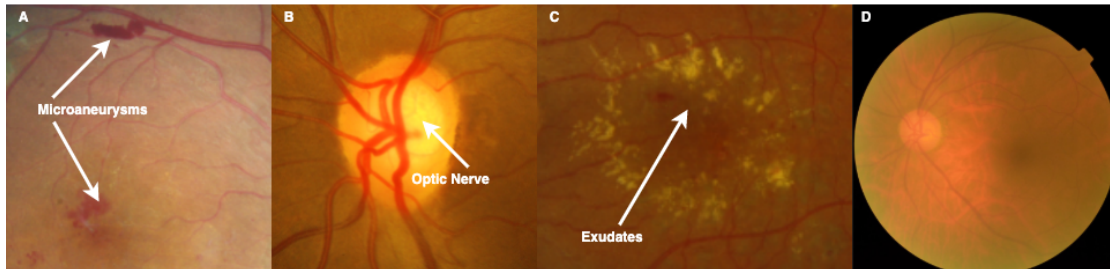


Figure 5.1: Complications of DED in fundus images; A. Microaneurysms; narrow bulges in the side of the blood vessel(Diabetic Retinopathy) B. Progressive damage of optic nerve damage(Glaucoma) C. Exudates formation in macular region and thickening of macula(Diabetic Macular Edema) D. Degeneration of lens (Cataract).

5.1 Introduction

The World Health Organisation (WHO) reports, 2.2 billion individuals globally have a blindness or vision loss, of which at least 1 billion have impaired vision, which could have been reversed¹. One of the reasons for this blindness is identified as diabetes mellitus or diabetes. Approximately one-third of those with diabetes expected to diagnosed with a DED, a chronic eye disease that can cause permanent visual impairment if left unattended [44]. DED includes diabetic retinopathy (DR), glaucoma (GI), diabetic macular edema (DME), and cataract² (Ca) (see Fig. 5.1). It is crucial to identify and diagnose these diseases for the treatment.

Motivated by the necessity of active strategies for diagnosis, and prevention to implement the broad spectrum of needs associated with retinal disorders and visual impairments throughout the lifespan. Automated DED diagnostic techniques using DL are vital to addressing these issues [2,75]. Timely screening of

¹<https://www.who.int/en/news-room/fact-sheets/detail/blindness-and-visual-impairment>

²The National Institute of Diabetes and Digestive and Kidney Diseases

DED, which is crucial to effective prognosis based on professional ophthalmologist, is time and labor intensive [66].

Although DL has generally achieved high validation accuracies for healthy and diseased (binary) classification, the results of mild and multi-class classification are less impressive, particularly for early stage impairment. Therefore, in this chapter, we present a Deep Convolutional Neural Network(DCNN) based automatic DED classification model that can classify healthy images from disease pathologies. To identify the best performing framework for the mild and multi-class DED classification tasks, we initially evaluate different DCNN architectures. We aim to achieve the highest performance levels than reported in the previous works. Thus, we trained and tested mild and multi-class classification models to improve sensitivities for the different DED classes, incorporating different preprocessing and augmentation approaches to boost the accuracy of the result and enhance adequate sample volume for the dataset.

Early rectification of retinal diseases is vital, but the diagnosis of these diseases utilizing neural networks requires a substantial amount of time and memory. Additional data must supply to enhance the precision, but this requires high computational power and a massive amount of time investment. Thus, a comparatively pretrained model can benefit the process as it adapts the design to reduce losses. Pretrained models or Transfer Learning(TL) [211] models has already been demonstrated and validated promising results in medical image classification and detection [20, 99, 116, 125]. As part of this analysis, we used the state of the art CNN models, pretrained on the broad public image repository ImageNet, following the TL principle. The top layers of the deep neural network were learned from the publicly accessible fundus image corpora for

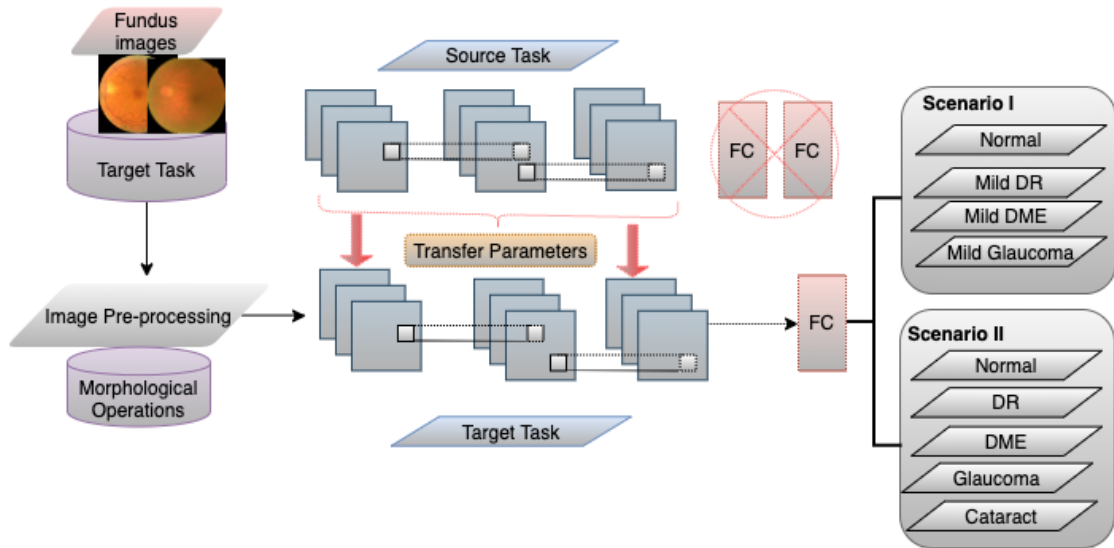


Figure 5.2: Transfer Learning process.

mild and multi-class classification by using initialized weights. The research performed in this chapter focuses solely on different DED instances, actually challenging to classify as opposed to previous approaches. Initially, the highest-performing CNN model is selected based on a comprehensive experiment conducted. Lastly, it evaluates the set of performance improvements, including fine-tuning, and optimizer selection. Finally, an ideal intermediate scenario of accuracy achieved is selected to facilitate efficient and effective fully automated DL based system development to improve outcomes to mass screening services among the at risk population.

5.2 Literature Review

Several previous research work concentrated on automated retinal disease detection by using machine learning algorithms [15, 46, 47, 221] to classify a substantial number of fundus images captured from retinal screening pro-

grams [29, 235]. Multiple machine learning techniques: Artificial Neural Network(ANN), K-nearest neighbour algorithm, Support Vector Machine(SVM), and Naive Bayes classifier, were implemented to the automated identification of retinal diseases [125]. Many studies implemented ANN models to identify the disparity between glaucoma and non glaucoma [38, 234]. A glaucoma research team observed visual field evaluation by discovering preperimetric glaucoma utilising DL feedforward neural networks(FNN) [16]. For the grading intensity of the nuclear cataract [64], an artificial DCNN has been applied. DL emerges as popular solution for various classification problems in the field of ML techniques [70, 81, 110, 119]. The Google research group has developed the advanced DL model capable of diagnosing Diabetes Mellitus Retinopathy(DMR) [75]. The study of the Age-related Macular degeneration(AMD) was carried out using similar DL methods, fundus photographs and optical coherence tomography [28, 111]. However, all retinal image classification studies selected binary classification through which problems of normal versus one disease were solved [107]. Furthermore, in order to classify mild and multi-class diabetic retinopathy, Lam et al. [109] employed pretrained networks (GoogleNet and AlexNet) in the Messidor dataset, authors applied selective contrast-limited adaptive histogram equalization(CLAHE) and documented improvement in the identification of subtle features. Multi-class DL algorithms for automatic detection of ten retinal disorders were studied by Choi et al. [42]. The results of this work showed that current DL algorithms were unsuccessful in classifying retinal images from small datasets of multiple groups. While research conducted in this area have published the result that high classification performance in standardized experimental settings, it is fundamentally difficult to implement the binary classification model to the actual medical practice where patients visit-

ing are suffering from various DED. Indeed, studies have been very limited on mild and multi-class classification aimed at recognising DED.

In this research, we adapted TL in mild and multi-class DED settings using a state of the art CNN for fundus image analysis. This chapter articulates a pilot study planned with the use of small open source fundus retinal image database for TL evaluation on mild and multi-class classification.

5.3 Dataset

Retinal fundus images are independently extracted from various publicly available datasets. The following sections discuss the data collection, selection and pre-processing employed in this study.

5.3.1 Data Collection

Data were obtained from the open source, including Messidor, Messidor-2, DRISHTI-GS, and retina datasets, which are publicly available. Messidor dataset includes high fidelity images with reliable labeling despite its relatively small scale. Similarly, Messidor-2 is a public database used by other individual people to evaluate DED algorithm performance. The database consists of 1,748 images of 874 subjects. Messidor-2 differs from the initial 1200 image Messidor set of data, and it has two images for each item, one for each eye. The Drishti-GS dataset contains 101 retinal images, with 31 normal images and 70 lesion images. Cataract dataset acquired from retina dataset Github³. This dataset

³https://github.com/yiweichen04/retina_dataset

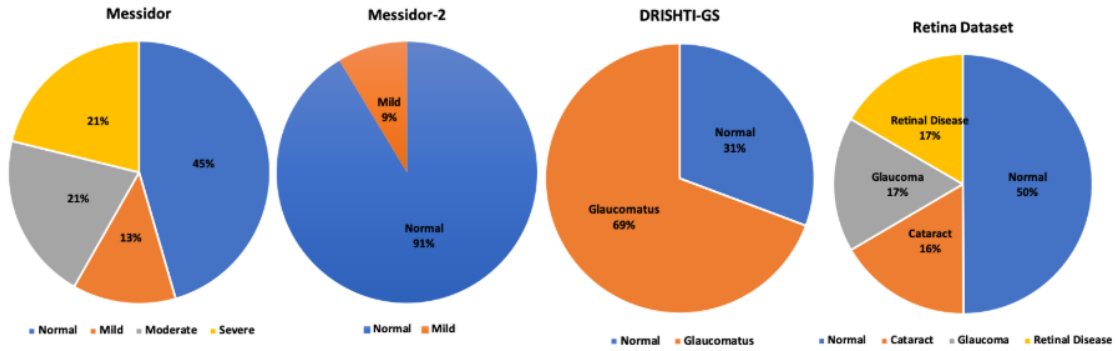


Figure 5.3: Data Distribution

consists of 100 cataract images.

5.3.2 Data Pre-processing

Data imbalance is the common problem encountered in machine learning applications and real-world data mining [115]. Image preprocessing plays a significant role: If the dataset have a small number of samples, in one or more categories that lead to the problem of misclassification. In this study, methods like under-sampling and over-sampling are performed to avoid misclassification. We implemented both the methodologies throughout the dataset better results obtained using the under-sampling method. Followed by morphological top-hat and bottom-hat transform to enhance the contrast [208] (see Fig. 5.4). Two morphological transformations, top-hat and bottom-hat, are commonly used for image enhancement. These are a very effective tool for improving clarity in the presence of shading or dark areas in medical imaging. The top-hat method is defined as the difference between the input image and its opening, whereas the bottom-hat is the difference between the input image and the closing. By implementing top-hat, we can extract objects or elements smaller than the SE and brighter than their environment. On the other hand, bottom-hat produces

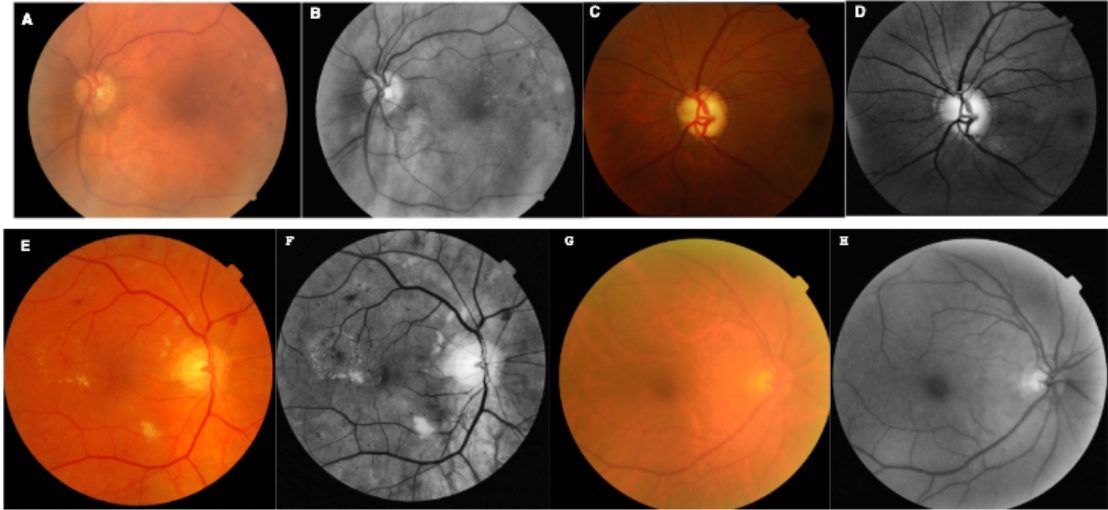


Figure 5.4: Contrast Enhancement (A) Original and (B) Enhanced Diabetic Retinopathy; (C) Original and (D) Enhanced Glaucoma; (E) Original and (F) Enhanced Diabetic Macular Edema; (G) Original and (H) Enhanced Cataract .

objects more trivial than the SE and darker than their environment. So we can take advantage of these two operators by adding the top-hat and subtracting the bottom-hat result.

5.4 Model Construction

This study's real objective is the performance enhancement of mild and multi-class DED identification via an experimental evaluation of various techniques for improving the classification. The associated goals and objectives can be identified as follows.

1. Comparative analysis of two CNN frameworks using TL concept,
2. Impact of a fine-tuning analysis on the performance of frameworks,
3. Impact of an optimizer analysis on the performance of frameworks,

4. Analysis of data improvement and contrast enhancement techniques for further classification improvements on mild and multi-class DED detection task.

The TL process is illustrated (see Fig. 5.2), to demonstrate the steps that followed.

5.4.1 Model Specification

In this study, we employ pretrained CNNs to incorporate the classification of the DED dataset. A deep convolutional neural network (CNN) converts a feature vector with a defined weight matrix to obtain particular feature representations without missing information about the spatial arrangement [230]. The concept uses features learned on the source task and its reuse to target jobs. TL is beneficial in areas of research that involve large quantities of data and significant computational resources [179]. Thus, we are exploring pretrained models to achieve the best possible classification outcomes. This section presents the specific information of the pretrained models.

Visual Geometry Group (VGG16): VGG was designed based on the deep convolutional neural network model in Oxford Robotics Institute by Andrew Zisserman and Karen Simonyan [183]. VGG became popular at the Large Scale Visual Recognition Challenge in 2014 (ILSVRC2014). The VGGNet operated well on the dataset of the ImageNet. To enhance the image extraction efficiency, the VGGNet used smaller 3×3 filters compared to the 11×11 AlexNet filters. There are two different versions of this deep network architecture (VGG16 and VGG19), which have different layers and depths. Moreover, the number of pa-

rameters for VGG19 is larger and more complex than VGG16 to train the model. Table.5.2 Explains the parameters we used to train a system.

InceptionV3: Inception network or GoogLeNet was 22 layers network and won 2014 Image net challenge with 93.3% top-5 accuracy [36]. Later versions are referred to as Inception VN , where, V is the version and N is the number so inceptionV1, inceptionV2 and inceptionV3. The InceptionV3 network has several symmetrical and asymmetrical building blocks, where each block has several branches of convolutions, average pooling, max-pooling, concatenated, dropouts, and fully-connected layers. In our dataset, VGG16 obtained high accuracy than other models. Table.5.3 Explains the parameters we used to train a system.

5.4.2 Classification Performance Analysis

The efficiency of each CNN is measured by different metrics applied to calculate the true and/or false classification for the diagnosed DED in the retinal fundus images evaluated as follows. First, the cross-validation estimator [192] is being used and resulted in a confusion matrix Table.6.2. When the classification model correctly classifies samples associated with a particular class, such samples placed in the TP indices. The other samples that relate to some other classes correctly identified are in the TN indices of the confusion matrix. Similarly, the FP and FN indices in the uncertainty matrix refer to the number of samples incorrectly estimated by the classifier. Thus, the following equations are used with which a diagnostic test correctly identifies and excludes a certain ailment measured.

Table 5.1: The layers and layer parameters of the VGG16 model

Layers	layer Type	Output Shape	Trainable parameters
1	Cov2d	[224, 224, 64]	1792
2	Cov2d	[224, 224, 64]	36928
4	Cov2d	[112, 112, 128]	73856
5	Cov2d	[112, 112, 128]	147585
6	Cov2d	[56, 56, 256]	295168
7	Cov2d	[56, 56, 256]	590080
8	Cov2d	[56, 56, 256]	590080
9	Cov2d	[56, 56, 256]	590080
10	Cov2d	[28, 28, 512]	1180160
11	Cov2d	[28, 28, 512]	2359808
12	Cov2d	[28, 28, 512]	2359808
13	Cov2d	[14, 14, 512]	2359808
14	Cov2d	[14, 14, 512]	2359808
15	Cov2d	[14, 14, 512]	2359808
16	Cov2d	[14, 14, 512]	2359808

Table 5.2: Parameters of the VGG16 model and preferred weights in this study.

Model	Platform Used	Image Size	Optimizer	Mini-Batch Size	fine-tune	Learning Rate
VGG16	Anaconda	224*224	ADAM	32	15	1e-3
	Python		RMSProp			1e-3
	Keras		SGD			1e-3
	Tensorflow		AdamGrad			1e-3

Table 5.3: Parameters of the InceptionV3 model and preferred weights in this study.

Model	Platform Used	Image Size	Optimizer	Mini-Batch Size	fine-tune	Learning Rate
InceptionV3	Anaconda	224*224	ADAM	32	100	1e-3
	Python		RMSProp			1e-3
	Keras		SGD			1e-3
	Tensorflow		AdamGrad			1e-3

$$Accuracy(\%) = \frac{TP + TN}{TP + FN + TN + FP}. \quad (5.1)$$

Similarly, *Recall*:

$$Sensitivity(Recall) = \frac{TP}{TP + FN} \quad (5.2)$$

Precision:

$$Precision = \frac{TP}{TP + FP} \quad (5.3)$$

5.5 Experimental Design

All the studies conducted used Python, Keras library, TensorFlow as a back-end. The resolution of the images has been standardized to a uniform size, following each model's input requirements. The epoch number set at 15 because of

the use of pretrained weights in our experiments. The distribution of training/testing dataset at 80/20. Stratified standard preference made to ensure a nearly similar dispersion of the class. Mini-batch size set to 32, and the categorical cross-entropy loss function was selected due to its suitability for multi-class classification tasks. The default ADAM was the Optimiser. The primary assessment metric for accuracy, specificity, and sensitivity of test data was used for final scores validation.

5.5.1 Performance enhancement

Fine-tune: The neural networks used in this chapter were pretrained on a large-scale ImageNet dataset covering 1000 classes, including birds, animals, and flowers. Systems obtain the highest performance in the classification tasks for objects with labeled datasets while demonstrating restricted in their assessment to specialty areas of study, such as DED detection. The diagnosis and treatment of possible pathological signs in the fundus images are based on a large number of complex characteristics and their orientation inside the fundus images [109]. There is a new representation of the feature vector on every layer of CNN by progressive extraction of the most distinguishing characteristics of [122]. The following constraints considered in the experimental work: (i) Eliminating the fully connected nodes at the end of the layer (where the true label class predictions made) and substitute the modules fully connected with those newly initialized (current pre-training approach); and (ii) eliminating the n layers and re-training the network (the suggested approach). The range of parameters used across CNN depends on the total hidden layers present on every system model. The possible classification enhancement of the DED detection

task assessed as a result of the models' proposed customization options. In the analysis with Zhang et al. [243] DL based DR detection device performance accuracy improved from 95.68% to 97.15% as a result of fine-tuning.

Table 5.4: Average performance of the models in mild DED classification (mild multi-classes).

Model	Optimiser	Learning Rate	Accuracy*	Accuracy**
VGG16	<i>Adam</i>	1e-3	82.42%	85.94%
	<i>RMSprop</i>	1e-3	83.52%	83.98%
	<i>SGD</i>	1e-3	75%	82.03%
	<i>Adagrad</i>	1e-3	75%	75.23%
InceptionV3	<i>Adam</i>	1e-3	74%	75%
	<i>RMSprop</i>	1e-3	71%	73%
	<i>SGD</i>	1e-3	78.52%	78.52%
	<i>Adagrad</i>	1e-3	76%	79.17%

Legend: Accuracy* = Results Before fine-tuning, Accuracy** = Results after fine-tuning.

Table 5.5: Average performance of the models in multi-class DED classification.

Model	Optimiser	Learning Rate	Accuracy*	Accuracy**
VGG16	<i>Adam</i>	1e-3	84.88%	88.3%
	<i>RMSprop</i>	1e-3	74%	80%
	<i>SGD</i>	1e-3	80%	80%
	<i>Adagrad</i>	1e-3	79.95%	80%
InceptionV3	<i>Adam</i>	1e-3	79%	81%
	<i>RMSprop</i>	1e-3	65%	78%
	<i>SGD</i>	1e-3	63%	63%
	<i>Adagrad</i>	1e-3	58%	64%

Legend: Accuracy* = Results Before fine-tuning, Accuracy** = Results after fine-tuning.

Optimizer Selection: In the training phase, the neural net nodes' parameters are updated automatically to reduce the loss function. However, the direction

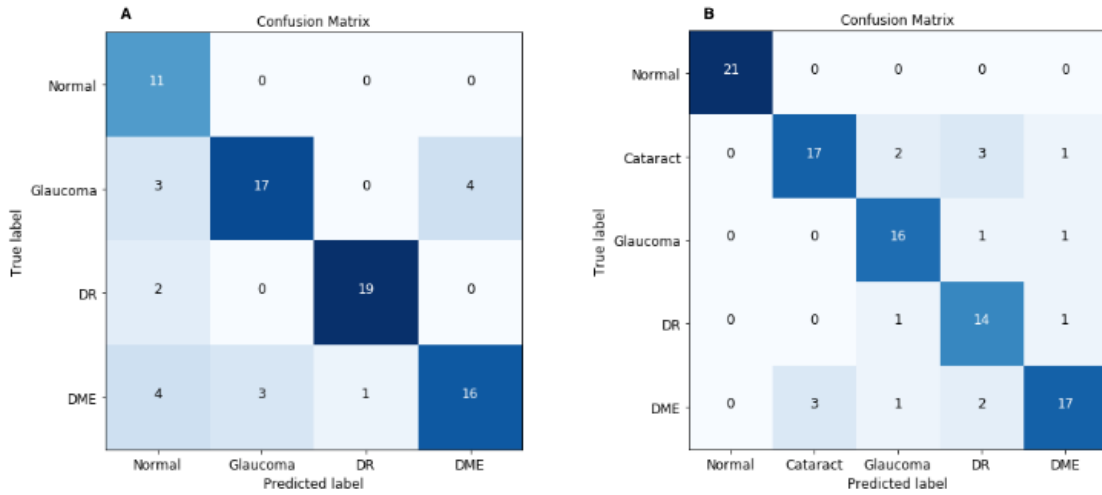


Figure 5.5: Confusion Matrix in VGG16 + Adam (A) scenario I and (B) Scenario II.

and magnitude of the parameter adjustment are highly dependant on the optimizer utilized. The most significant weight that evaluates the performance of the Optimiser is Regularisation and Learning Rate. Too high/too lower learning rate results either in non-convergence of the loss function or in the range of the local, but not the absolute minimum. Meanwhile, Regularisation makes it possible to avoid overfitting the model by penalizing the dominant weighting factors for correct predictions. As a consequence, the generalization capability of the classifier increases when exposed to new data. The optimization techniques used for the experiments were as follows : (1) RMSprop, (2) SGD, (3) Adagrad, (4) Adam.

5.5.2 Training and Prediction Results

The two pretrained CNN models were compared with the yielded accuracy on the test dataset. Also, fine-tuning was used as a substitute for the default setting. After deletion and retraining of n layers (n was CNN-dependent), the

efficiency acquired by each model was used for comparative purposes. The fine-tuning effect was evaluated in terms of accuracy (%) increment or reduction. The highest accuracy was identified by each model (either through default or after fine-tuning) in four different optimizers. Finally, the top 1 CNN architectures + optimizers with the higher accuracy performance for the target task have been selected in Table.5.4 and Table.5.5.

This study is an investigation of mild and multi-class DL algorithms for automated detection of DED. As per the British Diabetic Association (BDA) standards, a minimum amount of 80% sensitivity and 95% specificity for sight-threatening DED detection must be achieved by any method [18]. After testing our approach in DED detection tasks, the scenario I achieved maximum sensitivity of 85% and a maximum specificity of 96%. Similarly, the sensitivity of 85% and specificity of 98% for scenario II, respectively. Thus, according to the BDA standards, mild and multi-class DED detection is sufficient, in terms of its sensitivity and specificity.

5.5.3 Accuracy Evaluation

This study focuses on DL algorithms to automatically identify mild and multi-class DED. Previous researches in this topic showed the ineffectiveness of the latest DL algorithms in classifying fundus images from small datasets. It failed to demonstrate practical and effective results for a computer-aided medical applications. Therefore, this article adapted optimized DL architectures for the automated classification of normal, DR, DME, GL and Ca due to the significance of each disease in order to create an automated model for the classification.

The performance of DL models was dropped by 3%, in early stage multi-class DED classification. This finding is apparently very normal since early stage DED fundus images consist of subtle features that can be crucial for diagnosis. Interestingly, the architectures most commonly deployed were designed to identify object based features like those present in the ImageNet dataset. Then we may need a new paradigm such as lesion based (e.g. exudates) for diagnosing diseases through CNN models. Our future goals include DED lesion segmentation (region of interest) [141,142,233] for enhancing the identification of mild disease and moving to more complex and advantageous identification of multi-grade diseases.

5.6 Summary of Findings

Early identification and prompt diagnosis of DED are considered crucial to the prevention of permanent vision loss. Automated DED recognition has been the topic of several studies in the past, with the main emphasis on healthy/unhealthy binary retinal classification [153]. The results show that the identification of moderate to severe indications does not present significant difficulties due to the high visibility of the pathological features. The issue occurs with the mild identification of DED cases, in which only small lesions prove representative of the condition, sometimes undetected by the classifiers. Mild DED cases prognostication further questioned by the poor quality of fundus photography, which further complicates the recognition of subtle lesions in the eye. In the case of multi-class classification, the performance of DL models has been reduced as categories have multiplied. When categories increased, the predicted precision of the random distribution decreased. This finding corre-

sponded to the previous studies [51]. Recent research using the GoogLeNet model to identify skin cancer has shown that increase in the number of classes has underperformed (with an accuracy of 72.1% for a three class problem and 55.4% for a nine class problem) [56]. Thus it is essential to create disease-specific strategies to differentiate between DED to enhance the efficiency of multi-class classification. Therefore, the research proposed a system that focuses entirely on the identification of mild and multi-class DED among healthy instances, as discussed in previous studies. According to the empiric nature of DL, a variety of performance optimization techniques have been applied (i) fine-tuning, (ii) optimizer choice, (iii) data increase, and (iii) contrast enhancement. Besides, the study used combined datasets from different sources to evaluate the system's robustness in its flexibility to cope with real world scenarios. As Wan et al. [219] have pointed out, the single data collection environment presents difficulties in the validation of accurate models [171].

CHAPTER 6

AUTOMATED CLASSIFICATION AND DETECTION OF MULTI-CLASS DED USING PROPOSED CNN

A key tool commonly used for the initial diagnosis of patients with Diabetic Eye Disease (DED) or other eye disorders is the screening of retinal fundus images. In recent years, the methodology of deep learning has demonstrated impressive benefits in clinical practice. To detect retinal eye diseases from retinal fundus photographs, researchers have attempted to use Deep Learning (DL) methods. Prompt examination, therefore, increases the chances of effective treatment and reduces permanent deterioration of vision. Manual detection, however, can be labor-intensive and time-consuming. Furthermore, for ophthalmologists, the implementation of an automated diagnostic device reduces time and workload. The DL techniques in Machine Learning (ML) has achieved a state of the art performance in binary classification between healthy or diseased retinal fundus image. The classification of multi-class retinal eye diseases remains an open challenge, multi-class DED is therefore considered in this study to developed an automated classification framework for DED. Therefore, detecting multiple diabetic eye diseases from retinal fundus images is an important research topic with practical consequences. Our proposed model tested on various retinal fundus images gathered from the publicly available dataset, which is annotated by an ophthalmologist. This experiment is conducted employing proposed convolutional neural network (CNN) model. Maximum accuracy of 81.33%, sensitivity of 100%, and specificity of 100% of obtained on our proposed model for multi-class classification.

6.1 Introduction

A category of eye disorders that can affect people with diabetes is a diabetic eye disease. Diabetic retinopathy, diabetic macular edema, glaucoma, and cataract are among these diseases. Diabetes can cause eye damage over time, resulting in blurred vision or even vision impairment. However, by keeping track of diabetes, one can avoid DED or keep it from getting worse [44]. Around one-third of people with diabetes are likely to be diagnosed with DED. 2.2 billion people worldwide are confirmed by the World Health Organization (WHO) to have blindness or vision loss, of which at least 1 billion have a vision impairment, which could have been reversed¹. Identifying and diagnosing these diseases for treatment is critical.

Motivated by the need for successful development of detection and preventive measures to implement the wide range of lifespan needs associated with retinal conditions and visual impairments. For solving these problems, automated DED diagnostic techniques using DL are vital [2,75]. The time and labor intensive [66] nature of screening of DED make it a crucial inaccurate prognosis based on a competent ophthalmologist. While DL has generally achieved high accuracy of validity for healthy and diseased (binary) classification, the results of multi-class classification, particularly for early-stage disability, are less impressive. We, therefore, present in this chapter an automated DED classification model based on the Deep Convolutional Neural Network (DCNN) that can distinguish healthy images from disease pathology.

Initially, various DCNN architectures are evaluated to determine the best

¹<https://www.who.int/en/news-room/fact-sheets/detail/blindness-and-visual-impairment>

performing system for the mild and multi-class DED classification tasks [169]. We aspire to achieve the highest standards of output that the previous works have recorded. In order to enhance sensitivities for the various DED levels, we trained the proposed CNN model and tested a multi-class classification model, integrating different preprocessing models to improve sensitivities for the different DED classes, incorporating different preprocessing and augmentation approaches to boost the accuracy of the result and enhance adequate sample volume for the dataset.

Early amplification of retinal diseases is important; however, it takes a tremendous amount of time and memory to diagnose these diseases using neural networks. To improve accuracy, additional data must be given, but this requires high computing capacity and a large amount of time spent. Therefore, the method will benefit from a comparatively pre-trained model as it adapts the design to minimize losses. Pretrained models or models for Transfer Learning(TL) [211] have already shown and validated promising results in the classification and detection of medical images [20, 99, 116, 125]. As the phase of this research, following the TL theory, we used the state-of-the-art CNN models, pre-trained on the sizeable public image repository ImageNet in our previous study [169]. The deep neural network's top layers were learned from the publicly available fundus image corpora using initialized weights for mild and multi-class classification. In this study we proposed a new CNN model to solve the problem of multi-class classification. Initially, the highest-performing CNN model is developed based on a comprehensive experiment conducted in previous studies. Secondly, it evaluates the set of performance improvements, including image-processing and optimizer selection. Finally, an ideal specificity and sensitivity are achieved by the proposed model to facilitate efficient and ef-

fective fully automated DL-based system development to improve outcomes to mass screening services among the at-risk population.

6.2 Literature Review

By using machine learning algorithms [15,46,47,221] to identify a huge proportion of fundus images captured from ocular scanning programs [29,235], several previous researches focused on automatic retinal disease detection. Various machine learning techniques have been introduced for the automatic detection of retinal diseases [125]: Artificial Neural Network(ANN), K-nearest neighbor algorithm, Support Vector Machine(SVM), and Naive Bayes classifier. To define the difference between glaucoma and non-glaucoma [38,234], multiple studies have introduced ANN models. By finding preperimetric glaucoma using DL feedforward neural networks(FNN) [16], a glaucoma research team observed visual field assessment. An artificial DCNN was applied for the grading sensitivity of nuclear cataracts [64]. In the field of ML techniques, DL emerges as a common solution for different classification issues [70,81,110,119]. An advanced DL model capable of diagnosing Diabetes Mellitus Retinopathy(DMR) [75] has been developed by the Google research community. Using identical DL techniques, fundus photographs and optical coherence tomography [28,111], the Age-related Macular Degeneration(AMD) research was performed. However, binary classification was chosen by all retinal image classification studies from which problems with normal versus one disease were resolved [107]. Besides, Lam et al. [109] used pre-trained networks (GoogleNet and AlexNet) in the Messidor dataset to distinguish mild and multi-class diabetic retinopathy, researchers developed selective contrast-limited adaptive histogram equalization

(CLAHE) and reported enhancement in recognition of subtle characteristics. Multi-class DL architectures have been tested by Choi et al. [42] for automated detection of ten retinal disorders. This work's findings have shown that existing DL algorithms have failed to distinguish retinal images from small multi-group datasets. While the outcome of high classification success in structured experimental settings has been published in research conducted in this field, it is fundamentally difficult to apply the binary classification model in real medical practice where visiting patients suffer from different DEDs. Indeed, there have been minimal studies on mild and multi-class groups aimed at recognizing DED. This study used a state-of-the-art CNN for fundus image analysis to adapt TL in mild and multi-class DED environments. This chapter articulates a pilot study intended to evaluate TL on mild and multi-class classification using the small open-source fundus retinal image database.

6.3 Data Collection

Open-source data was collected, including publicly available Messidor, Messidor-2, DRISHTI-GS, and kaggle cataract datasets. Despite its relatively limited size, Messidor's dataset contains high-resolution photos with accurate labeling. Similarly, Messidor-2 is a public dataset for analyzing DED algorithm output used by other individuals. The data comprises 1,748 photographs of 874 topics. Messidor-2 varies from the primary 1200 image data set of Messidor, and for each object has two images, one for each eye. They acquired the cataract and glaucoma dataset from the retina dataset obtained by Kaggle. This dataset consists of 100 images of a cataract and 100 images of glaucoma. Distribution of data can be seen in Fig. 6.1

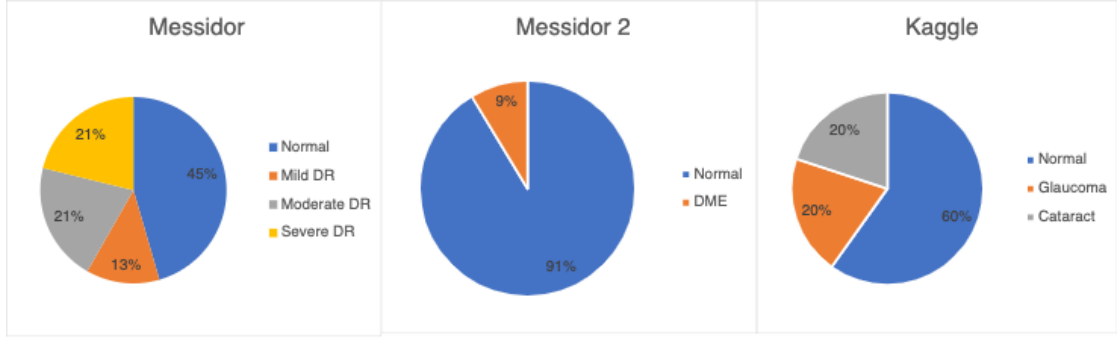


Figure 6.1: Data Distribution

6.3.1 Data Enhancement

To accomplish contrast enhancement in the retinal images, mathematical morphology has been used. Mathematical morphology approaches work hinged on the structural values of objects. To pull out the elements of an image, these methods use relationships between classes and mathematical fundamentals, which help explain areas. In morphological operators, the input consists of two data sets. The original image is included in the first set, and the second one illustrates the structural element (SE), which is also called a mask. The original image is in grey level or binary, and the mask is a 0s and 1s value matrix [198]. In morphological operators, if the gray-level image matrix is represented by $I(x, y)$ and the SE by $S(u, v)$, the erosion and dilation operators are defined as Equation 6.1 and 6.2 [80].

$$I \ominus S = \min_{u,v} \{I(x + u, y + v) - S(u, v)\} \quad (6.1)$$

$$I \oplus S = \max_{u,v} \{I(x - u, y - v) + S(u, v)\} \quad (6.2)$$

The erosion operator decreases the objects' size and increases the size of an image's holes and eliminates very tiny information from that image. It makes the final image appear darker than the original image by removing bright areas under the SE. The dilation operator operates in reverse; in other words, the size

of objects increases and holes in the image decreases, respectively. Therefore, the opening operator is similar to implementing the dilation and erosion operations on the same image Equation 6.3, while the closing operator acts in reverse Equation 6.3.

$$I \circ S = (I \ominus S) \oplus S \quad (6.3)$$

$$I \bullet S = (I \oplus S) \ominus S \quad (6.4)$$

The opening operator eliminates poor relations between artifacts and small information, while small gaps are eliminated, and the closing operator fills cracks. The size and shape of a SE are usually chosen arbitrarily; however, disk-shaped SE is used more frequently than other masks for medical images.

6.4 Study Design

The real aim of this study is to increase performance in automated multi-class DED classification and detection through an experimental assessment of different classification improvement techniques. It is possible to define the related priorities and goals are as follows.

1. Performance analysis of proposed CNN framework with multiple datasets collected from multiple sources,
2. Impact of an optimizer on the performance of proposed frameworks,
3. Visual representation of the performance of the model using heat-map.
4. Analysis of image quality improvement using contrast enhancement techniques for further classification improvements on multi-class DED detection task.

6.4.1 Model development

This layer comprises a filter set (kernel). Each filter is convoluted against the input image and then extract features by creating a new layer. Each layer signifies some of the important features or characteristics of the input image. The $*$ symbol identifies the operation of the convolution. The output (or function map) $F(t)$ is defined below when input $I_n(t)$ is convoluted with a filter or $f(a)$ kernel.

$$F(t) = (I_n * f)(t). \quad (6.5)$$

If t can only accept integer values, the following discrete convolution is provided by the following equation:

$$F(t) = \sum_a I_n(a) \cdot f(t - a). \quad (6.6)$$

The above assumes a one-dimensional convolutional operation. A two dimension convolution operation with input $I_n(m, n)$ and a kernel $f(a, b)$ is defined as:

$$F(t) = \sum_a \sum_b I_n(a, b) \cdot f(m - a, n - b). \quad (6.7)$$

By the commutative law, the kernel is flipped and the above is equivalent to:

$$F(t) = \sum_a \sum_b I_n(m - a, n - b) \cdot f(a, b). \quad (6.8)$$

Neural networks implement the cross-correlation function, which is the same as convolution but without flipping the kernel.

$$F(t) = \sum_a \sum_b I_n(m + a, n + b) \cdot f(a, b). \quad (6.9)$$

Rectified Linear Unit (ReLU) Layer

This layer is an activation function that sets the negative input value to zero, which optimizes and speeds up analyses and training, and helps prevent the gradient from disappearing. Mathematically, this is described as:

$$R(x) = \max(0, x). \quad (6.10)$$

In which x is input to the neuron.

Maxpooling Layer

This Layer is a sample-based discretization method. It is employed to down-sample an input design (input image, hidden-layers, output matrix, etc.), and compressing its dimensionality and enabling assumptions about the components available in the binned sub-regions to be made. This will decrease the size of learning parameters and provide fundamental interpretation invariance to internal depiction, thus further reducing the cost of computation. Our model adopted the kernel size of 3×3 during the Maxpooling process. After the final convolution block, the network flattened to one dimension.

Batch Normalization

Batch normalization enables every layer of the network to learn a little more independently of the other layers. It also normalizes the output from the previous activation layer by subtracting the batch mean and dividing the batch standard deviation [90] to improve the steadiness of the neural network.

Fully Connected Layer

This layer takes the output of the previous layer (Convolutional, ReLU, or Pooling) as its input and calculates the probability values for classification into the various groups.

Loss Function

This layer applies a soft-max function to the input data sample. This layer is used for the final prediction. Therefore, our loss function is given as:

$$L_i = -\log\left(\frac{e^{\beta_y}}{\sum_j^c e^{\beta_j}}\right) \quad (6.11)$$

Where β_j is the j th element of the vector of class scores β , β_y is the CNN score for the positive class and c is classes for each image. The softmax ensures a proper prediction probability in the log of the equation.

Regularization

An efficient regularization method named as a dropout is employed. This strategy was being proposed by Srivastava et al. [196]. During the training process, the dropout is conducted by maintaining the neuron active with a certain probability P or by setting it to 0. In our study, we set hyperparameter to 0.50 because it outputs in the maximum amount of regularization [19].

Table 6.1: Hyper-parameters of the build CNN model and preferred weights in this study.

R1	R2	R3	R4	R5	R6	R7	R8
CNN	224*224	RMSprop	32	10-fold	3e-4	BCE	50

Legend: R1 - Model, R2 - Image Size, R3 - Optimizers, R4 - Mini Batch Size, R5 - cross validation, R6 - Initial Learning Rate, R7 - Loss function, R8 - Epoch, BCE - Binary cross-entropy.

Table 6.2: Confusion Matrix

	Predictive Positive	Predictive Negative	Total
Actual Positive	TP	FN	$TP + FN$
Actual Negative	FP	TN	$FP + TN$
Total	$TP + FP$	$FN + TN$	

Legend: TP = True Positive, FN = False Negative, FP = False Positive, TN = True Negative.

6.4.2 Classification Description

Training and testing performed by new CNN architecture, as mentioned above, in Scenario I classification models.

- *Scenario I:* In this scenario, we will classify five classes of DED, such as healthy, DR, DME, Gl, and Ca retinal fundus images (multi-class classification)

6.4.3 Classification Performance Analysis

Retinal fundus images are evaluated as follows, the efficacy of each CNN is calculated by various metrics implemented to measure the true and false category for the diagnosed DED. Next, the cross-validation estimator [192] is used, resulting in a Table.6.2 confusion matrix. If the classification algorithm accurately

categorizes samples based on a specific category, they are included in the TP indices. The TN indices of the confusion matrix contain the other samples which relate correctly to some other classes defined. Similarly, in the confusion matrix, the FP and FN indices represent the number of samples that the classifier wrongly estimates. As a result, the equations below are employed to ensure that a diagnostic test correctly detects and excludes a specific condition.

$$Accuracy(\%) = \frac{TP + TN}{TP + FN + TN + FP}. \quad (6.12)$$

For experimental analytics, output parameters derived from the confusion matrix are used. Accuracy in eq 6.12 is essentially the fraction of the uncertainty matrix's total values between true positive and true negative. Therefore, the above elements of the confusion matrix should determine the classifier's efficacy in our present framework.

Similarly, we employed, following equations,

$$Sensitivity(Recall) = \frac{TP}{TP + FN} \quad (6.13)$$

$$Specificity = \frac{TN}{TN + FP} \quad (6.14)$$

$$Precision = \frac{TP}{TP + FP} \quad (6.15)$$

ROC curve: A ROC (receiver operating characteristic curve) curve is a graphical representation that demonstrates how a test's specificity and sensitivity differ concerning each other. Using the test, samples considered to be true or false

are calculated to create a ROC curve. To offer a graph identical to the one below, the TPR (sensitivity) is mapped against the FPR (1 - specificity) for specified cut-off values. Preferably, a point is selected across the curve's shoulder, reducing false positives while optimizing real positives.

6.5 Experimental Design

All the studies conducted used Python, Keras library, TensorFlow as a back-end. The resolution of the images has been standardized to a uniform size, following each model's input requirements. The epoch number set at 50 because of the use of new CNN trained on weights in our experiments. The distribution of training/testing dataset at 80/20. Stratified standard preference made to ensure a nearly similar dispersion of the class. Mini-batch size set to 32, and the categorical cross-entropy loss function was selected due to its suitability for multi-class classification tasks. The default RMSProp was the Optimiser. The primary assessment metric for accuracy, specificity, and sensitivity of test data was used for final scores validation.

6.5.1 Performance enhancement

In this article, CNN recommended that the classification of the DED dataset be included. A deep convolutionary neural network (CNN) converts a function vector with a fixed weight matrix to obtain specific representations of features without losing spatial arrangement information [230]. Optimizer selection is a vital component of the neural network, helping to pick which one to use for the

model by understanding how they function. Several hyperparameters could be modified to increase the efficiency of the neural network. Not all of them, however, have a significant influence on the efficiency of the network. Not all of them, however, have a significant influence on the efficiency of the network. The optimizer is one of the parameters that could allow the adjustment between the algorithm assemblies or set-off. There are different optimizers we have picked from, the most widely used ones.

RMSprop Optimizer The RMSprop is an unpublished method proposed by Geoff Hinton based on adaptive learning rate [84]. The RMSprop optimizer is equivalent with momentum to the gradient descent algorithm. In the vertical direction, this optimizer limits the oscillations. Thus, we can maximize our learning rate, and our algorithm will take larger steps to converge faster in the horizontal direction. The discrepancy in how the gradients are measured is between RMSprop. For the RMSprop with momentum, the following equations illustrate how the gradients are determined. Hinton suggested the momentum value is normally set to 0.9 and a good default value for the learning rate η is 0.001.

$$D[f^2]_t = 0.9D[f^2]_{t-1} + 0.1f_t^2 \quad (6.16)$$

$$\beta_{t+1} = \beta_t - \frac{\eta}{\sqrt{D[f^2]_t + \epsilon}} f_t \quad (6.17)$$

RMSprop's gist is to maintain a moving average of the gradient square and divide the gradient by the root of this average ².

²<https://keras.io/api/optimizers/rmsprop/>

Table 6.3: Average performance of the models in multi-class DED classification.

Model	Optimiser	Learning Rate	Accuracy	Sensitivity	Specificity
CNN	<i>RMSprop</i>	1e-3	81.33%	100%	100%

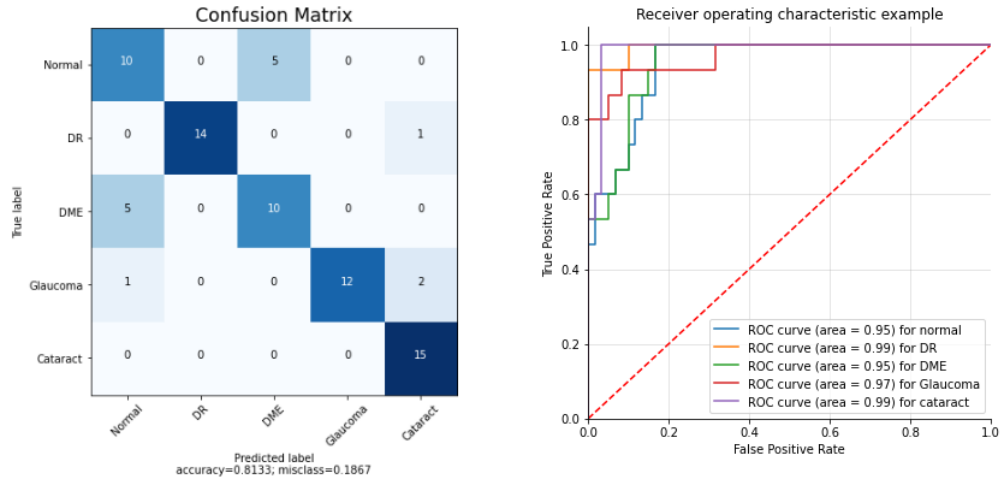


Figure 6.2: Confusion Matrix and ROC Curve obtained by proposed CNN

6.6 Results

The proposed CNN model has obtained accuracy in the test dataset. The efficiency acquired by the model has been used to demonstrate That multi-class classification in DED can be improved by improving the quality of the training images and using the right parameters for the model. The highest sensitivity and specificity was identified by proposed model in RMSprop optimizer. Finally, the accuracy obtained is shown in Table.6.3.

This analysis is a study of multi-class DED classification using the DL algorithm. A minimum of 80 percent sensitivity and 95 percent precision for sight-threatening DED identification must be obtained by any method [18] under the British Diabetic Association (BDA) guidelines. In scenario I, we achieved a max-

imum sensitivity of 100 percent and a maximum specificity of 100 percent, respectively, after checking our strategy in DED detection tasks. Thus, according to the BDA criteria, multi-class DED detection is adequate for its sensitivity and specificity.

6.6.1 Visualizing feature map

The feature maps, or activation maps, record the input applied with filters, such as the source images or other feature maps. The purpose of visualizing a feature map for particular source images would explain what attributes in the feature maps are observed or retained. The idea would be that the feature maps near the input detect fine-grained or small information while featuring maps near the model output to capture more distinctive characteristics. The first layer of CNN always learns features like edges, line patterns, color, and deeper layer network to identify more complex features like pathological lesions. Later layers construct their features by merging features from previous layers. To analyze the visualization of feature maps, we used the highest performed model with fundus retinal images, i.e., proposed CNN model, and used to create activations. The activations for CNN network models shown in Fig. 6.3.

6.6.2 Explaining Proposed Model using Grad-CAM

To make deep learning more practical and explainable, a range of work was performed. It is also essential to make the deep neural network more interpretative in various deep learning applications linked to medical imaging. A technique

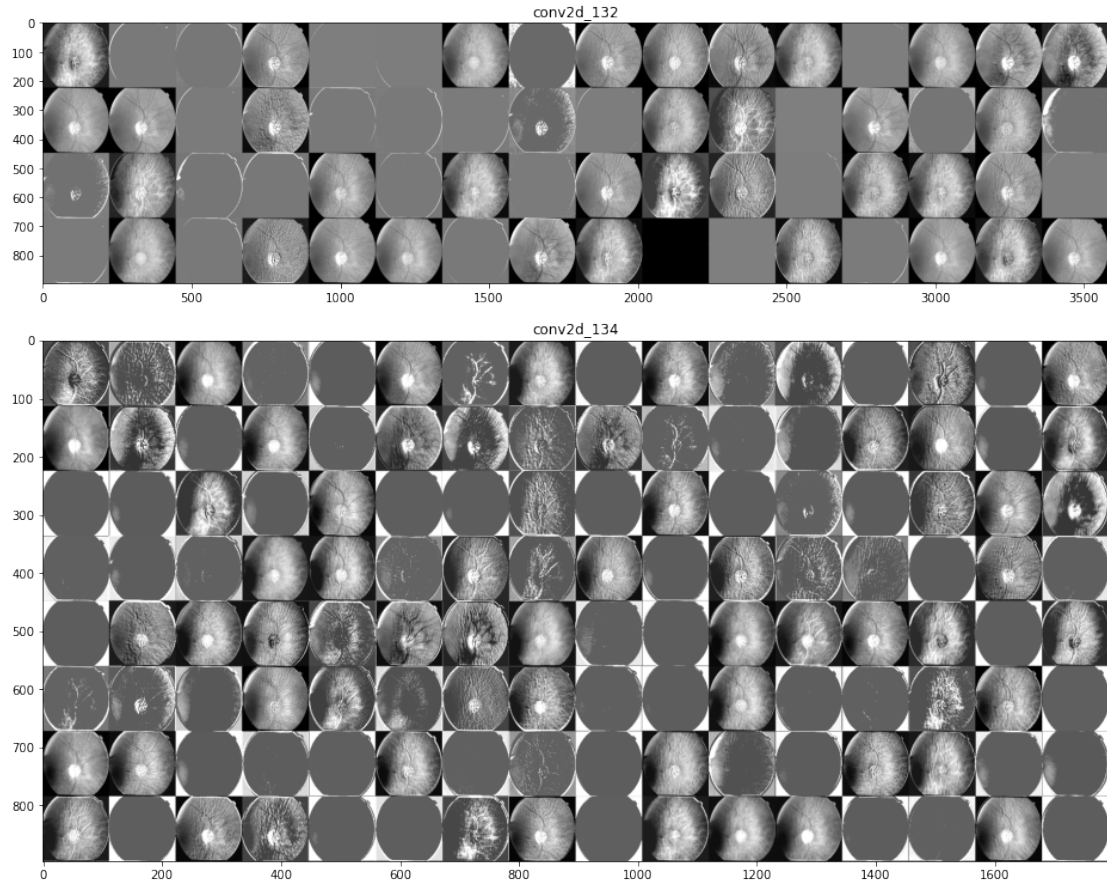


Figure 6.3: Visual feature maps in first layer and deep layer

of Gradient Weighted Class Activation Mapping (Grad-CAM) is developed by Selvaraju et al. [174], which provides an illustrative view of deep learning techniques. The technique of Grad-CAM offers a visual description for any deeply related neural network. This helps to decide more about the model when conducting identification or prediction tasks. The simple retinal fundus image is given as input and uses the proposed model as a detection method. After calculating the predicted label using the full model, Grad-CAM is applied to the last Convolution layer. Fig. 6.4 shows the heatmap visualization on various retinal fundus images by the proposed model.

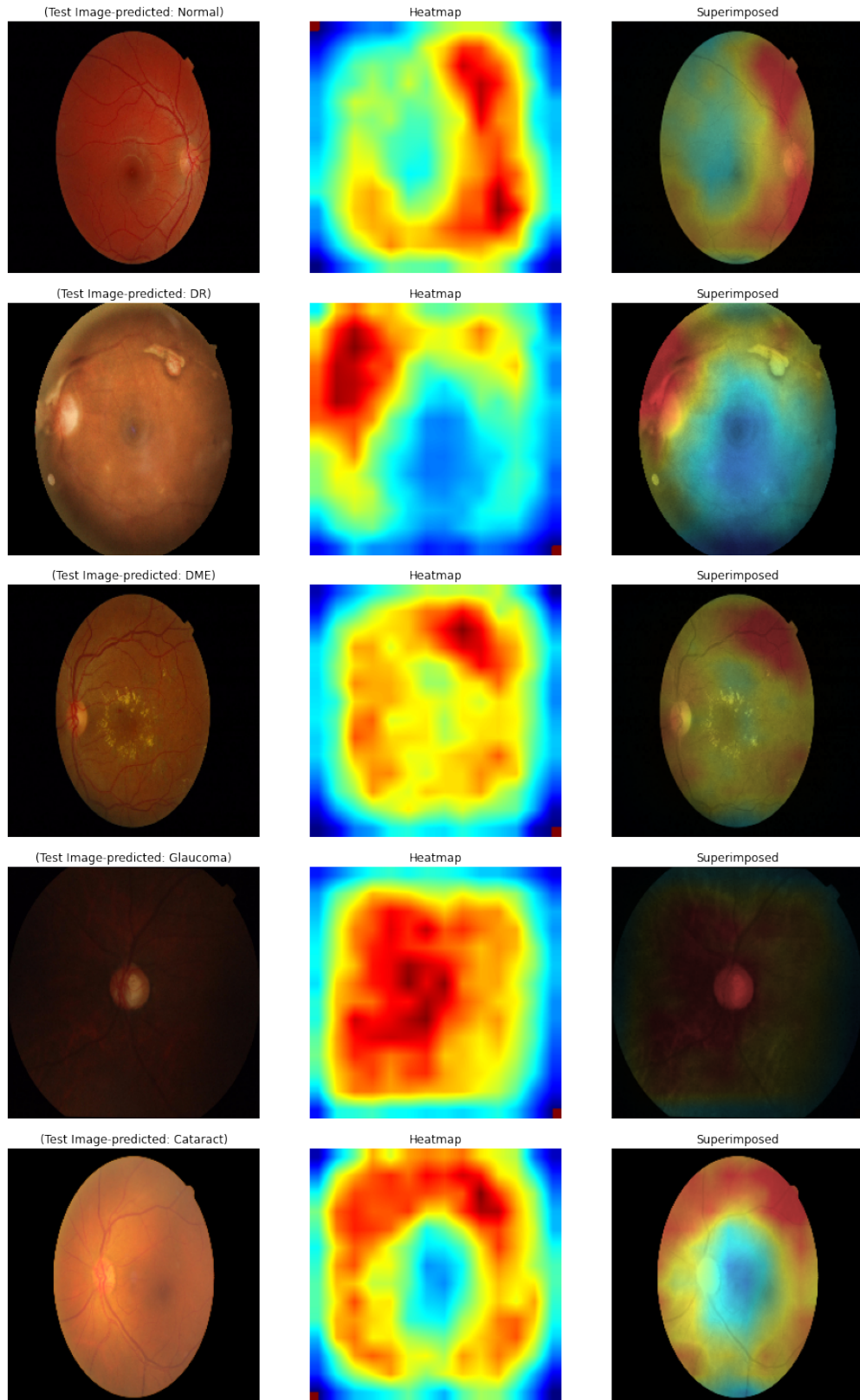


Figure 6.4: Visualisation on fundus retinal images of Normal / DR/ DME/ Glaucoma/ Cataract infected using Grad-CAM on the proposed model.

6.7 Summary of Findings

Automated DED recognition has been the topic of several studies in the past, with the main emphasis on healthy/unhealthy binary retinal classification [153]. In the case of multi-class classification, DL models' performance has been reduced as categories have multiplied. When categories increased, the predicted precision of the random distribution decreased. This finding corresponded to the previous studies [51]. Recent research using the GoogLeNet model to identify skin cancer has shown that an increase in the number of classes has underperformed (with an accuracy of 72.1% for a three-class problem and 55.4% for a nine-class problem) [56]. Thus it is essential to create disease-specific strategies to differentiate between DED to enhance multi-class classification efficiency. Therefore, this research proposed a system that focuses entirely on identifying multi-class DED among healthy instances, as discussed in previous studies. According to the empiric nature of DL, a variety of performance optimization techniques have been applied (i) optimizer choice, (ii) data augmentation, and (iii) contrast enhancement. The study also used combined datasets from different sources to evaluate the system's robustness in its flexibility to cope with real-world scenarios. As Wan et al. [219] have pointed out, the single data collection environment presents difficulties in the validation of accurate models [171].

Images of the retinal fundus are a popular and useful instrument and are used to provide accurate DED details. Such photographs can easily show injuries, anomalies and help to prevent permanent loss of vision. However, it is challenging to identify diabetic eye diseases through retinal fundus images accurately, and even highly experienced ophthalmologists are prone to misdiagnosis of eye lesions. Severe diabetic eye diseases, which require rapid diagnosis

and treatment, cause irreversible vision loss, visual imparities, and vision distortion disorders. Consequently, to assist in the diagnosis, it is essential to use deep learning methods. Multiple diseases may represent one collection of fundus photos. Using a single picture for diagnosis in a fundus image, which is well examined in traditional methods, is inaccurate. Besides, it requires a large amount of time to mark a series of retinal fundus images one by one. For this analysis, we, therefore, used publicly accessible and annotated photographs of the fundus. This research suggested a model that learns the characteristics of fundus images in retinal fundus photography and their feature dependencies for multi-class classification. We have grouped images of the retinal fundus into five types of diabetic eye disease. The findings presented in this work show that deep learning algorithms can automatically identify the form of diabetic eye disease. This technology may have a possible clinical application and may enhance healthcare delivery by identifying different acute DED diseases.

CHAPTER 7

CONCLUSION AND FUTURE WORK

This chapter presents the study's key contributions, including the drawbacks, potential directions, and its wider influence in the research field of computational health science.

7.1 Summary of Contributions

Diabetes is a life-threatening illness that affects multiple organs of the human body, including the eye's retina and causes DED disorder. Advanced DED leads to permanent vision loss, thus early detection of DED symptoms is essential to preventing disease escalation and ensuring timely treatment. This thesis addresses the research challenges in mild and multi-class DED detection reported in previous studies [42, 109]. Changes in eye anatomy during the early stages of DED are frequently untraceable by the human eye due to the subtle nature of their features. Large volumes of fundus images put a significant strain on limited specialist resources, rendering manual analysis practically infeasible. In response, this thesis introduced deep learning-based methods to facilitate early DED detection and address the current issues. Although deep learning applications have been used to detect severe anatomical changes to the eye, the detection of mild and multi-class disease has remained a problem. Consequently, in this thesis, we aim to address the main research gaps and propose a framework for mild and multi-class automated DED detection systems using fundus images through Deep Learning.

Detection of anatomical changes in the eye using fundus photography has brought up several challenges:

- The continuously increasing amount of information on patients' health, such as medical images, poses a significant strain on limited specialist diagnosis, treatment, and check-ups resources. Manual identification of features from high volumes of retinal images causes unnecessary time delays between detection and treatment. Diagnosis time taken further depends on specialists' years of practice experience
- Manual retinal image analysis and grading of DED performed by the ophthalmologist does not always produce accurate results as the very minute changes in the eye anatomy are not always detectable by the human eye
- Human evaluation tends to suffer from subjectivity leading to potentially inconsistent diagnoses across practices. At this point, early automated detection proves essential to providing early treatment and minimizing the risk of future vision loss
- Automated retinal image analysis plays an important role in screening for early DED detection.

In the last few decades, much efforts has been expended to establish reliable computer-based DED analysis systems. With the help of image processing techniques and deep learning methods, the workload associated with manual detection can be avoided, reducing the time and cost associated with DED diagnosis. The most common binary classification of severe-DED and non-DED using deep learning has already achieved high validation accuracy. Therefore, this research aimed to develop a robust system for mild and multi-class DED classification using colour fundus images.

The literature review revealed that previous work focuses on developing a classification system for the severity level of DR (mild, moderate, severe), and that classification of all four DED (DR, DME, Gl, Ca) jointly in one system is lacking. Detection of all four DED in one system is considered a crucial factor for treatment because it helps to specify the areas of abnormalities. Thus, we aimed to develop a system where mild and multi-class DED can be classified and detected effectively. In order to address the current challenges in automatic DED detection using deep learning, this thesis set out the main research question as a response: " *What deep learning approaches provide the highest accuracy for the classification task of mild and multi-class DED features, and how can they be further enhanced for clinical practice?*" The thesis focused on creating an advanced classification method to enhance the efficacy of the DED classification system in order to answer the question asked. Thus, the research goals were as follows:

- To develop an approach for retinal image enhancement to improve the validation accuracy before deep learning
- To introduce a robust framework for automatic classification and identification of mild DED
- To propose a new deep learning method for automated DED detection systems to achieve accuracy for clinical practice.

To achieve the goals set, the thesis proposed different image processing techniques in retinal fundus images, with the extensive study of 13 different pre-trained deep learning techniques with *seven* different optimizers in fundus images. In addition, we built a new deep learning framework and trained it from the scratch with the same retinal images. We used supervised methods of deep

learning for this research. These parameterized algorithms are capable of learning the patterns in the data, which must be considered carefully to distinguish the images and provided a class distinction based on empirical characteristics found in the data. Convolutional neural networks, powerful computational models designed to exploit high local correlations that exist in images, are employed in this thesis.

Machine learning techniques, particularly deep learning, are models that learn from data in general. Therefore, a primary aspect of success is to provide a statistically relevant sample dataset from which we can forecast a particular class of disease. To construct models with good generalization, it is essential to have a labelled dataset with appropriate samples (that is, the order of magnitude of thousands of elements per class). For this reason, we used various public datasets. In Chapter 2 this dataset is defined.

In Chapter 3 we implemented pre-trained deep learning methods for normal and mild DR classification. In this case, different high-resolution image values are obtained from the original images. Ideally, the use of images with the highest available resolution is interesting, but the processing and memory time needed make it challenging to use CNN architectures in such circumstances. In addition, the architecture of neural networks is a parameterized structures that requires regular input size. Moreover, with more adequate resolutions, abnormalities existing in images can be identified through presumed classification. In this chapter we also discuss the use of various input sizes, combinations of datasets, data augmentation approaches, fine-tuning, and optimization techniques which form the basis for choosing the right hyper-parameters. Ensemble methods are often used to enhance outcomes, averaging a range of estimates

from the measurement of different distorted representations of the same input image and image enhancement, comparing one patient's eye predictions with probability distributions of developing the disease by other. A near-human-level output model is derived from this preliminary work. The loss feature used for neural network parameter optimization in this chapter is the proven mild-DR classification norm, i.e. loss of logarithmics.

It is advantageous to use an immense amount of data, when building neural networks. The greater the number of instances of both No DR and Mild DR the better the model's validity, enabling the identification of more distinctive patterns. The small-scale Messidor dataset was then merged with the massive Kaggle dataset, i.e., the healthy and mild DR groups were merged in Chapter 3. Despite the enormous amount and ratio of Kaggle data from healthy to mild DR cases, resulting augmentation was conducted to mitigate the resulting problem of data imbalance. The following pre-processing steps were performed to improve classification: (1) *crop*, (2) *resize*, (3) *rotate* and (4) *mirror*. The device effectively promotes the standardization of the labour-intensive ocular process, while avoiding human subjectivity, acts as an auxiliary diagnostic reference.

Chapter 4 presents a way to use traditional image processing techniques for the performance enhancement of neural networks. Various image segmentation algorithms were combined to facilitate its usage with neural network pre-trained and build methods. These studies show that further research on automatic diagnosis utilizing fundus image analysis could define the mild DED classification. Traditional image processing to enhance mild DED characteristics was the first part of the experiment. Since mild DED appears to be extremely difficult to distinguish from a normal retina due to a few subtle signs

of deficiency, pathological features' visibility was expected to be increased by an increase in quality data. *VGG16* were the top 1 CNN architectures with the top layer removed and retrained, yielding an accuracy of 83.43%, 89.13%, 88% respectively. *Xception* and *DenseNet21* obtained the lowest results. Across the versions, the influence of fine-tuning varied. The observed increase in accuracy was only slight, suggesting the relative appropriateness for DED classification tasks of default pre-trained networks for DED classification tasks. In other words, despite having been educated on various images from the ImageNet repository, the CNN networks were able to distinguish mild DED from a healthy retina. If no progress in precision is made, unfreezing is not recommended, resulting in an excessive cost of measurement and time accumulated. The accuracy of 93.33%, 91.43%, 100%, was achieved for the CNN model build. The maximum sensitivity of 100 %, 94.44%, 100% and the maximum specificity of 86.67%, 88.24%, 100% was obtained after testing our high-performance approach on the detection task of mild DR, mild DME and mild GL. Thus, the early DED detection proved adequate, but still fell 9% and 6% short in terms of its specificity.

Chapter 5 concentrates on deep learning algorithms to classify mild and multi-class DEDs automatically. Previous studies in this field found that the new deep learning algorithms are ineffective in classifying DED disease from small datasets. For computer-aided medical applications, new deep learning algorithms failed to produce realistic and efficient results with less datasets. Therefore, because of each disease's significance, this research adapted the optimized deep learning architectures for the automated classification of healthy, DR, DME, GL, and Ca to construct an automated framework for the classification. The performance of deep learning models was dropped by 3%, in early

stage multi-class DED classification. This finding is apparently very normal since early stage DED fundus images consist of subtle features that can be crucial for diagnosis. Interestingly, the architectures most commonly deployed were designed to identify object based features like those present in the ImageNet dataset. A new paradigm such as lesion-based (e.g., exudates) were employed to diagnose multi-class DED using deep learning models. Following the work performed in this thesis, we can conclude that constructed frameworks can be used effectively as a diagnostic tool of high confidence to help clinical experts in mild DED diagnostic and reduce DED disease occurrence in the general population.

Chapter 6 Automated DED recognition has been the topic of several studies in the past, with the main emphasis on healthy/unhealthy binary retinal classification [153]. In the case of multi-class classification, the performance of pre-trained deep learning models reduces as categories multiply. In Chapter 5, it is observed that the predicted precision of the random distribution decreased when categories increase. This finding corresponded to the previous study by [51]. Thus, it is essential to create disease-specific strategies to differentiate between DED to enhance multi-class classification efficiency. Therefore, this research proposed a system that focuses entirely on identifying multi-class DED among healthy instances. According to the empiric nature of deep learning, a new built deep learning model with variety of performance optimization techniques have been applied (i) batch-size, (ii) epochs, (iii) learning rates and (iv) loss functions. Besides, this research used combined datasets from different sources to evaluate the system's robustness in its flexibility to cope with real-world scenarios. As Wan et al. [219] have pointed out, the single data collection environment presents difficulties in the validation of accurate models [171].

7.2 Study Limitations

Dataset Size: Several deficiencies of the research have been established. First, the datasets acquired for this experiment were publicly available which limited the number of high quality mild DED images. Only limited to moderate data set sizes were employed in the research. This approach also emphasises the value of an effective annotation process as having a direct effect on the output of the classifier. The Kaggle, Messidor, and Messidor-2, retinal datasets were validated and marked by professional ophthalmologists.

Dataset Source: Numerous datasets used in selected primary studies for DED detection suffer from a data imbalance problem in which images are not distributed uniformly throughout groups. The Kaggle data is a publicly accessible dataset, and the training data set is equipped with class labels. The training dataset consists of 35,126 images, and there are 53,576 images of the eye fundus in the test set. The training dataset given is imbalanced in such a way that there are 25,810 fundus images with class label 0 (normal diabetic retinopathy 73.5%), 2443 with label 1 (mild diabetic retinopathy 6.90%), 5292 with label 2 (moderate diabetic retinopathy 15.10%), 873 with label 3 (severe diabetic retinopathy 2.50%), and 708 with label 4 (proliferative diabetic retinopathy 2.00%). Such imbalanced data requires that the researcher either reduce the training data (resulting in a loss of extensive data) or update some specific class's training data using some image augmentation technique (resulting in biased classification results). The technique of image augmentation to deal with data imbalance is sufficient for better classification performance. However, only in the training set, and not the testing, image augmentation used. If the test set gives a higher classification accuracy (with no augmented images), then the results of the classification can

be used on a broader scale.

Technique Novelty: Transfer learning is used as a compensation procedure. Pre-trained CNN models in the wide-scale ImageNet database have been adopted in this study. To increase the size of the training sample set and to ease the data imbalance problem, data were rotated, flipped, mirrored, etc. Second, the default model parameters were adopted for the classification task (i.e. dropout, batch size, loss function, optimizer etc.). Finally, the 'black-box' nature of the deep learning-based solution is often criticized, causing resistance in the broader approach adopted by practitioners. However, with a CNN build using binary classifiers, we achieved state-of-the-art accuracy; the model performance degrades with the use of transfer learning. However, it is tough to ensure that more data help in developing more robust model. Previous field research has confirmed that CNN's ability to accommodate differences in size is limited, and some have indicated that more data can not overcome this inherent weakness in the case of retinal images [75].

7.3 Future Research Directions

This segment poses numerous research issues that researchers have not been able to solve in previous DED detection studies. Significant research is, therefore, needed to improve the effectiveness of various DED detection techniques. The gaps and research challenges that need to be addressed are set out below.

Developing stronger deep learning models: Deep learning has already shown extremely promising success in binary classification in the field of medical imaging and retinal disease diagnosis. To further refine and create more

effective deep neural networks for multiclass classification, another solution may be to increase computational power by increasing the capacity of the network [183,200]. Another approach could be to create a different object-based model rather than an image-based model. For example, if researchers are interested in detecting a region of interest (e.g. optic nerve only), they could design such a deep convolutional neural network that only learns with the optic nerve. It is argued in [138] that object-based identification is more effective than image-based identification.

Training on minimal data: deep learning software typically involves a large number of retinal fundus images for learning. If the training set is small, it may not produce satisfactory results in terms of accuracy. There are two solutions available. First, using a range of enhancement methods including image augmentation. Second, employ transfer learning algorithms to retrieve learned parameters and use these in the target task. Further, investigations shows Generative Adversal Network (GAN) is useful for the generation of training data, so that the DL architecture can be trained with robustness and more distinctive features [37].

Similar deep learning architecture for medical imaging: Several transfer learning frameworks for object recognition are available for retraining on a new collection of images such as medical images. These architectures are less suitable for medical images. This is because such TL frameworks are designed for objects such as animals, flowers, etc. As a result, such frameworks may be unsuitable for real time medical images. Potential study could implement a TL architectural design which has been learned on appropriate medical images rather than objects, functioning as a generic architecture, and eventually retrained to

improve the accuracy of medical image classification.

Automated choice of the optimum values for deep learning architectures:

Neural networks have provided promising results primarily in the area of computer vision and particularly in DED detection, but the complexity of modulating is not well known and is considered to be a black box. It is, therefore, hard to determine the effective model and optimum values for the number of layers and modules. Thus, in the future, automated optimization algorithms could be proposed to find optimal rates for various DL architectures on various DED datasets and other similar resources for medical images.

Integrating deep learning with telehealth and cloud computing: For remote regions in particular, mobile health can play an essential role in overcoming isolation. Neural networks in mobile devices can be used in the future to diagnose DED from eye fundus images. For example, in remote communities, the patient could use their mobile phone with a mobile camera to capture an image of the eye fundus. This image could also be classified using a DED detection model (constructed through a machine learning or deep learning approach). The configured system could identify DED from the image file and return the detection results.

BIBLIOGRAPHY

- [1] Qaisar Abbas, Irene Fondon, Auxiliadora Sarmiento, Soledad Jiménez, and Pedro Alemany. Automatic recognition of severity level for diagnosis of diabetic retinopathy using deep visual features. *Medical & biological engineering & computing*, 55(11):1959–1974, 2017.
- [2] Michael D Abramoff, Meindert Niemeijer, and Stephen R Russell. Automated detection of diabetic retinopathy: barriers to translation into clinical practice. *Expert review of medical devices*, 7(2):287–296, 2010.
- [3] Michael David Abramoff, Yiyue Lou, Ali Erginay, Warren Clarida, Ryan Amelon, James C Folk, and Meindert Niemeijer. Improved automated detection of diabetic retinopathy on a publicly available dataset through integration of deep learning. *Investigative ophthalmology & visual science*, 57(13):5200–5206, 2016.
- [4] Udyavara R Acharya, Choo M Lim, E Yin Kwee Ng, Caroline Chee, and Toshiyo Tamura. Computer-based detection of diabetes retinopathy stages using digital fundus images. *Proceedings of the institution of mechanical engineers, part H: journal of engineering in medicine*, 223(5):545–553, 2009.
- [5] Jin Mo Ahn, Sangsoo Kim, Kwang-Sung Ahn, Sung-Hoon Cho, Kwan Bok Lee, and Ungsoo Samuel Kim. A deep learning model for the detection of both advanced and early glaucoma using fundus photography. *PloS one*, 13(11):e0207982, 2018.
- [6] Jin Mo Ahn, Sangsoo Kim, Kwang-Sung Ahn, Sung-Hoon Cho, Kwan Bok Lee, and Ungsoo Samuel Kim. Correction: A deep learning model for the detection of both advanced and early glaucoma using fundus photography. *PloS one*, 14(1):e0211579, 2019.
- [7] Baidaa Al-Bander, Waleed Al-Nuaimy, Majid A Al-Tae, Bryan M Williams, and Yalin Zheng. Diabetic macular edema grading based on deep neural networks. *Proceedings of the Ophthalmic Medical Image Analysis Third International Workshop (OMIA 2016)*, 2016.
- [8] Baidaa Al-Bander, Waleed Al-Nuaimy, Majid A Al-Tae, and Yalin Zheng. Automated glaucoma diagnosis using deep learning approach. In *2017 14th International Multi-Conference on Systems, Signals & Devices (SSD)*, pages 207–210. IEEE, 2017.

- [9] Manal Al Ghamdi, Mingqi Li, Mohamed Abdel-Mottaleb, and Mohamed Abou Shousha. Semi-supervised transfer learning for convolutional neural networks for glaucoma detection. In *ICASSP 2019-2019 IEEE International Conference on Acoustics, Speech and Signal Processing (ICASSP)*, pages 3812–3816. IEEE, 2019.
- [10] Mohammad A Al-Jarrah and Hadeel Shatnawi. Non-proliferative diabetic retinopathy symptoms detection and classification using neural network. *Journal of medical engineering & technology*, 41(6):498–505, 2017.
- [11] Ahmed Almazroa, Sami Alodhayb, Essameldin Osman, Eslam Ramadan, Mohammed Hummadi, Mohammed Dlaim, Muhannad Alkatee, Kaamran Raahemifar, and Vasudevan Lakshminarayanan. Retinal fundus images for glaucoma analysis: the riga dataset. In *Medical Imaging 2018: Imaging Informatics for Healthcare, Research, and Applications*, volume 10579, page 105790B. International Society for Optics and Photonics, 2018.
- [12] Ahmed Almazroa, Ritambhar Burman, Kaamran Raahemifar, and Vasudevan Lakshminarayanan. Optic disc and optic cup segmentation methodologies for glaucoma image detection: a survey. *Journal of ophthalmology*, 2015, 2015.
- [13] Guangzhou An, Kazuko Omodaka, Kazuki Hashimoto, Satoru Tsuda, Yukihiko Shiga, Naoko Takada, Tsutomu Kikawa, Hideo Yokota, Masahiro Akiba, and Toru Nakazawa. Glaucoma diagnosis with machine learning based on optical coherence tomography and color fundus images. *Journal of Healthcare Engineering*, 2019, 2019.
- [14] Bálint Antal and András Hajdu. An ensemble-based system for automatic screening of diabetic retinopathy. *Knowledge-based systems*, 60:20–27, 2014.
- [15] R Arunkumar and P Karthigaikumar. Multi-retinal disease classification by reduced deep learning features. *Neural Computing and Applications*, 28(2):329–334, 2017.
- [16] Ryo Asaoka, Hiroshi Murata, Aiko Iwase, and Makoto Araie. Detecting preperimetric glaucoma with standard automated perimetry using a deep learning classifier. *Ophthalmology*, 123(9):1974–1980, 2016.
- [17] Ryo Asaoka, Masaki Tanito, Naoto Shibata, Keita Mitsuhashi, Kenichi Nakahara, Yuri Fujino, Masato Matsuura, Hiroshi Murata, Kana Tokumo, and Yoshiaki Kiuchi. Validation of a deep learning model to screen for

- glaucoma using images from different fundus cameras and data augmentation. *Ophthalmology Glaucoma*, 2019.
- [18] British Diabetic Association et al. Retinal photography screening for diabetic eye disease. *London: BDA*, 1997.
- [19] Pierre Baldi and Peter J Sadowski. Understanding dropout. In *Advances in neural information processing systems*, pages 2814–2822, 2013.
- [20] Ghazal Bargshady, Xujuan Zhou, Ravinesh C Deo, Jeffrey Soar, Frank Whittaker, and Hua Wang. Enhanced deep learning algorithm development to detect pain intensity from facial expression images. *Expert Systems with Applications*, 149:113305, 2020.
- [21] Buket D Barkana, Inci Saricicek, and Burak Yildirim. Performance analysis of descriptive statistical features in retinal vessel segmentation via fuzzy logic, ann, svm, and classifier fusion. *Knowledge-Based Systems*, 118:165–176, 2017.
- [22] James C Bezdek, James Keller, Raghu Krishnapuram, and Nikhil Pal. *Fuzzy models and algorithms for pattern recognition and image processing*, volume 4. Springer Science & Business Media, 1999.
- [23] RS Biyani and BM Patre. A clustering approach for exudates detection in screening of diabetic retinopathy. In *2016 International Conference on Signal and Information Processing (ICONSIP)*, pages 1–5. IEEE, 2016.
- [24] Patrick Bond. South africa’s vulnerability to the world capitalist crisis: How it worsened and how it might be reversed. *OF THE NATION*, page 609.
- [25] Rupert RA Bourne, Jost B Jonas, Alain M Bron, Maria Vittoria Cicinelli, Aditi Das, Seth R Flaxman, David S Friedman, Jill E Keeffe, John H Kempen, Janet Leasher, et al. Prevalence and causes of vision loss in high-income countries and in eastern and central europe in 2015: magnitude, temporal trends and projections. *British Journal of Ophthalmology*, 102(5):575–585, 2018.
- [26] Jean-Pierre Briot, Gaëtan Hadjeres, and François-David Pachet. Deep learning techniques for music generation—a survey. *arXiv preprint arXiv:1709.01620*, 2017.

- [27] Toan Bui, Noppadol Maneerat, and Ukrit Watchareeruetai. Detection of cotton wool for diabetic retinopathy analysis using neural network. In *2017 IEEE 10th International Workshop on Computational Intelligence and Applications (IWCI/A)*, pages 203–206. IEEE, 2017.
- [28] Philippe Burlina, David E Freund, Neil Joshi, Y Wolfson, and Neil M Bressler. Detection of age-related macular degeneration via deep learning. In *2016 IEEE 13th International Symposium on Biomedical Imaging (ISBI)*, pages 184–188. IEEE, 2016.
- [29] Miguel Caixinha and Sandrina Nunes. Machine learning techniques in clinical vision sciences. *Current eye research*, 42(1):1–15, 2017.
- [30] Enrique J Carmona, Mariano Rincón, Julián García-Feijoó, and José M Martínez-de-la Casa. Identification of the optic nerve head with genetic algorithms. *Artificial Intelligence in Medicine*, 43(3):243–259, 2008.
- [31] Darwin Yi Carson Lam, Margaret Guo, and Tony Lindsey. Automated detection of diabetic retinopathy using deep learning. *AMIA Summits on Translational Science Proceedings*, 2017:147, 2018.
- [32] Allan Cerentinia, Daniel Welfera, Marcos Cordeiro d’Ornellasa, Carlos Jesus Pereira Haygertb, and Gustavo Nogara Dottob. Automatic identification of glaucoma sing deep learning methods u. In *MEDINFO 2017: Precision Healthcare Through Informatics: Proceedings of the 16th World Congress on Medical and Health Informatics*, volume 245, page 318. IOS Press, 2018.
- [33] Juliana CN Chan, Vasanti Malik, Weiping Jia, Takashi Kadowaki, Chittaranjan S Yajnik, Kun-Ho Yoon, and Frank B Hu. Diabetes in asia: epidemiology, risk factors, and pathophysiology. *Jama*, 301(20):2129–2140, 2009.
- [34] CP Reshma Chand and J Dheeba. Automatic detection of exudates in color fundus retinopathy images. *Indian Journal of Science and Technology*, 8(26), 2015.
- [35] Subhasis Chaudhuri, Shankar Chatterjee, Norman Katz, Mark Nelson, and Michael Goldbaum. Detection of blood vessels in retinal images using two-dimensional matched filters. *IEEE Transactions on medical imaging*, 8(3):263–269, 1989.
- [36] Guanmin Chen, Peter Faris, Brenda Hemmelgarn, Robin L Walker, and Hude Quan. Measuring agreement of administrative data with chart data

using prevalence unadjusted and adjusted kappa. *BMC medical research methodology*, 9(1):5, 2009.

- [37] Hanlin Chen and Peng Cao. Deep learning based data augmentation and classification for limited medical data learning. In *2019 IEEE International Conference on Power, Intelligent Computing and Systems (ICPICS)*, pages 300–303. IEEE, 2019.
- [38] Xiangyu Chen, Yanwu Xu, Damon Wing Kee Wong, Tien Yin Wong, and Jiang Liu. Glaucoma detection based on deep convolutional neural network. In *2015 37th annual international conference of the IEEE engineering in medicine and biology society (EMBC)*, pages 715–718. IEEE, 2015.
- [39] Xiao Chen, Fazhi He, and Haiping Yu. A matting method based on full feature coverage. *Multimedia Tools and Applications*, 78(9):11173–11201, 2019.
- [40] Ching-Yu Cheng, Ningli Wang, Tien Y Wong, Nathan Congdon, Mingguang He, Ya Xing Wang, Tasanee Braithwaite, Robert J Casson, Maria Vittoria Cicinelli, Aditi Das, et al. Prevalence and causes of vision loss in east asia in 2015: magnitude, temporal trends and projections. *British Journal of Ophthalmology*, 104(5):616–622, 2020.
- [41] Carol Y Cheung, Fangyao Tang, Daniel Shu Wei Ting, Gavin Siew Wei Tan, and Tien Yin Wong. Artificial intelligence in diabetic eye disease screening. *The Asia-Pacific Journal of Ophthalmology*, 8(2):158–164, 2019.
- [42] Joon Yul Choi, Tae Keun Yoo, Jeong Gi Seo, Jiyong Kwak, Terry Taewoong Um, and Tyler Hyungtaek Rim. Multi-categorical deep learning neural network to classify retinal images: a pilot study employing small database. *PloS one*, 12(11):e0187336, 2017.
- [43] François Chollet. Xception: Deep learning with depthwise separable convolutions. In *Proceedings of the IEEE conference on computer vision and pattern recognition*, pages 1251–1258, 2017.
- [44] Nathan G Congdon, David S Friedman, and Thomas Lietman. Important causes of visual impairment in the world today. *Jama*, 290(15):2057–2060, 2003.
- [45] Tyler Coye. A novel retinal blood vessel segmentation algorithm for fundus images. *MATLAB Central File Exchange (Jan 2017)*, 2015.

- [46] Jeffrey De Fauw, Pearse Keane, Nenad Tomasev, Daniel Visentin, George van den Driessche, Mike Johnson, Cian O Hughes, Carlton Chu, Joseph Ledsam, Trevor Back, et al. Automated analysis of retinal imaging using machine learning techniques for computer vision. *F1000Research*, 5, 2016.
- [47] Jeffrey De Fauw, Joseph R Ledsam, Bernardino Romera-Paredes, Stanislav Nikolov, Nenad Tomasev, Sam Blackwell, Harry Askham, Xavier Glorot, Brendan O’Donoghue, Daniel Visentin, et al. Clinically applicable deep learning for diagnosis and referral in retinal disease. *Nature medicine*, 24(9):1342–1350, 2018.
- [48] Jordi de La Torre, Aida Valls, and Domenec Puig. A deep learning interpretable classifier for diabetic retinopathy disease grading. *Neurocomputing*, 2019.
- [49] Alan Carlos de Moura Lima, Lucas Bezerra Maia, Roberto Matheus Pinheiro Pereira, Geraldo Braz Junior, Joao Dallyson Sousa de Almeida, and Anselmo Cardoso de Paiva. Glaucoma diagnosis over eye fundus image through deep features. In *2018 25th International Conference on Systems, Signals and Image Processing (IWSSIP)*, pages 1–4. IEEE, 2018.
- [50] Etienne Decencière, Xiwei Zhang, Guy Cazuguel, Bruno Lay, Béatrice Cochener, Caroline Trone, Philippe Gain, Richard Ordonez, Pascale Massin, Ali Erginay, et al. Feedback on a publicly distributed image database: the messidor database. *Image Analysis & Stereology*, 33(3):231–234, 2014.
- [51] Jia Deng, Alexander C Berg, Kai Li, and Li Fei-Fei. What does classifying more than 10,000 image categories tell us? In *European conference on computer vision*, pages 71–84. Springer, 2010.
- [52] Steven Diamond, Vincent Sitzmann, Stephen Boyd, Gordon Wetzstein, and Felix Heide. Dirty pixels: Optimizing image classification architectures for raw sensor data. *arXiv preprint arXiv:1701.06487*, 2017.
- [53] Andres Diaz-Pinto, Sandra Morales, Valery Naranjo, Thomas Köhler, Jose M Mossi, and Amparo Navea. Cnns for automatic glaucoma assessment using fundus images: an extensive validation. *Biomedical engineering online*, 18(1):29, 2019.
- [54] Yanyan Dong, Qinyan Zhang, Zhiqiang Qiao, and Ji-Jiang Yang. Classification of cataract fundus image based on deep learning. In *2017 IEEE*

International Conference on Imaging Systems and Techniques (IST), pages 1–5. IEEE, 2017.

- [55] Darshit Doshi, Aniket Shenoy, Deep Sidhpura, and Prachi Gharpure. Diabetic retinopathy detection using deep convolutional neural networks. In *2016 International Conference on Computing, Analytics and Security Trends (CAST)*, pages 261–266. IEEE, 2016.
- [56] Andre Esteva, Brett Kuprel, Roberto A Novoa, Justin Ko, Susan M Swetter, Helen M Blau, and Sebastian Thrun. Dermatologist-level classification of skin cancer with deep neural networks. *Nature*, 542(7639):115–118, 2017.
- [57] Damian JJ Farnell, FN Hatfield, P Knox, M Reakes, S Spencer, D Parry, and Simon P Harding. Enhancement of blood vessels in digital fundus photographs via the application of multiscale line operators. *Journal of the Franklin institute*, 345(7):748–765, 2008.
- [58] Robert P Finger, Rolf Fimmers, Frank G Holz, and Hendrik PN Scholl. Incidence of blindness and severe visual impairment in germany: projections for 2030. *Investigative ophthalmology & visual science*, 52(7):4381–4389, 2011.
- [59] Nita Gandhi Forouhi and Nicholas J Wareham. Epidemiology of diabetes. *Medicine*, 38(11):602–606, 2010.
- [60] Nita Gandhi Forouhi and Nicholas J Wareham. Epidemiology of diabetes. *Medicine*, 47(1):22–27, 2019.
- [61] M Moazam Fraz, Waqas Jahangir, Saqib Zahid, Mian M Hamayun, and Sarah A Barman. Multiscale segmentation of exudates in retinal images using contextual cues and ensemble classification. *Biomedical Signal Processing and Control*, 35:50–62, 2017.
- [62] Francisco Fumero, Silvia Alayón, José L Sanchez, Jose Sigut, and M Gonzalez-Hernandez. Rim-one: An open retinal image database for optic nerve evaluation. In *2011 24th international symposium on computer-based medical systems (CBMS)*, pages 1–6. IEEE, 2011.
- [63] Karthikeyan Ganesan, Roshan Joy Martis, U Rajendra Acharya, Chua Kuang Chua, Lim Choo Min, EYK Ng, and Augustinus Laude. Computer-aided diabetic retinopathy detection using trace transforms

- on digital fundus images. *Medical & biological engineering & computing*, 52(8):663–672, 2014.
- [64] Xinting Gao, Stephen Lin, and Tien Yin Wong. Automatic feature learning to grade nuclear cataracts based on deep learning. *IEEE Transactions on Biomedical Engineering*, 62(11):2693–2701, 2015.
- [65] GG Gardner, D Keating, Tom H Williamson, and Alex T Elliott. Automatic detection of diabetic retinopathy using an artificial neural network: a screening tool. *British journal of Ophthalmology*, 80(11):940–944, 1996.
- [66] Rishab Gargeya and Theodore Leng. Automated identification of diabetic retinopathy using deep learning. *Ophthalmology*, 124(7):962–969, 2017.
- [67] Nasr Y Gharaibeh. A novel approach for detection of microaneurysms in diabetic retinopathy disease from retinal fundus images. *Computer and Information Science*, 10(1):1–15, 2017.
- [68] Ratul Ghosh, Kuntal Ghosh, and Sanjit Maitra. Automatic detection and classification of diabetic retinopathy stages using cnn. In *2017 4th International Conference on Signal Processing and Integrated Networks (SPIN)*, pages 550–554. IEEE, 2017.
- [69] Luca Giancardo, Fabrice Meriaudeau, Thomas P Karnowski, Yaqin Li, Seema Garg, Kenneth W Tobin Jr, and Edward Chaum. Exudate-based diabetic macular edema detection in fundus images using publicly available datasets. *Medical image analysis*, 16(1):216–226, 2012.
- [70] Evgin Goceri and Numan Goceri. Deep learning in medical image analysis: recent advances and future trends. 2017.
- [71] James Kang Hao Goh, Carol Y Cheung, Shaun Sebastian Sim, Pok Chien Tan, Gavin Siew Wei Tan, and Tien Yin Wong. Retinal imaging techniques for diabetic retinopathy screening. *Journal of diabetes science and technology*, 10(2):282–294, 2016.
- [72] Juan J Gómez-Valverde, Alfonso Antón, Gianluca Fatti, Bart Liefers, Alejandra Herranz, Andrés Santos, Clara I Sánchez, and María J Ledesma-Carbayo. Automatic glaucoma classification using color fundus images based on convolutional neural networks and transfer learning. *Biomedical optics express*, 10(2):892–913, 2019.

- [73] Waleed M Gondal, Jan M Köhler, René Grzeszick, Gernot A Fink, and Michael Hirsch. Weakly-supervised localization of diabetic retinopathy lesions in retinal fundus images. In *2017 IEEE International Conference on Image Processing (ICIP)*, pages 2069–2073. IEEE, 2017.
- [74] Early Treatment Diabetic Retinopathy Study Research Group et al. Grading diabetic retinopathy from stereoscopic color fundus photographs—an extension of the modified airleie house classification: Etdrs report number 10. *Ophthalmology*, 98(5):786–806, 1991.
- [75] Varun Gulshan, Lily Peng, Marc Coram, Martin C Stumpe, Derek Wu, Arunachalam Narayanaswamy, Subhashini Venugopalan, Kasumi Widner, Tom Madams, Jorge Cuadros, et al. Development and validation of a deep learning algorithm for detection of diabetic retinopathy in retinal fundus photographs. *Jama*, 316(22):2402–2410, 2016.
- [76] Fatih C Gundogan, Umit Yolcu, Fahrettin Akay, Abdullah Ilhan, Gokhan Ozge, and Salih Uzun. Diabetic macular edema. *Pakistan journal of medical sciences*, 32(2):505, 2016.
- [77] Yuki Hagiwara, Joel En Wei Koh, Jen Hong Tan, Sulatha V Bhandary, Augustinus Laude, Edward J Ciaccio, Louis Tong, and U Rajendra Acharya. Computer-aided diagnosis of glaucoma using fundus images: A review. *Computer methods and programs in biomedicine*, 165:1–12, 2018.
- [78] Balazs Harangi, Janos Toth, Agnes Baran, and Andras Hajdu. Automatic screening of fundus images using a combination of convolutional neural network and hand-crafted features. In *2019 41st Annual International Conference of the IEEE Engineering in Medicine and Biology Society (EMBC)*, pages 2699–2702. IEEE, 2019.
- [79] Taimur Hassan, M Usman Akram, M Furqan Masood, and Ubaidullah Yasin. Biomisa retinal image database for macular and ocular syndromes. In *International Conference Image Analysis and Recognition*, pages 695–705. Springer, 2018.
- [80] Hamid Hassanpour, Najmeh Samadiani, and SM Mahdi Salehi. Using morphological transforms to enhance the contrast of medical images. *The Egyptian Journal of Radiology and Nuclear Medicine*, 46(2):481–489, 2015.
- [81] Jinyuan He, Jia Rong, Le Sun, Hua Wang, Yanchun Zhang, and Jiangang Ma. A framework for cardiac arrhythmia detection from iot-based ecgs. *World Wide Web*, pages 1–16, 2020.

- [82] Kaiming He, Xiangyu Zhang, Shaoqing Ren, and Jian Sun. Deep residual learning for image recognition. In *Proceedings of the IEEE conference on computer vision and pattern recognition*, pages 770–778, 2016.
- [83] D Jude Hemanth, Omer Deperlioglu, and Utku Kose. An enhanced diabetic retinopathy detection and classification approach using deep convolutional neural network. *Neural Computing and Applications*, 32(3):707–721, 2020.
- [84] Geoffrey Hinton, Nitish Srivastava, and Kevin Swersky. Neural networks for machine learning lecture 6a overview of mini-batch gradient descent. *Cited on*, 14(8), 2012.
- [85] Daniel T Hogarty, David A Mackey, and Alex W Hewitt. Current state and future prospects of artificial intelligence in ophthalmology: a review. *Clinical & experimental ophthalmology*, 47(1):128–139, 2019.
- [86] Andrew G Howard, Menglong Zhu, Bo Chen, Dmitry Kalenichenko, Weijun Wang, Tobias Weyand, Marco Andreetto, and Hartwig Adam. Mobilenets: Efficient convolutional neural networks for mobile vision applications. *arXiv preprint arXiv:1704.04861*, 2017.
- [87] Gao Huang, Zhuang Liu, Laurens Van Der Maaten, and Kilian Q Weinberger. Densely connected convolutional networks. In *Proceedings of the IEEE conference on computer vision and pattern recognition*, pages 4700–4708, 2017.
- [88] A Hutchinson, A McIntosh, J Peters, C O’keeffe, K Khunti, R Baker, and A Booth. Effectiveness of screening and monitoring tests for diabetic retinopathy—a systematic review. *Diabetic medicine*, 17(7):495–506, 2000.
- [89] National Eye institute. Facts About Diabetic Eye Disease. <https://nei.nih.gov/health/diabetic/retinopathy>, 2015. [Online; Last Reviewed: September-2015].
- [90] Sergey Ioffe and Christian Szegedy. Batch normalization: Accelerating deep network training by reducing internal covariate shift. *arXiv preprint arXiv:1502.03167*, 2015.
- [91] Uzair Ishtiaq, Sameem Abdul Kareem, Erma Rahayu Mohd Faizal Abdullah, Ghulam Mujtaba, Rashid Jahangir, and Hafiz Yasir Ghafoor. Diabetic retinopathy detection through artificial intelligent techniques: a review and open issues. *Multimedia Tools and Applications*, pages 1–44, 2019.

- [92] Md Tariqul Islam, Sheikh Asif Imran, Asiful Arefeen, Mahmudul Hasan, and Celia Shahnaz. Source and camera independent ophthalmic disease recognition from fundus image using neural network. In *2019 IEEE International Conference on Signal Processing, Information, Communication & Systems (SPICSCON)*, pages 59–63. IEEE, 2019.
- [93] T Jaya, J Dheeba, and N Albert Singh. Detection of hard exudates in colour fundus images using fuzzy support vector machine-based expert system. *Journal of Digital Imaging*, 28(6):761–768, 2015.
- [94] Yuping Jiang, Huiqun Wu, and Jiancheng Dong. Automatic screening of diabetic retinopathy images with convolution neural network based on caffe framework. In *Proceedings of the 1st International Conference on Medical and Health Informatics 2017*, pages 90–94. ACM, 2017.
- [95] Shilpa Joshi and PT Karule. A review on exudates detection methods for diabetic retinopathy. *Biomedicine & Pharmacotherapy*, 97:1454–1460, 2018.
- [96] Mamta Juneja, Shaswat Singh, Naman Agarwal, Shivank Bali, Shubham Gupta, Niharika Thakur, and Prashant Jindal. Automated detection of glaucoma using deep learning convolution network (g-net). *Multimedia Tools and Applications*, pages 1–23, 2019.
- [97] Rim Kahloun, Moncef Khairallah, Serge Resnikoff, Maria Vittoria Cicinelli, Seth R Flaxman, Aditi Das, Jost B Jonas, Jill E Keeffe, John H Kempen, Janet Leasher, et al. Prevalence and causes of vision loss in north africa and middle east in 2015: magnitude, temporal trends and projections. *British Journal of Ophthalmology*, 103(7):863–870, 2019.
- [98] Asha Gowda Karegowda, Asfiya Nasiha, MA Jayaram, and AS Manjunath. Exudates detection in retinal images using back propagation neural network. *International Journal of Computer Applications*, 25(3):25–31, 2011.
- [99] Sri Phani Krishna Karri, Debjani Chakraborty, and Jyotirmoy Chatterjee. Transfer learning based classification of optical coherence tomography images with diabetic macular edema and dry age-related macular degeneration. *Biomedical optics express*, 8(2):579–592, 2017.
- [100] Manpreet Kaur and Mandeep Kaur. A hybrid approach for automatic exudates detection in eye fundus image. *Int. J.*, 5(6):411–417, 2015.
- [101] Jill Elizabeth Keeffe, Robert J Casson, Konrad Pesudovs, Hugh R Taylor, Maria Vittoria Cicinelli, Aditi Das, Seth R Flaxman, Jost B Jonas, John H

- Kempen, Janet Leasher, et al. Prevalence and causes of vision loss in south-east asia and oceania in 2015: magnitude, temporal trends and projections. *British Journal of Ophthalmology*, 103(7):878–884, 2019.
- [102] Nour Eldeen M Khalifa, Mohamed Loey, Mohamed Hamed N Taha, and Hamed Nasr Eldin T Mohamed. Deep transfer learning models for medical diabetic retinopathy detection. *Acta Informatica Medica*, 27(5):327, 2019.
- [103] Tehmina Khalil, Muhammad Usman Akram, Samina Khalid, and Amina Jameel. Improved automated detection of glaucoma from fundus image using hybrid structural and textural features. *IET Image Processing*, 11(9):693–700, 2017.
- [104] Helga Kolb. Simple anatomy of the retina by helga kolb. *Webvision: The Organization of the Retina and Visual System*, 2011.
- [105] Alex Krizhevsky, Ilya Sutskever, and Geoffrey E Hinton. Imagenet classification with deep convolutional neural networks. In *Advances in neural information processing systems*, pages 1097–1105, 2012.
- [106] Worapan Kusakunniran, Qiang Wu, Panrasee Ritthipravat, and Jian Zhang. Hard exudates segmentation based on learned initial seeds and iterative graph cut. *Computer methods and programs in biomedicine*, 158:173–183, 2018.
- [107] Arkadiusz Kwasigroch, Bartłomiej Jarzembinski, and Michal Grochowski. Deep cnn based decision support system for detection and assessing the stage of diabetic retinopathy. In *2018 International Interdisciplinary PhD Workshop (IIPhDW)*, pages 111–116. IEEE, 2018.
- [108] Kris A Kwiterovich, Maureen G Maguire, Robert P Murphy, Andrew P Schachat, Neil M Bressler, Susan B Bressler, and Stuart L Fine. Frequency of adverse systemic reactions after fluorescein angiography: results of a prospective study. *Ophthalmology*, 98(7):1139–1142, 1991.
- [109] Carson Lam, Darvin Yi, Margaret Guo, and Tony Lindsey. Automated detection of diabetic retinopathy using deep learning. *AMIA Summits on Translational Science Proceedings*, 2018:147, 2018.
- [110] Yann LeCun, Yoshua Bengio, and Geoffrey Hinton. Deep learning. *nature*, 521(7553):436–444, 2015.

- [111] Cecilia S Lee, Doug M Baughman, and Aaron Y Lee. Deep learning is effective for classifying normal versus age-related macular degeneration oct images. *Ophthalmology Retina*, 1(4):322–327, 2017.
- [112] Ryan Lee, Tien Y Wong, and Charumathi Sabanayagam. Epidemiology of diabetic retinopathy, diabetic macular edema and related vision loss. *Eye and vision*, 2(1):1–25, 2015.
- [113] Fei Li, Zhe Wang, Guoxiang Qu, Diping Song, Ye Yuan, Yang Xu, Kai Gao, Guangwei Luo, Zegu Xiao, Dennis SC Lam, et al. Automatic differentiation of glaucoma visual field from non-glaucoma visual field using deep convolutional neural network. *BMC medical imaging*, 18(1):35, 2018.
- [114] Guo Li, Shibao Zheng, and Xinzhe Li. Exudate detection in fundus images via convolutional neural network. In *International Forum on Digital TV and Wireless Multimedia Communications*, pages 193–202. Springer, 2017.
- [115] Hu Li, Ye Wang, Hua Wang, and Bin Zhou. Multi-window based ensemble learning for classification of imbalanced streaming data. *World Wide Web*, 20(6):1507–1525, 2017.
- [116] Xiaogang Li, Tiantian Pang, Biao Xiong, Weixiang Liu, Ping Liang, and Tianfu Wang. Convolutional neural networks based transfer learning for diabetic retinopathy fundus image classification. In *2017 10th International Congress on Image and Signal Processing, BioMedical Engineering and Informatics (CISP-BMEI)*, pages 1–11. IEEE, 2017.
- [117] Xiaomeng Li, Xiaowei Hu, Lequan Yu, Lei Zhu, Chi-Wing Fu, and Pheng-Ann Heng. Canet: Cross-disease attention network for joint diabetic retinopathy and diabetic macular edema grading. *IEEE transactions on medical imaging*, 2019.
- [118] Geert Litjens, Thijs Kooi, Babak Ehteshami Bejnordi, Arnaud Arindra Adiyoso Setio, Francesco Ciompi, Mohsen Ghafoorian, Jeroen AWM Van Der Laak, Bram Van Ginneken, and Clara I Sánchez. A survey on deep learning in medical image analysis. *Medical image analysis*, 42:60–88, 2017.
- [119] Jiangang Ma, Le Sun, Hua Wang, Yanchun Zhang, and Uwe Aickelin. Supervised anomaly detection in uncertain pseudoperiodic data streams. *ACM Transactions on Internet Technology (TOIT)*, 16(1):1–20, 2016.

- [120] G Mahendran and R Dhanasekaran. Investigation of the severity level of diabetic retinopathy using supervised classifier algorithms. *Computers & Electrical Engineering*, 45:312–323, 2015.
- [121] Romany F Mansour. Deep-learning-based automatic computer-aided diagnosis system for diabetic retinopathy. *Biomedical engineering letters*, 8(1):41–57, 2018.
- [122] Muhammad Mateen, Junhao Wen, Sun Song, Zhouping Huang, et al. Fundus image classification using vgg-19 architecture with pca and svd. *Symmetry*, 11(1):1, 2019.
- [123] Prasanna Porwal; Samiksha Pachade; Ravi Kamble; Manesh Kokare; Girish Deshmukh; Vivek Sahasrabudde; Fabrice Meriaudeau. Indian diabetic retinopathy image dataset (idrid), 2018.
- [124] Volodymyr Mnih, Koray Kavukcuoglu, David Silver, Andrei A Rusu, Joel Veness, Marc G Bellemare, Alex Graves, Martin Riedmiller, Andreas K Fidjeland, Georg Ostrovski, et al. Human-level control through deep reinforcement learning. *nature*, 518(7540):529–533, 2015.
- [125] Muthu Rama Krishnan Mookiah, U Rajendra Acharya, Chua Kuang Chua, Choo Min Lim, EYK Ng, and Augustinus Laude. Computer-aided diagnosis of diabetic retinopathy: A review. *Computers in biology and medicine*, 43(12):2136–2155, 2013.
- [126] Vinay Nangia, Jost B Jonas, Ronnie George, Vijaya Lingam, Leon Ellwein, Maria Vittoria Cicinelli, Aditi Das, Seth R Flaxman, Jill E Keeffe, John H Kempen, et al. Prevalence and causes of blindness and vision impairment: magnitude, temporal trends and projections in south and central asia. *British Journal of Ophthalmology*, 103(7):871–877, 2019.
- [127] Syed Ali Gohar Naqvi, Muhammad Faisal Zafar, and Ihsan ul Haq. Referral system for hard exudates in eye fundus. *Computers in biology and medicine*, 64:217–235, 2015.
- [128] Quang H Nguyen, Ramasamy Muthuraman, Laxman Singh, Gopa Sen, Anh Cuong Tran, Binh P Nguyen, and Matthew Chua. Diabetic retinopathy detection using deep learning. In *Proceedings of the 4th International Conference on Machine Learning and Soft Computing*, pages 103–107, 2020.
- [129] Pradeep Nijalingappa and B Sandeep. Machine learning approach for the identification of diabetes retinopathy and its stages. In *2015 International*

Conference on Applied and Theoretical Computing and Communication Technology (iCATccT), pages 653–658. IEEE, 2015.

- [130] Jan H Noordik. *Cheminformatics Developments: History, Reviews and Current Research*. IOS Press, 2004.
- [131] Kevin Noronha, Jagadish Nayak, and SN Bhat. Enhancement of retinal fundus image to highlight the features for detection of abnormal eyes. In *TENCON 2006-2006 IEEE Region 10 Conference*, pages 1–4. IEEE, 2006.
- [132] Maxime Oquab, Leon Bottou, Ivan Laptev, and Josef Sivic. Learning and transferring mid-level image representations using convolutional neural networks. In *Proceedings of the IEEE conference on computer vision and pattern recognition*, pages 1717–1724, 2014.
- [133] World Health Organization et al. Global report on diabetes. 2016.
- [134] José Ignacio Orlando, Huazhu Fu, João Barbosa Breda, Karel van Keer, Deepti R Bathula, Andrés Diaz-Pinto, Ruogu Fang, Pheng-Ann Heng, Jeyoung Kim, JoonHo Lee, et al. Refugee challenge: A unified framework for evaluating automated methods for glaucoma assessment from fundus photographs. *Medical image analysis*, 59:101570, 2020.
- [135] José Ignacio Orlando, Elena Prokofyeva, Mariana del Fresno, and Matthew B Blaschko. Convolutional neural network transfer for automated glaucoma identification. In *12th international symposium on medical information processing and analysis*, volume 10160, page 101600U. International Society for Optics and Photonics, 2017.
- [136] José Ignacio Orlando, Elena Prokofyeva, Mariana del Fresno, and Matthew B Blaschko. An ensemble deep learning based approach for red lesion detection in fundus images. *Computer methods and programs in biomedicine*, 153:115–127, 2018.
- [137] Alireza Osareh, Majid Mirmehdi, Bari Thomas, and Richard Markham. Automated identification of diabetic retinal exudates in digital colour images. *British Journal of Ophthalmology*, 87(10):1220–1223, 2003.
- [138] Wanli Ouyang, Ping Luo, Xingyu Zeng, Shi Qiu, Yonglong Tian, Hongsheng Li, Shuo Yang, Zhe Wang, Yuanjun Xiong, Chen Qian, et al. Deepidnet: multi-stage and deformable deep convolutional neural networks for object detection. *arXiv preprint arXiv:1409.3505*, 2014.

- [139] Abhishek Pal, Manav Rajiv Moorthy, and A Shahina. G-eyenet: A convolutional autoencoding classifier framework for the detection of glaucoma from retinal fundus images. In *2018 25th IEEE International Conference on Image Processing (ICIP)*, pages 2775–2779. IEEE, 2018.
- [140] Sinno Jialin Pan and Qiang Yang. A survey on transfer learning. *IEEE Transactions on knowledge and data engineering*, 22(10):1345–1359, 2009.
- [141] Dinesh Pandey, Xiaoxia Yin, Hua Wang, Min-Ying Su, Jeon-Hor Chen, Jianlin Wu, and Yanchun Zhang. Automatic and fast segmentation of breast region-of-interest (roi) and density in mris. *Heliyon*, 4(12):e01042, 2018.
- [142] Dinesh Pandey, Xiaoxia Yin, Hua Wang, and Yanchun Zhang. Accurate vessel segmentation using maximum entropy incorporating line detection and phase-preserving denoising. *Computer Vision and Image Understanding*, 155:162–172, 2017.
- [143] Sumaiya Pathan, Preetham Kumar, Radhika M Pai, and Sulatha V Bhandary. Automated segmentation and classification of retinal features for glaucoma diagnosis. *Biomedical Signal Processing and Control*, 63:102244, 2021.
- [144] Oscar Perdomo, John Arevalo, and Fabio A González. Convolutional network to detect exudates in eye fundus images of diabetic subjects. In *12th International Symposium on Medical Information Processing and Analysis*, volume 10160, page 101600T. International Society for Optics and Photonics, 2017.
- [145] Oscar Perdomo, Sebastian Otalora, Francisco Rodríguez, John Arevalo, and Fabio A González. A novel machine learning model based on exudate localization to detect diabetic macular edema. 2016.
- [146] Sang Phan, Shin’ichi Satoh, Yoshioki Yoda, Kenji Kashiwagi, Tetsuro Oshika, Japan Ocular Imaging Registry Research Group, et al. Evaluation of deep convolutional neural networks for glaucoma detection. *Japanese journal of ophthalmology*, pages 1–8, 2019.
- [147] Ramon Pires, Sandra Avila, Jacques Wainer, Eduardo Valle, Michael D Abramoff, and Anderson Rocha. A data-driven approach to referable diabetic retinopathy detection. *Artificial Intelligence in Medicine*, 2019.

- [148] M Ponni Bala and S Vijayachitra. Early detection and classification of microaneurysms in retinal fundus images using sequential learning methods. *International Journal of Biomedical Engineering and Technology*, 15(2):128–143, 2014.
- [149] M Ponnibala and S Vijayachitra. A sequential learning method for detection and classification of exudates in retinal images to assess diabetic retinopathy. *Journal of Biological Systems*, 22(03):413–428, 2014.
- [150] Ryan Poplin, Avinash V Varadarajan, Katy Blumer, Yun Liu, Michael V McConnell, Greg S Corrado, Lily Peng, and Dale R Webster. Prediction of cardiovascular risk factors from retinal fundus photographs via deep learning. *Nature Biomedical Engineering*, 2(3):158, 2018.
- [151] Prasanna Porwal, Samiksha Pachade, Ravi Kamble, Manesh Kokare, Girish Deshmukh, Vivek Sahasrabuddhe, and Fabrice Meriaudeau. Indian diabetic retinopathy image dataset (idrid): A database for diabetic retinopathy screening research. *Data*, 3(3):25, 2018.
- [152] Turimerla Pratap and Priyanka Kokil. Computer-aided diagnosis of cataract using deep transfer learning. *Biomedical Signal Processing and Control*, 53:101533, 2019.
- [153] Harry Pratt, Frans Coenen, Deborah M Broadbent, Simon P Harding, and Yalin Zheng. Convolutional neural networks for diabetic retinopathy. *Procedia Computer Science*, 90:200–205, 2016.
- [154] Pavle Prentasic and Sven Loncaric. Weighted ensemble based automatic detection of exudates in fundus photographs. In *2014 36th Annual International Conference of the IEEE Engineering in Medicine and Biology Society*, pages 138–141. IEEE, 2014.
- [155] Pavle Prentašić and Sven Lončarić. Detection of exudates in fundus photographs using deep neural networks and anatomical landmark detection fusion. *Computer methods and programs in biomedicine*, 137:281–292, 2016.
- [156] Pavle Prentašić, Sven Lončarić, Zoran Vatauvuk, Goran Benčić, Marko Subašić, Tomislav Petković, Lana Dujmović, Maja Malenica-Ravlić, Nikolina Budimlija, and Rašeljka Tadić. Diabetic retinopathy image database (dridb): a new database for diabetic retinopathy screening programs research. In *2013 8th International Symposium on Image and Signal Processing and Analysis (ISPA)*, pages 711–716. IEEE, 2013.

- [157] Gwenolé Quéllec, Katia Charrière, Yassine Boudi, Béatrice Cochener, and Mathieu Lamard. Deep image mining for diabetic retinopathy screening. *Medical image analysis*, 39:178–193, 2017.
- [158] U Raghavendra, Hamido Fujita, Sulatha V Bhandary, Anjan Gudigar, Jen Hong Tan, and U Rajendra Acharya. Deep convolution neural network for accurate diagnosis of glaucoma using digital fundus images. *Information Sciences*, 441:41–49, 2018.
- [159] Sarni Suhaila Rahim, Chrisina Jayne, Vasile Palade, and James Shuttleworth. Automatic detection of microaneurysms in colour fundus images for diabetic retinopathy screening. *Neural computing and applications*, 27(5):1149–1164, 2016.
- [160] Jing Ran, Kai Niu, Zhiqiang He, Hongyan Zhang, and Hongxin Song. Cataract detection and grading based on combination of deep convolutional neural network and random forests. In *2018 International Conference on Network Infrastructure and Digital Content (IC-NIDC)*, pages 155–159. IEEE, 2018.
- [161] Pallab Roy, Ruwan Tennakoon, Khoa Cao, Suman Sedai, Dwarikanath Mahapatra, Stefan Maetschke, and Rahil Garnavi. A novel hybrid approach for severity assessment of diabetic retinopathy in colour fundus images. In *2017 IEEE 14th International Symposium on Biomedical Imaging (ISBI 2017)*, pages 1078–1082. IEEE, 2017.
- [162] Olga Russakovsky, Jia Deng, Hao Su, Jonathan Krause, Sanjeev Satheesh, Sean Ma, Zhiheng Huang, Andrej Karpathy, Aditya Khosla, Michael Bernstein, et al. Imagenet large scale visual recognition challenge. *International journal of computer vision*, 115(3):211–252, 2015.
- [163] Jaakko Sahlsten, Joel Jaskari, Jyri Kivinen, Lauri Turunen, Esa Jaanio, Kustaa Hietala, and Kimmo Kaski. Deep learning fundus image analysis for diabetic retinopathy and macular edema grading. *Scientific reports*, 9(1):1–11, 2019.
- [164] Patrick J Saine and Marshall E Tyler. *Ophthalmic photography: retinal photography, angiography, and electronic imaging*, volume 132. Butterworth-Heinemann Boston, 2002.
- [165] Mark Sandler, Andrew Howard, Menglong Zhu, Andrey Zhmoginov, and Liang-Chieh Chen. Mobilenetv2: Inverted residuals and linear bottle-

- necks. In *Proceedings of the IEEE Conference on Computer Vision and Pattern Recognition*, pages 4510–4520, 2018.
- [166] M Sankar, K Batri, and R Parvathi. Earliest diabetic retinopathy classification using deep convolution neural networks. pdf. *Int. J. Adv. Eng. Technol.*, 10:M9, 2016.
- [167] D Santhi, D Manimegalai, S Parvathi, and S Karkuzhali. Segmentation and classification of bright lesions to diagnose diabetic retinopathy in retinal images. *Biomedical Engineering/Biomedizinische Technik*, 61(4):443–453, 2016.
- [168] Iqbal H Sarker, Md Faisal Faruque, Hamed Alqahtani, and Asra Kalim. K-nearest neighbor learning based diabetes mellitus prediction and analysis for ehealth services.
- [169] Rubina Sarki, Khandakar Ahmed, Hua Wang, and Yanchun Zhang. Automated detection of mild and multi-class diabetic eye diseases using deep learning. *Health Information Science and Systems*, 8(1):1–9, 2020.
- [170] Rubina Sarki, Khandakar Ahmed, Hua Wang, and Yanchun Zhang. Automatic detection of diabetic eye disease through deep learning using fundus images: A survey. *IEEE Access*, 8:151133–151149, 2020.
- [171] Rubina Sarki, Khandakar Ahmed, and Yanchun Zhang. Early detection of diabetic eye disease through deep learning using fundus images. *EAI Endorsed Transactions on Pervasive Health and Technology*, 6(22), 5 2020.
- [172] Rory Sayres, Ankur Taly, Ehsan Rahimy, Katy Blumer, David Coz, Naama Hammel, Jonathan Krause, Arunachalam Narayanaswamy, Zahra Rastegar, Derek Wu, et al. Using a deep learning algorithm and integrated gradients explanation to assist grading for diabetic retinopathy. *Ophthalmology*, 126(4):552–564, 2019.
- [173] Strategic Policy Sector et al. State of the nation 2012. 2013.
- [174] Ramprasaath R Selvaraju, Michael Cogswell, Abhishek Das, Ramakrishna Vedantam, Devi Parikh, and Dhruv Batra. Grad-cam: Visual explanations from deep networks via gradient-based localization. In *Proceedings of the IEEE international conference on computer vision*, pages 618–626, 2017.
- [175] Syamimi Mardiah Shahrarum, Nurul Hajar Hashim, Nurhafizah Abu

- Talip, Mohamad Shaiful Abdul Karim, Ahmad Afif Mohd Faudzi, et al. Automatic detection of diabetic retinopathy retinal images using artificial neural network. In *Proceedings of the 10th National Technical Seminar on Underwater System Technology 2018*, pages 495–503. Springer, 2019.
- [176] Ambika Sharma, Monika Agrawal, Sumantra Dutta Roy, and Vivek Gupta. Automatic glaucoma diagnosis in digital fundus images using deep cnns. In *Advances in Computational Intelligence Techniques*, pages 37–52. Springer, Singapore, 2020.
- [177] Naoto Shibata, Masaki Tanito, Keita Mitsuhashi, Yuri Fujino, Masato Matsuura, Hiroshi Murata, and Ryo Asaoka. Development of a deep residual learning algorithm to screen for glaucoma from fundus photography. *Scientific reports*, 8(1):1–9, 2018.
- [178] Frank Y Shih. *Image processing and pattern recognition: fundamentals and techniques*. John Wiley & Sons, 2010.
- [179] Hoo-Chang Shin, Holger R Roth, Mingchen Gao, Le Lu, Ziyue Xu, Isabella Nogues, Jianhua Yao, Daniel Mollura, and Ronald M Summers. Deep convolutional neural networks for computer-aided detection: Cnn architectures, dataset characteristics and transfer learning. *IEEE transactions on medical imaging*, 35(5):1285–1298, 2016.
- [180] SD Shirbahadurkar, Vijay M Mane, and Dattatray V Jadhav. Early stage detection of diabetic retinopathy using an optimal feature set. In *International Symposium on Signal Processing and Intelligent Recognition Systems*, pages 15–23. Springer, 2017.
- [181] Nathan Silberman, Kristy Ahrlich, Rob Fergus, and Lakshminarayanan Subramanian. Case for automated detection of diabetic retinopathy. In *2010 AAAI Spring Symposium Series*, 2010.
- [182] David Silver, Aja Huang, Chris J Maddison, Arthur Guez, Laurent Sifre, George Van Den Driessche, Julian Schrittwieser, Ioannis Antonoglou, Veda Panneershelvam, Marc Lanctot, et al. Mastering the game of go with deep neural networks and tree search. *nature*, 529(7587):484–489, 2016.
- [183] Karen Simonyan and Andrew Zisserman. Very deep convolutional networks for large-scale image recognition. *arXiv preprint arXiv:1409.1556*, 2014.

- [184] Amitojdeep Singh, Sourya Sengupta, and Vasudevan Lakshminarayanan. Glaucoma diagnosis using transfer learning methods. In *Applications of Machine Learning*, volume 11139, page 111390U. International Society for Optics and Photonics, 2019.
- [185] Law Kumar Singh, Hitendra Garg, et al. Automated glaucoma type identification using machine learning or deep learning techniques. In *Advancement of Machine Intelligence in Interactive Medical Image Analysis*, pages 241–263. Springer, Singapore, 2020.
- [186] Chanjira Sinthanayothin, James F Boyce, Tom H Williamson, Helen L Cook, Evelyn Mensah, Shantanu Lal, and David Usher. Automated detection of diabetic retinopathy on digital fundus images. *Diabetic medicine*, 19(2):105–112, 2002.
- [187] Dilip Singh Sisodia, Shruti Nair, and Pooja Khobragade. Diabetic retinal fundus images: Preprocessing and feature extraction for early detection of diabetic retinopathy. *Biomedical and Pharmacology Journal*, 10(2):615–626, 2017.
- [188] Siuly Siuly, Smith K Khare, Varun Bajaj, Hua Wang, and Yanchun Zhang. A computerized method for automatic detection of schizophrenia using eeg signals. *IEEE Transactions on Neural Systems and Rehabilitation Engineering*, 2020.
- [189] Sobha Sivaprasad, Joana C Vasconcelos, A Toby Prevost, Helen Holmes, Philip Hykin, Sheena George, Caroline Murphy, Joanna Kelly, Geoffrey B Arden, Frank Ahfat, et al. Clinical efficacy and safety of a light mask for prevention of dark adaptation in treating and preventing progression of early diabetic macular oedema at 24 months (cleopatra): a multicentre, phase 3, randomised controlled trial. *The Lancet Diabetes & Endocrinology*, 6(5):382–391, 2018.
- [190] Jayanthi Sivaswamy, SR Krishnadas, Gopal Datt Joshi, Madhulika Jain, and A Ujjwaft Syed Tabish. Drishti-gs: Retinal image dataset for optic nerve head (onh) segmentation. In *2014 IEEE 11th international symposium on biomedical imaging (ISBI)*, pages 53–56. IEEE, 2014.
- [191] Alvy Ray Smith. Color gamut transform pairs. *ACM Siggraph Computer Graphics*, 12(3):12–19, 1978.
- [192] Marina Sokolova and Guy Lapalme. A systematic analysis of perfor-

- mance measures for classification tasks. *Information processing & management*, 45(4):427–437, 2009.
- [193] Chris Solomon and Toby Breckon. *Fundamentals of Digital Image Processing: A practical approach with examples in Matlab*. John Wiley & Sons, 2011.
- [194] SK Somasundaram and P Alli. A machine learning ensemble classifier for early prediction of diabetic retinopathy. *Journal of Medical Systems*, 41(12):1–12, 2017.
- [195] Akara Sopharak and Bunyarit Uyyanonvara. Automatic exudates detection from diabetic retinopathy retinal image using fuzzy c-means and morphological methods. In *Proceedings of the third IASTED international conference Advances in Computer Science and Technology*, pages 359–364, 2007.
- [196] Nitish Srivastava, Geoffrey Hinton, Alex Krizhevsky, Ilya Sutskever, and Ruslan Salakhutdinov. Dropout: a simple way to prevent neural networks from overfitting. *The journal of machine learning research*, 15(1):1929–1958, 2014.
- [197] Ruchir Srivastava, Lixin Duan, Damon WK Wong, Jiang Liu, and Tien Yin Wong. Detecting retinal microaneurysms and hemorrhages with robustness to the presence of blood vessels. *Computer methods and programs in biomedicine*, 138:83–91, 2017.
- [198] KQ Sun and N Sang. Morphological enhancement of vascular angiogram with multiscale detected by gabor filters. *Electronics Letters*, 44(2):86–87, 2008.
- [199] Christian Szegedy, Sergey Ioffe, Vincent Vanhoucke, and Alexander A Alemi. Inception-v4, inception-resnet and the impact of residual connections on learning. In *Thirty-First AAAI Conference on Artificial Intelligence*, 2017.
- [200] Christian Szegedy, Wei Liu, Yangqing Jia, Pierre Sermanet, Scott Reed, Dragomir Anguelov, Dumitru Erhan, Vincent Vanhoucke, and Andrew Rabinovich. Going deeper with convolutions. In *Proceedings of the IEEE conference on computer vision and pattern recognition*, pages 1–9, 2015.
- [201] Christian Szegedy, Vincent Vanhoucke, Sergey Ioffe, Jon Shlens, and Zbigniew Wojna. Rethinking the inception architecture for computer vision. In

Proceedings of the IEEE conference on computer vision and pattern recognition, pages 2818–2826, 2016.

- [202] Syed Amin Tabish. Is diabetes becoming the biggest epidemic of the twenty-first century? *International Journal of health sciences*, 1(2):V, 2007.
- [203] Hidenori Takahashi, Hironobu Tampo, Yusuke Arai, Yuji Inoue, and Hidetoshi Kawashima. Applying artificial intelligence to disease staging: Deep learning for improved staging of diabetic retinopathy. *PloS one*, 12(6):e0179790, 2017.
- [204] Jen Hong Tan, Hamido Fujita, Sobha Sivaprasad, Sulatha V Bhandary, A Krishna Rao, Kuang Chua Chua, and U Rajendra Acharya. Automated segmentation of exudates, haemorrhages, microaneurysms using single convolutional neural network. *Information sciences*, 420:66–76, 2017.
- [205] Wei Ren Tan, Chee Seng Chan, Hernán E Aguirre, and Kiyoshi Tanaka. Artgan: Artwork synthesis with conditional categorical gans. In *2017 IEEE International Conference on Image Processing (ICIP)*, pages 3760–3764. IEEE, 2017.
- [206] Ning Tang, Fei Zhou, Zhaorui Gu, Haiyong Zheng, Zhibin Yu, and Bing Zheng. Unsupervised pixel-wise classification for chaetoceros image segmentation. *Neurocomputing*, 318:261–270, 2018.
- [207] Roy Taylor and Deborah Batey. *Handbook of retinal screening in diabetes*. Wiley Online Library, 2006.
- [208] Suman Thapar and Shevani Garg. Study and implementation of various morphology based image contrast enhancement techniques. *International Journal of Computing and Business Research*, pages 2229–6166, 2012.
- [209] Daniel Shu Wei Ting, Carol Yim-Lui Cheung, Gilbert Lim, Gavin Siew Wei Tan, Nguyen D Quang, Alfred Gan, Haslina Hamzah, Renata Garcia-Franco, Ian Yew San Yeo, Shu Yen Lee, et al. Development and validation of a deep learning system for diabetic retinopathy and related eye diseases using retinal images from multiethnic populations with diabetes. *Jama*, 318(22):2211–2223, 2017.
- [210] Daniel Shu Wei Ting, Louis R Pasquale, Lily Peng, John Peter Campbell, Aaron Y Lee, Rajiv Raman, Gavin Siew Wei Tan, Leopold Schmetterer, Pearse A Keane, and Tien Yin Wong. Artificial intelligence and deep

- learning in ophthalmology. *British Journal of Ophthalmology*, 103(2):167–175, 2019.
- [211] Lisa Torrey and Jude Shavlik. Transfer learning. In *Handbook of research on machine learning applications and trends: algorithms, methods, and techniques*, pages 242–264. IGI Global, 2010.
- [212] Anjana Umopathy, Anusha Sreenivasan, Divya S Nairy, S Natarajan, and B Rao. Image processing, textural feature extraction and transfer learning based detection of diabetic retinopathy. In *Proceedings of the 2019 9th International Conference on Bioscience, Biochemistry and Bioinformatics*, pages 17–21. ACM, 2019.
- [213] Deepika Vallabha, Ramprasath Dorairaj, Kamesh Namuduri, and Hilary Thompson. Automated detection and classification of vascular abnormalities in diabetic retinopathy. In *Conference Record of the Thirty-Eighth Asilomar Conference on Signals, Systems and Computers, 2004.*, volume 2, pages 1625–1629. IEEE, 2004.
- [214] P Vamsi and Anjali Chahuan. Machine learning based hybrid model for fault detection in wireless sensors data. *EAI Endorsed Transactions on Scalable Information Systems*, 7(24), 2020.
- [215] Mark JJP van Grinsven, Bram van Ginneken, Carel B Hoyng, Thomas Theelen, and Clara I Sánchez. Fast convolutional neural network training using selective data sampling: Application to hemorrhage detection in color fundus images. *IEEE transactions on medical imaging*, 35(5):1273–1284, 2016.
- [216] RRRCR Vanithamani and R Renee Christina. Exudates in detection and classification of diabetic retinopathy. In *International Conference on Soft Computing and Pattern Recognition*, pages 252–261. Springer, 2016.
- [217] Rohit Varma, Paul P Lee, Ivan Goldberg, and Sameer Kotak. An assessment of the health and economic burdens of glaucoma. *American journal of ophthalmology*, 152(4):515–522, 2011.
- [218] Praveen Vashist, Sameeksha Singh, Noopur Gupta, and Rohit Saxena. Role of early screening for diabetic retinopathy in patients with diabetes mellitus: an overview. *Indian journal of community medicine: official publication of Indian Association of Preventive & Social Medicine*, 36(4):247, 2011.

- [219] Shaohua Wan, Yan Liang, and Yin Zhang. Deep convolutional neural networks for diabetic retinopathy detection by image classification. *Computers & Electrical Engineering*, 72:274–282, 2018.
- [220] Su Wang, Hongying Lilian Tang, Yin Hu, Saeid Sanei, George Michael Saleh, Tunde Peto, et al. Localizing microaneurysms in fundus images through singular spectrum analysis. *IEEE Transactions on Biomedical Engineering*, 64(5):990–1002, 2016.
- [221] Yu Wang, Yaonan Zhang, Zhaomin Yao, Ruixue Zhao, and Fengfeng Zhou. Machine learning based detection of age-related macular degeneration (amd) and diabetic macular edema (dme) from optical coherence tomography (oct) images. *Biomedical optics express*, 7(12):4928–4940, 2016.
- [222] Zhiguang Wang and Jianbo Yang. Diabetic retinopathy detection via deep convolutional networks for discriminative localization and visual explanation. *arXiv preprint arXiv:1703.10757*, 2017.
- [223] Zhiguang Wang and Jianbo Yang. Diabetic retinopathy detection via deep convolutional networks for discriminative localization and visual explanation. In *Workshops at the Thirty-Second AAAI Conference on Artificial Intelligence*, 2018.
- [224] Tien Y Wong, Jennifer Sun, Ryo Kawasaki, Paisan Ruamviboonsuk, Neeru Gupta, Van Charles Lansingh, Mauricio Maia, Wanjiku Mathenge, Sunil Moreker, Mahi MK Muqit, et al. Guidelines on diabetic eye care: the international council of ophthalmology recommendations for screening, follow-up, referral, and treatment based on resource settings. *Ophthalmology*, 125(10):1608–1622, 2018.
- [225] Tien Yin Wong and Neil M Bressler. Artificial intelligence with deep learning technology looks into diabetic retinopathy screening. *Jama*, 316(22):2366–2367, 2016.
- [226] Jiayi Wu, Jingmin Xin, Lai Hong, Jane You, and Nanning Zheng. New hierarchical approach for microaneurysms detection with matched filter and machine learning. In *2015 37th Annual International Conference of the IEEE Engineering in Medicine and Biology Society (EMBC)*, pages 4322–4325. IEEE, 2015.
- [227] Di Xiao, Shuang Yu, Janardhan Vignarajan, Dong An, Mei-Ling Tay-Kearney, and Yogi Kanagasingam. Retinal hemorrhage detection by rule-based and machine learning approach. In *2017 39th Annual International*

Conference of the IEEE Engineering in Medicine and Biology Society (EMBC), pages 660–663. IEEE, 2017.

- [228] Zhitao Xiao, Xinpeng Zhang, Lei Geng, Fang Zhang, Jun Wu, Jun Tong, Philip O Ogunbona, and Chunyan Shan. Automatic non-proliferative diabetic retinopathy screening system based on color fundus image. *Biomedical engineering online*, 16(1):1–19, 2017.
- [229] Kele Xu, Dawei Feng, and Haibo Mi. Deep convolutional neural network-based early automated detection of diabetic retinopathy using fundus image. *Molecules*, 22(12):2054, 2017.
- [230] Rikiya Yamashita, Mizuho Nishio, Richard Kinh Gian Do, and Kaori Togashi. Convolutional neural networks: an overview and application in radiology. *Insights into imaging*, 9(4):611–629, 2018.
- [231] Ji-Jiang Yang, Jianqiang Li, Ruifang Shen, Yang Zeng, Jian He, Jing Bi, Yong Li, Qinyan Zhang, Lihui Peng, and Qing Wang. Exploiting ensemble learning for automatic cataract detection and grading. *Computer methods and programs in biomedicine*, 124:45–57, 2016.
- [232] Yehui Yang, Tao Li, Wensi Li, Haishan Wu, Wei Fan, and Wensheng Zhang. Lesion detection and grading of diabetic retinopathy via two-stages deep convolutional neural networks. In *International Conference on Medical Image Computing and Computer-Assisted Intervention*, pages 533–540. Springer, 2017.
- [233] Xiaoxia Yin, Brian WH Ng, Jing He, Yanchun Zhang, and Derek Abbott. Accurate image analysis of the retina using hessian matrix and binarisation of thresholded entropy with application of texture mapping. *PLoS One*, 9(4):e95943, 2014.
- [234] Tae Keun Yoo and Samin Hong. Artificial neural network approach for differentiating open-angle glaucoma from glaucoma suspect without a visual field test. *Investigative Ophthalmology & Visual Science*, 56(6):3957–3966, 2015.
- [235] Tae Keun Yoo and Eun-Cheol Park. Diabetic retinopathy risk prediction for fundus examination using sparse learning: a cross-sectional study. *BMC medical informatics and decision making*, 13(1):106, 2013.
- [236] Jason Yosinski, Jeff Clune, Anh Nguyen, Thomas Fuchs, and Hod Lip-

- son. Understanding neural networks through deep visualization. *arXiv preprint arXiv:1506.06579*, 2015.
- [237] Aliaa AA Youssif, Atef Z Ghalwash, Amr S Ghoneim, et al. Comparative study of contrast enhancement and illumination equalization methods for retinal vasculature segmentation. In *Cairo International Biomedical Engineering Conference*, pages 1–5, 2006.
- [238] Haiping Yu, Fazhi He, and Yiteng Pan. A novel region-based active contour model via local patch similarity measure for image segmentation. *Multimedia Tools and Applications*, 77(18):24097–24119, 2018.
- [239] Haiping Yu, Fazhi He, and Yiteng Pan. A novel segmentation model for medical images with intensity inhomogeneity based on adaptive perturbation. *Multimedia Tools and Applications*, 78(9):11779–11798, 2019.
- [240] Shuang Yu, Di Xiao, and Yogesan Kanagasigam. Exudate detection for diabetic retinopathy with convolutional neural networks. In *2017 39th Annual International Conference of the IEEE Engineering in Medicine and Biology Society (EMBC)*, pages 1744–1747. IEEE, 2017.
- [241] Hongyan Zhang, Kai Niu, Yanmin Xiong, Weihua Yang, ZhiQiang He, and Hongxin Song. Automatic cataract grading methods based on deep learning. *Computer methods and programs in biomedicine*, 182:104978, 2019.
- [242] Linglin Zhang, Jianqiang Li, He Han, Bo Liu, Jijiang Yang, Qing Wang, et al. Automatic cataract detection and grading using deep convolutional neural network. In *2017 IEEE 14th International Conference on Networking, Sensing and Control (ICNSC)*, pages 60–65. IEEE, 2017.
- [243] Wei Zhang, Jie Zhong, Shijun Yang, Zhentao Gao, Junjie Hu, Yuanyuan Chen, and Zhang Yi. Automated identification and grading system of diabetic retinopathy using deep neural networks. *Knowledge-Based Systems*, 175:12–25, 2019.
- [244] Zhuo Zhang, Feng Shou Yin, Jiang Liu, Wing Kee Wong, Ngan Meng Tan, Beng Hai Lee, Jun Cheng, and Tien Yin Wong. Origa-light: An online retinal fundus image database for glaucoma analysis and research. In *2010 Annual International Conference of the IEEE Engineering in Medicine and Biology*, pages 3065–3068. IEEE, 2010.
- [245] Haiyong Zheng, Ruchen Wang, Zhibin Yu, Nan Wang, Zhaorui Gu, and Bing Zheng. Automatic plankton image classification combining multiple

- view features via multiple kernel learning. *BMC bioinformatics*, 18(16):570, 2017.
- [246] Stephan Zheng, Yang Song, Thomas Leung, and Ian Goodfellow. Improving the robustness of deep neural networks via stability training. In *Proceedings of the IEEE conference on computer vision and pattern recognition*, pages 4480–4488, 2016.
- [247] Wei Zhou, Chengdong Wu, Dali Chen, Yugen Yi, and Wenyong Du. Automatic microaneurysm detection using the sparse principal component analysis-based unsupervised classification method. *IEEE access*, 5:2563–2572, 2017.
- [248] Yiren Zhou, Sibong Song, and Ngai-Man Cheung. On classification of distorted images with deep convolutional neural networks. In *2017 IEEE International Conference on Acoustics, Speech and Signal Processing (ICASSP)*, pages 1213–1217. IEEE, 2017.
- [249] Yue Zhou, Guoqi Li, and Huiqi Li. Automatic cataract classification using deep neural network with discrete state transition. *IEEE transactions on medical imaging*, 2019.
- [250] Barret Zoph, Vijay Vasudevan, Jonathon Shlens, and Quoc V Le. Learning transferable architectures for scalable image recognition. In *Proceedings of the IEEE conference on computer vision and pattern recognition*, pages 8697–8710, 2018.
- [251] Karel Zuiderveld. Contrast limited adaptive histogram equalization. In *Graphics gems IV*, pages 474–485. Academic Press Professional, Inc., 1994.